An Atomic Force Microscopy Study of Bacterial Adhesion to Natural Organic Matter-Coated Surfaces In the Environment

by

Laila Ibrahim Abu Lail

A Thesis

submitted to the faculty of

WORCESTER POLYTECHNIC INSTITUTE

in partial fulfillment of the requirements for the

Degree of Master of Science

in

Civil and Environmental Engineering

by

24 April, 2006

Terri A. Camesano, Ph.D.,
Major Advisor
Assistant Professor of Chemical Engineering
Worcester Polytechnic Institute

John Bergendahl, Ph.D.
Assistant Professor of Civil and Environmental Engineering
Worcester Polytechnic Institute

Frederick L. Hart, Ph.D.
Professor and Department Head of Civil and Environmental Engineering
Worcester Polytechnic Institute

Table of Contents

List of Tables

List of Figures

Acknowledgments

First, I am grateful for the guidance and support of my advisor, Professor Terri A. Camesano. She is not only my advisor; she is my best friend, with whom I shared very special moments. I will never forget you.

Further, I would like to thank Professor John Bergendahl for having always the time for me, and for giving me the encouragement to do more work.

I would like also to thank:

- My lab mates: Dr. Ray Emerson, Dr. Nehal Abu-Lail, Yatao Liu, Arzu Atabek, and Paola Pinzon-Arango
- Civil & Environmental Engineering Department
- Chemical Engineering Department
- Professor George Pins from Biomedical Engineering Department
- Eftim Milkani from the Chemistry Department
- NSF grant BES-0238627 for funding this project
- All my friends for the time we spent together, laughing, crying, talking, and listening, specially; Mariana Jbantova, Ikram, Mohammad Nassar, Caitlin Callaghan, Wael Al-nahhal, Amparo, Olly, Hala Mokbel, Majed Alsyd, Alpna, Amesha, Natalie, and Ruba
- My family: They were the most who helped me in this work, gave me the strength to continue this work, everyone did a great job.

Mom and Dad; Salemah Alyousef and the late Ibrahim Abu-Lail

Sisters; Nehal, Seren, Areej, and Alaa

Brother, Abd Almajeed

Brothers in Law: Abd alhamed, Nor alden, and my sister in law, Amneah.

Parents in Law: Sameha and Omar Abu-Lail

My lovely nieces: Tala, Hala, and Lema

- My world: Hussein Abu-Lail and Omar Abu-Lail.

This work is dedicated to the memory of my father Ibrahim Abu-Lail, without his faith in me and his encouragement all the time I could never have finished this work. I am so proud to be your daughter.

Abstract

Studying the interactions between bacteria and soil colloidal particles in the environment is important for bioaugmentation purposes. Different factors affect the transport of the bacteria in porous media. For example, the soil type, the ionic strength of the substrate, and biological properties, such as the bacterial cell motility. Since organic materials are present in almost all subsurface media, the presence of natural organic matter (NOM) is considered an important factor influencing bacterial transport in porous media.

In this work, a model system was developed to examine the interactions between natural colloidal particles and environmental bacteria using Atomic Force Microscopy (AFM). The natural colloids in the environment were modeled by a surface film of adsorbed NOM onto spherical SiO2 particles. Poly(methacrylic acid) (PMA), a simple linear polyelectrolyte, was used to mimic NOM since both are dominated by carboxylic acid functional groups.

Soil Humic Acid (SHA) and Suwannee River Humic Acid (SRHA), two acidic polyelectrolytes, were used in further experiments to represent more complicated NOM. A smooth strain of Pseudomonas aeruginosa (PAO1) that coexpresses A-band and B-band polysaccharides, and its rough mutant (AK1401) that only expresses the A-band polysaccharides, were chosen to represent environmental bacteria. The model system was characterized through analysis of the measured forces between the chemically-modified colloidal probes and the bacterial cells. Interestingly, we found that PMA was not a good model for the more complex NOM substances. Differences were also observed in how each bacterium interacted with the three forms of NOM. For example, P. aeruginosa

PAO1 had the highest adhesion with both complex forms of NOM, while P. aeruginosa AK1401 had the lowest adhesion with the complex forms of NOM. Since the lipopolysaccharide (LPS) structure is the only difference between the two strains, we attribute the different interactions to differences in LPS structure. The polymer density on the bacterial surface was found to be the most important factor in controlling the nature of the interaction forces.

Introduction:

Numerous cities around the world rely on groundwater as their major source of drinking water. For this reason, the microbial quality of groundwater is very important to public health (90). According to the latest estimates, over 100 million people use groundwater as their source of drinking water in the United States. The United States Environmental Protection Agency (USEPA) estimates that currently over 200,000 illnesses and 18 deaths occur each year due to viral and bacterial contamination of public ground water systems (3). Groundwater can become contaminated by leaking sewer lines, pathogen infiltration from improperly designed septic tank systems, as well as infiltration from other sources (71). Therefore, understanding the fate and transport of bacteria in soil and groundwater is critical for designing protective zones around water supply wells (100).

Studying bacterial transport through soil aquifers has two main applications. In the process of bioaugmentation, bacterial transport is enhanced by injecting certain bacterial strains into the aquifer. These bacteria are selected based on their ability to degrade organic pollutants in contaminated soils. Conversely, reduced bacterial transport is needed to prevent pathogenic bacteria from migrating long distances from discharge points in the ground such as septic tanks.

Many laboratory and field studies have been conducted to investigate sorption, inactivation, and transport of various bacterial strains in porous media (12, 21, 42, 64, 72, 101).

Temperature, soil properties, solution chemistry, the presence of metal oxides, the degree of saturation of the solid media, and the presence and composition of natural organic matter are the primary factors influencing bacterial transport in subsurface environment (41, 100).

The presence of organic material is an important factor influencing bacterial transport in porous media (30). Organic materials are present in almost all subsurface media, although their quantities vary. In most natural soils, the organic matter content is lower than 50 g/kg (51, 80). In these natural media, organic materials can influence transport of contaminants directly (58) as well as indirectly by being adsorbed as a film on the surface of solid grains. The latter alters the surface charge and aggregation behavior of reactive mineral oxides and layered silicate minerals (49). These reactions can greatly affect bacterial interactions at the solid-liquid interface and, thereby, affect the mobility of the bacteria.

Much research has centered on investigating the effect of natural organic matter on bacterial transport into porous media by monitoring bacterial retention in quartz sand and glass bead columns (25, 45, 76). Bacterial attachment efficiencies are estimated from bacterial retention using a steady-state filtration equation (55, 66, 98). Prior studies suggested that sediment organic matter (SOM) and dissolved organic matter (DOM) can enhance bacterial transport into the porous media by either sorption onto the bacterial cell walls, and increasing the negative charge of the bacterial surface, or by the competition between DOM and bacteria for sediment sorption sites (44).

Atomic force microscopy (AFM) has been extensively applied as a spectroscopy technique for measuring interfacial forces between bacteria and surfaces (37, 46). In this

work, the AFM is used to study the interactions between each of two well-defined bacterial strains with NOM-coated surfaces. A model system is being built in order to closely represent the properties of colloidal particles present in the environment. In this system, the natural colloids were represented by a surface film of adsorbed natural organic matter on spherical SiO_2 particles. Interaction force-separation curves were recorded between the adsorbed NOM-coated surfaces and two well defined strains of *Pseudomonas aeruginosa*.

1 Literature Review

1.1 Bacterial Transport in Porous Media

For more than 100 years, there has been debate among microbiologists and public health practitioners concerning monitoring drinking water for either pathogens or indicators (50).

In the time period 1970-1985, it was recognized that bacteria could travel considerable distances in aquifers and saturated soils, posing a contamination threat to surface and well waters (50). As a result, a large number of outbreaks of water-borne diseases have been attributed to contaminated groundwater. A review of pathogen transport through aquifers by Gerba et al. (30) considered the distances that bacteria traveled in different soil types, or in areas with different underlying geology. In aquifers that allow high pump rates, and contain small amounts of clays or dissolved solids, the chance is greater to enhance the movement of microorganisms. They observed bacteria to travel 0.6 m in fine loamy sand while they have shown bacteria to move for more than 1 km in sand-gravel aquifers. Field and laboratory studies at the time relevant to microbial

transport in porous media have focused on factors affecting adsorption of microbes to solids (29), and on the development of models for microbial transport based on adsorption.

Recently, field and laboratory studies relevant to bacterial transport in porous media have focused on the different physical, chemical, and biological factors influencing microbial transport (16, 25, 28, 33, 59, 71, 100, 101). These studies rigorously employed column experiments, and used the colloid filtration theory as a model for one-dimensional bacterial transport in soil.

The transport of microorganisms in soil aquifers can be both beneficial and harmful. It is undesirable, for example, for pathogenic bacteria to migrate long distances from discharge points in the ground such as septic tanks.

Table 1 shows the most important pathogenic bacteria and viruses that may either actively or passively transport into the water path. The remediation of soils contaminated with organic pollutants can be enhanced via bioaugementation (54). There are also a number of engineering applications in which the transport of microorganisms in subsurface environments is important, including river bank filtration, reuse of domestic wastewater for irrigation and land disposal of treated wastewater effluents.

In this section, a general review on the main physical, chemical, and biological factors influencing transport of microorganisms into groundwater is presented. Table 2 summarizes the different factors influencing bacterial transport through porous media (16, 25, 28, 33, 52, 59, 71, 100, 101).

Table 1: Important pathogenic bacteria and viruses that might be transported in groundwater (63).

Pathogenic bacteria	Pathogenic viruses
Salmonella sp.	Hepatitis virus
Shigella sp.	Polio virus
Yersinia enterocolitica	Coxsackie viruses
Y. pseudotuberculosis	Adenovirus
Leptospira sp.	Rotavirus
Francisella tularensis	Norwalk like virus
Dyspepsia coli	
Enterotoxigenic E.coli (ETEC)	
Pseudomonads	
Vibrio sp.	
Legionella sp.	

Table 2: Factors influencing bacterial transport through porous media.

Physical properties	Chemical properties	Biological properties
Soil type	Ionic strength	Surface charge
Soil texture	Surface modifying chemicals	Cell size
Depth of bedrock	pH value of the groundwater	Cell motility
Grain size	Natural organic matter	Hydrophobicity
Heterogeneity		Nutrient medium
		Growth phase
		Surface Macromolecules

1.1.1 Physical Properties Affecting Bacterial Transport in Porous Media:

Many studies have focused on demonstrating the role of the different physical properties on enhancing or reducing bacterial transport onto porous media. Physical properties that have been examined are: soil type (30), soil texture (25), the depth of soil over the bedrock (18), grain size (25) and soil heterogeneity (25).

Soil type can be an important factor in bacterial transport. Several studies have examined the distances that bacteria traveled in different soil types. Gerba et al (30) observed that coliform bacteria could travel 0.6 m in fine loamy sand and more than 1 km in sand-gravel.

Other studies showed that depth to bedrock was a factor affecting groundwater quality (18). If the depth of soil over the bedrock was shallow, there would be little chance for the soil to interact with water and any contaminants percolating within it. Therefore, a relatively unrestricted flow of water would take place, allowing contaminants to enter groundwater. Bacteria have been shown to move through soil columns at pore velocities of 3-30 m/day in laboratory experiments (25, 76, 93) as well as in field studies (34, 35).

The soil provides a natural filtering action and adsorption site for the removal of bacteria. The extent of bacterial movement through saturated soil is mainly related to water movement, which is affected by soil properties. Smaller pore size, resulting from increased bulk density, may yield better filtration, as there is more soil available for adsorption along the same length of flow path (18). Van Elsas (39, 86) found a strong

influence of soil bulk density on the migration of bacteria. Small increases in bulk density resulted in up to 60% decrease in transport of bacteria due to reduction in flow.

Grain size and soil texture are important factors in measuring the ease and speed with which water and contaminants can move through the soil to groundwater. Fontes et al. (25) demonstrated that grain size was the most important factor controlling transport of bacteria over the range of values tested for all of the factors examined. They investigated two particles types with different properties namely clay and coarse sand. Clay particles contain 40-70% pore space, while in coarse sand the pore space ranges between 25-50%. Clay pores are small and poorly connected, making clay deposits less permeable. The pores in sand are large and interconnected, making these types of deposits much more permeable, allowing water to move more easily and rapidly through this medium (18). Sands and clays also have very different surface areas available for nutrient accumulation and microbial adhesion. The surface area ranges from approximately 20 cm^2/g for coarse sands to more than 20,000 cm^2/g for certain clays.

The clay and sand content markedly affect the structure of soil, its bulk density, permeability and its ability to adsorb water and cations from solution. All of these factors influence whether bacteria can transport through or survive in soil (18).

Smith et al. (76) showed that surface soil type has a strong impact on the bacterial motility by comparing the movement of *Escherichia coli* through both undisturbed and repacked soils of different textures. They found that bacteria moved the greatest distance in coarse sand and least in fine sand for a given suspending solution.

Fontes et al. (25) found that heterogeneity in the subsurface environment is an important factor influencing transport of bacteria and may be responsible for much of the long range transport of microbes.

1.1.2 Chemical Properties Affecting Bacterial Transport in Porous Media:

Chemical properties have been studied extensively in order to enhance bacterial transport in the subsurface, either by changes in the solution chemistry or by changes in the surface properties of the bacteria or substratum. The effect of ionic strength, surface modifying chemicals, pH, and natural organic matter on bacterial transport onto porous media is presented here.

1.1.2.1 Effect of Ionic Strength on Bacterial Transport.

The effect of ionic strength on bacterial retention in porous media has been studied by performing column transport experiments for bacterial suspensions in three different buffers (45). The solution buffers were; phosphate, [3-(N- morpholino) propanesulfonic acid] (MOPS), and Tris (33). Decreasing the ionic strength has lowered the bacterial retention on borosilicate glass beads irrespective of the type of buffer. At the lowest ionic strength the attachment efficiency was equal to 0.0016, while at high ionic strength, the attachment efficiency approached unity. The surface charge of the bacteria and the glass beads under the conditions of these experiments was negative. The experiments showed that the bacterial retention and colloid retention increased with ionic strength under unfavorable conditions. Particle retention under unfavorable conditions is governed by the net result of electrostatic repulsion and van der Waals attraction. The

separation distance between the bacteria and the porous media surface at which van der Waals attraction dominates electrostatic repulsion is highly sensitive to the ionic strength of the solution. High ionic strengths compress the electrostatic repulsive layer, and hence increase particle retention. However, since the bacterial surface is characterized by differing degrees of hydrophobicity and surface charge, the effects of the different treatments investigated for ionic strength changes may vary significantly for different bacterial strains (45).

1.1.2.2 Effect of Surface Modifying Chemicals on Bacterial Transport.

The use of experimental mini-columns provides an efficient means of determining bacterial attachment efficiencies in a system approximating the transport conditions in an aquifer. A variety of chemical additives have been shown to modify bacterial retention in porous media mini-columns (45). Among these chemicals, seven had the greatest effect on bacterial retention in the mini-columns. These seven chemicals are: (two surfactants, Tween-20 (a nonionic surfactant that affects hydrophobic interactions) and sodium dodecyl sulfate (an anionic surfactant) (SDS), EDTA (a cell membrane permeabilizer that removes outer membrane lipopolysaccharides), sodium periodate (an oxidizer that cleaves surface polysaccharides), sodium pyrophosphate (a surface charge modifier), proteinase-K (a nonspecific protease that cleaves peptide bonds), and lysozyme (an enzyme that cleaves cell wall components)) (33). Chemical additions to the bacterial suspension can be used to modify either the bacterial or sediment grain surfaces, or both (30). Of the chemical treatments used, surfactant addition resulted in the largest decreases in bacterial retention, and hence was the most effective in facilitating bacterial transport.

Tween-20 reduced the bacterial attachment efficiency from 0.38 in the absence of Tween-20, to 0.0016 in the presence of 0.1 vol. % Tween-20. SDS lowered the bacterial attachment efficiency from 0.064 in the absence of SDS to 0.0067 in the presence of 10 mg/L SDS. Three of the treatments increased bacterial retention. Lysozyme, sodium periodate, and EDTA resulted in increasing the attachment efficiencies depending on the buffer used (45).

The effect of surface modifying chemicals on the cell morphology of *Bacillus cereus* was studied by Xiaopeng et al. using the atomic force microscope (AFM). They studied the changes in the cell surface structures including the size, shape and properties of the bacteria under different media conditions, they found that bacteria without any treatment usually have a smooth surface and after treatment with 0.1 mol/L HNO_3 or EDTA overnight they became rougher. However, they were able to preserve their overall cell structure, such as the shape and size, implying that treatment with 0.1 mol/L HNO_3 or EDTA does not cause any major change in the cell structure (95).

1.1.2.3 Effect of pH Values for Groundwater.

Scandura et al. studied the effect of the pH value of the groundwater on viral and bacterial contamination of groundwater (71). They found that detection of viruses was greater in the groundwater of typically acidic soils which have a low pH value. This is due to the fact that low pH value of the groundwater allows rapid movement of bacteria and other contaminants, especially under saturated flow conditions. Thus, such groundwater may experience extensive viral and bacterial contamination by specific effluent.

1.1.2.4 Effect of Natural Organic Matter on Bacterial Transport.

The presence of organic material (NOM) is an important factor influencing bacterial transport in porous media (30), since organic materials are present in almost all subsurface media. Studies have shown that there is an adsorbed film composed mainly of organic matter formed on the surface of most of the solid particles in soil and sea water (53). Neihof and Loeb studied the properties of the adsorbed film using micro-electrophoresis, ellipsometry, and contact angle measurements. Their results showed that a film forms very rapidly during the first few minutes, continues to grow at an appreciable rate for a period of hours, and continues to build even after 20 hrs. They found that there are many possible humic substances which may lead to electronegative films on adsorption (53).

Humic substances are derived from soil and are also produced within natural water and sediments by chemical and biological processes such as the decomposition of organisms after death. These decomposition products are then acted on by microorganisms, affected by environmental factors, and transformed into the humic and fulvic acids (65).

Humic substances are anionic polyelectrolytes of low to moderate molecular weight; their charge is primarily caused by carboxyl and phenolic groups. Humic substances are refractive, have both aromatic and aliphatic components, can persist for centuries or longer and can be surface active. Humic substances are defined operationally by the methods used to extract them from water or soil (65). Typically humic substances are divided into fulvic acids (FAs) and humic acids (HAs). Fulvic acids are humic

substances soluble in both acidic and basic solutions. While humic acids (HAs) are not soluble in acidic conditions and only soluble at high pHs (73).

Many studies done using mini-column experiments have shown that bacterial transport may be facilitated by aqueous phase dissolved organic matter (DOM) and sediment organic matter (SOM) (29, 44). DOM has been shown to facilitate bacterial transport through aquifer sediment by sorbing onto bacterial cell walls and increasing the negative charge of the bacterial surface (30, 44, 64).

Other studies on the effect of NOM in facilitating the transport of contaminants in aquifer sediments have shown that the transport of hydrophobic contaminants in the presence of humic substances at environmentally feasible concentrations should be facilitated relative to transport of such contaminants alone in both batch and column transport experiments (43). The association of hydrophobic contaminants with humic substances holds promise for the use of humic substances as a solubilizing agent for the removal of hydrophobic contaminants from the sediment (43).

Two humic substances were mainly used in most of the studies; Suwannee River humic acid (SRHA), and soil humic acid (SHA). Ultrafiltration measurements were performed on the two NOM sources to separate them into three fractions (bulk, < 10000 Da, < 1000 Da) (43). These fractions were then measured for dissolved organic carbon (DOC) in order to obtain a relative measure of molecular mass. The results indicated that over 80% of SHA is of molecular mass greater than 10000 Da whereas less than 50% of SRHA exceeds 10000 Da, indicating that SHA has a higher average molecular weight than SRHA.

1.1.3 Biological Properties Affecting Bacterial Transport in Porous Media:

The following biological properties are the major biological properties that affect bacterial transport through porous media: bacterial surface charge (33, 89), hydrophobicity (89), cell size (25, 28), cell motility (48, 59), nutrient medium (45), cell growth phase (87), and surface polymers. Bacterial surface charge is typically measured by electrophoresis (85). The electrostatic interaction predicts that a negative cell surface charge promotes bacterial attachment to positively charged Fe and Al oxide surfaces but inhibits attachment to negatively charged quartz surfaces (33, 89). In reality, this simple relationship is complicated by the presence of organic matter, which can alter the surface charges of both bacteria and sediment. van Loosdrecht et al. determined the effect of both cell surface electrokinetic potential and hydrophobicity and found that both parameters have an influence on bacterial adhesion (87). They observed that the influence of electrokinetic potential became obvious when combined with the hydrophobicity results. At high contact angle for water, hydrophobicity was the dominant characteristic irrespective of mobility. However, electrokinetic potential became more influential at more hydrophilic cell surfaces (87). They reasoned their results as a cause of the classical Derjaguin, Landau, Verwey, and Overbeek (DLVO) theory of electrostatic-double layer interactions. Rijnaarts et al. demonstrated that the isoelectric point (IEP) of the bacterium is a more appropriate parameter than the electrophoretic mobility for predicting cell adhesion, and that steric interactions rather than DLVO-type interactions control cell adhesion at high ionic strength (68). They studied nine strains of Gram-negative bacteria including *Pseudomonas*. They found a specific relation between hydrophobicity and IEP

but no correlation between IEP and electrophoretic mobility. Their results showed low adhesion on glass when the IEP was ≤ 3.0 and on Teflon when the IEP was ≤ 2.8. An IEP below these values suggests the presence of cell surface polymers that inhibits adhesion by steric interactions (68).

Cell hydrophobicity has been investigated in relation to bacterial transport by different groups (28, 61). Forexample, Gannon et al. (28) studied the retention of 19 strains including *Pseudomonas* by soil particles and found no correlation between bacterial transport and cell hydrophobicity. Retention was statistically related to cell size, with bacteria shorter than 1.0 μm usually showing higher percentages of cells being transported through the soil.

Experiments on the effects of cell motility on bacterial transport have also resulted in different outcomes. In some cases, motile cells have been shown to be transported further (59), and in other cases, motile cells have been shown to attach to mineral grain surfaces more than nonmotile cells (48). The discrepancy may be related to substrate surface characteristics. Camesano and Logan (16) observed that motile cells were retained less in sediments due to the ability of the bacteria to swim and avoid collisions with grain surfaces. McClaine and Ford studied the effect of fluid velocity on the attachment and detachment of motile and non-motile bacteria to glass surfaces using a parallel-plate flow chamber they also examined the possible role of flagella on bacterial adhesion (56). They found that transport of motile bacteria to surfaces is dominated by diffusion. Whereas transport of non-motile bacteria is dominated by settling at low velocities, and by Brownian diffusion at high velocities. Their results showed that the attachment rate of motile cells is five times higher than the attachment rate of non-motile

cells at the highest fluid velocity. They found also that the presence of flagella has no effect on the initial attachment rate of non-motile bacteria. However, the movement of the flagella helped the attached motile bacteria to detach at low flow rates, and strengthened their adhesion at high flow rates (56).

The effect of cell size on bacterial transport in porous media has been studied (28), and it is generally recognized that smaller cells are transported more readily than larger cells. On the basis of a regression analysis of the relationship between the percentages of cells transported and cell surface properties, Gannon et al. (28) concluded that cell size was the only statistically significant parameter responsible for the observed differences in transport of 19 strains through soil columns. Fontes et al. (25) performed bacterial transport experiments by injecting two strains that had the same hydrophobicity but were different sizes into a number of columns of clean quartz sand in which the grain sizes were different and the ionic strengths of the pore water were different. They concluded that cell size and ionic strength were of equal importance but were less important than grain size.

Nutrient medium is another factor that affects the transport of bacteria in porous media. Enriched bacteria have a larger size, a more hydrophobic surface, and hence a much stronger tendency for attachment to sediment, than do microbes which have been starved prior to introduction to sediment. Although starved bacteria are more easily transported, nutrient-enriched bacteria may have greater ability to degrade contaminants if they have been acclimated to these contaminants prior to introduction to the subsurface (45). van Loosdrecht et al. found that most lacustrine and near-shore microorganisms

tend to adhere under optimal growth conditions, while some open-ocean microorganisms adhere during starvation (87).

Cell growth phase affects bacterial adhesion through changes in cell hydrophobicity. van Loosdrecht et al. observed that bacteria becomes more hydrophobic during the exponential growth phase and during continuous cultivation at high dilution rates many bacteria tend to form flocks or adhere to surfaces present in the culture flask (87). The significant impact of cell growth phase on adhesion characteristics was also studied by Smets and his group (32). They studied the changes in both the hydrophobic and the electrostatic character of the cell surface with altering growth phases. They found that *Pseudomonas aeruginosa* Olin exhibited increased ζ-potential in the stationary phase as compared with logarithmic growth and decay phases. They showed also that cells in the logarithmic growth and decay phases exhibited increased hydrophilic repulsion, while cells in the stationary phase exhibited less hydrophilic repulsion (32).

Bacterial surface polymers are of importance in the field of bacterial adhesion (68).Their ability to inhibit or to promote adhesion is determined by their affinities for the substratum. Rijnaarts et al. demonstrated that in addition to hydrophobicity the isoelectric point (IEP) of the bacterium is a more appropriate parameter than the electrophoretic mobility for predicting the steric properties of cell surface polymers and their consequences for cell adhesion. They found that IEP $\leq$ 2.8 indicates the presence of significant amounts of cell surface polymers which inhibit adhesion onto both hydrophilic (Glass) and hydrophobic (Teflon) surfaces (68).

Proteins are among the surface polymers which have been studied extensively by AFM (19, 74). In one study AFM has been used to determine the forces that control

protein-ligand and protein-protein interactions. The study considered measurements of the specific and the nonspecific forces that jointly control protein interactions and reviewed some of the recent studies in determining the unbinding forces and mechanical properties of proteins (74). In another study, AFM was used to provide insights into the structure, function, and assembly of water-soluble and membrane proteins. The signal-to-noise ratio of the AFM was used to image the individual proteins under physiological relevant conditions at a lateral resolution of 0.5-1 nm and a vertical resolution of 0.1-0.2 nm (19).

1.2 Colloid Filtration Theory:

Filtration theory (15, 55, 66, 98) has been widely used to model the transport of bacteria in porous media, and used to make engineering calculations on aquasol removal in filters. The one dimensional steady-state clean-bed filtration model describes the fraction of bacteria retained in a column of length L as

$$F_R = \left(1 - \frac{C}{C_0}\right) = 1 - \left(exp\left(-3(1-\theta)\frac{\alpha\eta L}{2d_c}\right)\right) \qquad (1)$$

Where F_R is the fraction of bacteria retained in the column, C and C_0 are the effluent and influent bacterial concentrations, θ is the porosity of the media, d_c is the collector diameter, α is the collision efficiency, and η is the collector efficiency (15). This model was developed by Yao et al. (98) (1971) for flow in packed bed, assuming that the bed consists of spherical collectors, and conducting a mass balance over a control volume around a spherical collector.

The collision efficiency term in equation (1) is the fraction of colliding particles that attach to the soil, and represents the affinity of the particle for the collector. The magnitude of the collision efficiency depends on the forces between the particle, the fluid, and the collector as the separation distance between the surfaces decreases.

The collision efficiency is often calculated using the steady state breakthrough concentrations, C/C_0, over a whole column of length L (11, 15, 52, 59).

The collector efficiency (η) is a parameter dependent on diffusion, interception, and gravitational settling, which are the mechanisms that cause collisions. It indicates the fraction of particles flowing toward a grain of media, or collector that actually collides with the collector.

Rajagopalan and Tien (RT) (66) developed a semiempirical filtration equation, which has been preferred by scientists for predicting particle transport in soil columns and groundwater aquifers, since it provides the best agreement with the experimental data.

All filtration mechanisms in the RT model are based on the Happel model (1958) (15, 55). In which the flow was assumed to be completely within a concentric spherical space surrounding the collectors, and that dispersion was negligible in comparison to advection. Rajagopalan and Tien modeled particle removal by interception and gravitational sedimentation, and assumed that the Happel cell solution for diffusion which accounts for the fact that the collectors are not isolated spheres could be added on their final expression for the collector efficiency. Their model also includes attractive effects due to London-van der Waals forces.

According to Rajagopalan and Tien, the collector efficiency (15, 66) has been modeled as

$$\eta = 4.04 A_s^{1/3} N_{pe}^{-2/3} + A_s N_{L_0}^{1/8} N_R^{15/8} + 0.00338 A_s N_G^{1.2} N_R^{-0.4} \qquad (2)$$

The dimensionless numbers A_s, N_{pe}, N_{L0}, N_R, and N_G account for the effects of neighboring particles, diffusion, London-van der Waals forces, interception, and sedimentation on particle collisions. These parameters are calculated as follows:

A_s is a porosity-dependent term of the Happel model, defined as:

$$A_s = 2\frac{\left(1-\gamma^5\right)}{\left(2-3\gamma+3\gamma^5-2\gamma^6\right)} \qquad (3)$$

Where $\gamma = (1-\theta)^{1/3}$. N_{pe} is the Peclet number defined as:

$$N_{pe} = \frac{3\mu\pi U d_c d_p}{kT} \qquad (4)$$

Where d_p is the suspended particle diameter, μ is the dynamic fluid viscosity (8.94 x 10^{-4} N.s/m^2), U is the superficial fluid velocity, k is Boltzmann constant (1.38 x 10^{-23} kg.m^2/s^2.K), and T is the fluid temperature (298 K).

N_{L0} is a dimensionless number that accounts for London-van der Waals attractive forces, and is defined as

$$N_{L0} = \frac{4H}{9\pi\mu d_p^2 U} \qquad (5)$$

Where H is the Hamaker constant, assumed to be 10^{-20} J, based on interactions between water, quartz, and air (40).

N_R is the ratio of the bacterial cell diameter to the sand diameter,

$$N_R = \frac{d_p}{d_c} \quad (6)$$

N_G is the dimensionless ratio of the bacteria's Stokes settling velocity to the stream fluid approach velocity $N_G = \frac{u_{p,s}}{U}$; where the settling velocity is given by:

$$u_{p,s} = \frac{g(\rho_p - \rho_f)d_p^2}{18\mu} \quad (7)$$

Where ρ_p is the suspended particle density, ρ_f is the fluid density, and g is the gravitational constant.

Tufenkji and Elimelech (TE) (2004) (82) have proposed a different model to calculate the collector efficiency based on a numerical solution of the convective-dispersion equation. In this model the effect of the hydrodynamics interactions and the effect of the London-Van der Waals forces was included as part of all of the particle deposition terms (diffusion, interception, and settling terms).

One advantage of this model over the RT model is to overcome the limitations of the later which excluded the effect of hydrodynamic interactions and van der Waals forces on the deposition of particles that are dominated by Brownian diffusion. It also showed a remarkable agreement with exact theoretical values based on numerical solution of the convective-diffusion equation as well as a closer agreement with the experimental data compared to other available models.

In the TE model (TE), the collector efficiency is calculated as

$$\eta = 2.4A_s^{1/3}N_R^{-0.081}N_{pe}^{-0.715}N_{vdW}^{0.052} + 0.55A_sN_R^{1.675}N_A^{0.125} + 0.22N_R^{0.24}N_G^{1.11}N_{vdW}^{0.053}$$

(8)

Where $N_G = u_{p,s}$, N_{vdW} the van der Waals number defined as $N_{vdW} = \frac{H}{kT}$, and N_A, the attraction number, which combine the influence of van der Waals attraction and fluid velocity in particle collisions due to interception, and is defined as

$N_A = \frac{d_p^2(\rho_p - \rho_f)}{18\mu U}$, and all other parameters are the same as were defined for the RT model.

1.3 Pseudomonas aeruginosa

Pseudomonas aeruginosa is a Gram-negative, aerobic, rod, belonging to the bacterial family *pseudomonadaceae* (81). *P. aeruginosa* is an opportunistic pathogen that causes urinary tract infections, soft tissue infections, respiratory system infections, bacteremia, and a variety of systemic infections, particularly in patients with severe burns, and in cancer and AIDS patients who are immunosuppressed (81). It is well known for it is resistance to antibiotics and, therefore, it is a particularly dangerous and dreaded pathogen (81). These bacteria are common inhabitants of soil and water, and are motile by means of a single polar flagellum. *P. aeruginosa* can live in a biofilm form, or it can live in a planktonic form, as a free-swimming cell (81). Minimum organic growth factors are required for *Pseudomonas aeruginosa*, and it can use more than thirty organic compounds for growth (81). Its optimum temperature for growth is 37°C, and it is able to grow at temperature as high as 42°C. *P. aeruginosa* does grow in moist environments, a reflection of its natural existence in soil and water (81).

Pseudomonas aeruginosa has been mainly isolated from natural environments, such as soil or water, or from clinical settings. The environmental isolates typically

produce a small rough colony (81). There are two main phenotypes of *P. aeruginosa* clinical samples: a nonmucoid, lipopolysaccharide (LPS)-smooth phenotype mostly isolated from patients with nosocomial and community-acquired infections, and a muciod, LPS-rough phenotype mostly isolated from cystic fibrosis (CS) patients with chronic respiratory infections (36, 81).

Lipopolysaccharides are cell-surface molecules common to all Gram-negative bacteria. They consist of three regions; a lipid A portion, a core oligosaccharide, which can be subdivided into inner, and outer core units, and a high molecular weight side chain polysaccharide. The carbohydrate (core oligosaccharide) portion is linked to the lipid A by a very acid labile linkage involving 2-Keto-3-deoxyoctulosonic acid (KDO). The side chain structure is called O-antigen. This side chain consist of repeating units composed of 2-5 monosaccharides, and commonly contain uronic acids, amino sugars, and some unusual sugars (10).

Smooth LPS strains refers to strains possessing O-side chain, while rough LPS strains do not express the O-chain side (36).

The mucoid LPS (rough) strains produce alginate slime, or capsule, or muciod exopolysaccharide (MEP). Alginate slime is a repeating polymer of mannuronic and glucuronic acid which forms the matrix of the pseudomonas biofilm that anchors the cells to their environment (36). On the other hand, alginate genes are not expressed or required during the formation of the exopolysaccharide for the nonmucoid, LPS-smooth type (94).

Pseudomonas aeruginosa strains can co-express two chemically and antigenically distinct forms of the O-side chains; a serotype-specific O-antigen containing B-band LPS, and a common antigen referred to as A-band LPS. The high molecular mass B-band

polysaccharide determines the antigenic specificity of the bacterium since it is an electronegative component, whereas the antigenically conserved A-band LPS consists of α-D-rhamnose containing trisaccharide repeating units. Typically smooth *Pseudomonas aeruginosa* strains express long chain molecules, containing up to 50 repeating units (69).

Two strains of *Pseudomonas aeruginosa* have been chosen in this work as model organisms. These two strains are; PAO1 a smooth strain of *Pseudomonas aeruginosa* and AK1401 which is a semi-rough mutant of PAO1 *Pseudomonas aeruginosa*. Both strains have well-defined LPS surface characteristics. Composition analysis of the LPS from both strains indicated that the complete core oligosaccharide was composed of D-glucose, L-rhamnose, 2-amino-2-deoxy-D-galactose, L-glycero-D-manno-heptose, 3-deoxy-D-manno-octulosonic acid, L-alanine, and phosphate (70). Structural studies done on the polysaccharide portion of AK1401 strain have shown that the A-band LPS from AK1401 consists of D-rhamnose, with smaller amounts of 3-O-methylrhamnose, ribose, mannose, glucose, and a 3-O-methylhexose (10).

The PAO1 strain expresses the O-antigen side chain, and coexpresses both the A-band and the B-band polysaccharides (10). While AK1401 is a semi-rough mutant that does express only one repeating unit of the O-antigen side and does express the A-band polysaccharides (10).

The complete sequence of the genome of *Pseudomonas aeruginosa* PAO1 has been reported (79). Analysis of its genome sequence has identified genes involved in attachment, transport and utilization of nutrients, antibiotic efflux, and systems involved in sensing and responding to environmental changes (79).

1.4 Atomic Force Microscopy (AFM)

The use of atomic force microscopy (AFM) in environmental science and engineering applications has increased rapidly in the last few years. Besides the main use of AFM in high resolution imaging of different material surfaces including metals, polymers, biomolecules or cells, AFM made significant contributions to various research areas dealing with the structure, properties and dynamic processes of material surfaces and interfaces (46). Using traditional imaging and spectroscopy techniques requires sophisticated sample preparation methods, such as etching techniques or metal evaporation onto the samples, which can cause changes in the sample structure and properties. AFM does not require such preparations, hence leaving the sample and its properties in its native state. Another advantage of the AFM is its ability to work under a variety of environmental conditions and in a real time with the use of its fluid cell (46). AFM can operate in a number of different modes (contact mode, tapping mode and non-contact mode) making it possible to image a variety of samples with different degrees of softness and with the use of different kinds of tips (46, 99). In contact mode the tip is in permanent physical contact with the surface. Therefore, contact mode can be used to image hard samples which are not affected by the frictional force components the tip applies to the sample. Tapping mode uses an oscillating tip which moves toward the surface and starts to tap the surface. In tapping mode the cantilever's oscillation amplitude is used as a feedback signal to measure topographic variations of the surface. Tapping mode in liquid environments is the most suitable mode to study soft and viable cells such as bacteria (46). In non-contact mode, the tip is placed at the attractive force region, and force gradients are detected. The force gradients can be detected from shifts

in the resonance frequency of the cantilever (57). This mode has a high sensitivity of gradient measurements and offers the lowest possible interaction between sample and tip which make it suitable for work on soft surfaces, but it is more complicated than the tapping mode and has a much smaller operation range of cantilever amplitude (46).

1.4.1 AFM operating Principles

An AFM consists of a tip attached to a flexible cantilever of a known spring constant. The cantilever deflects in the z-direction due to the surface topography during tip scanning over the sample surface. This deflection movement of the cantilever is recorded to produce the image of the sample. A photodiode of four segments detects the deflection of the cantilever through a laser beam focused on and reflected from the back of the cantilever. This special photodiode gives the information about cantilever position to compiler which generates the image of the surface of the sample (46). The tip that moves across the sample plays an important role in depicting the right picture, since the resolution of an image captured by AFM depends on the radius of the tip. The radius of the tip should be smaller than the features on the sample to get a well resolved image. Depending on the kind of surface under observation, tips with different spring constant are chosen. AFM in air can be used to get very clear images, but it is not possible to get good force measurements in air due to high capillary forces caused by thin water films present on the tip and on the sample surface. These capillary forces are so large that they can hide the actual force of interaction between the tip and the sample. Using AFM under liquid makes it possible to capture realistic force measurements of the sample surface. Taking force curves for bacterial cells in water using AFM is more relevant since

bacterial adhesion usually takes place in liquid systems in nature. Therefore, AFM gives a closer picture of the actual interaction forces that a bacterium experiences during the attachment process.

1.4.2 AFM Applications

Since it is invention, AFM has proven that it is a valuable technique for obtaining precise images as well as measuring surface forces of biological systems (46). AFM does not affect the morphology of biological samples and can operate in a variety of environments especially under liquids, which represents the most relevant environmental conditions (46).

AFM has been widely applied in the field of bacterial adhesion. Studying the surface polysaccharides of the bacteria is one of the AFM applications. For example, *Escherichia coli* JM109 were used to understand the role of surface lipopolysaccharides in the adhesion of bacteria to silicon nitride tip (8). Characterizing the surface polysaccharides was done using appropriate polymer stretching models. From application of those models as the wormlike chain model, physicochemical properties of the polysaccharides such as the contour length, persistence length, and segment elasticity or spring constant was calculated (6).

Another AFM application is to study the relation ship between microscopic and macroscopic cell surface properties (84). Vadillo-Rodriguez et al. studied the interaction forces between a silicon nitride AFM tip and the surface of nine different oral bacterial strains. They compared the microscopic features of the force-distance curves to some macroscopic cell surface properties such as hydrophobicity, and cell surface charge (84).

AFM was also applied in studying the adhesion forces between colloids and biopolymer surfaces. Abu-Lail and Camesano characterized the physicochemical properties of biopolymers with AFM high-resolution images (5). Images of single molecules of DNA, proteins, and polysaccharides were studied to provide quantitative information on molecular properties of these surfaces. Among the more interesting examples of probing biopolymers with AFM are DNA sequencing, protein folding and unfolding, and identifying polysaccharide components from mixtures (5). Xu et al. used the AFM to study the effect of residence time, loading force, pH, and ionic strength on adhesion forces between two proteins and a polysaccharide (Bovine serum albumin (BSA), lysozyme, or dextran) and colloids (96).

Modification of the surface properties of the AFM tip with specific functionalities became a desirable way to obtain data from AFM measurements (83). One of the common ways of modifying the probe surface is by binding alkanethiols to a gold-coated probe surface (27). The main advantage of thiol functionalization is that such tips are ready to have a wide range of functional groups that can be used (e.g. $–CH_3$, –OH and –COOH) at their free end. Another way to functionalize tips is using polymer coatings. These coatings are chemically and structurally heterogeneous. Polymer-coated tips can be prepared by chemisorption (77), physisorption or plasma vapor deposition (47).

1.4.3 AFM to measure Steric Interactions

Steric interactions occur when two polymer-covered surfaces approach each other and their outer segments start to overlap. These interactions usually lead to a repulsive force due to the unfavorable entropy associated with compressing the chains between the

surfaces (40). The steric forces depend on the coverage of polymer on each surface, on whether the polymer is adsorbed in a reversible process or irreversibly grafted onto the surfaces, and on the quality of the solvent. For interactions in poor and theta solvents, the theories are well developed (40). A theta or ideal solvent is a solvent in which the polymer experiences no interactions with itself, either attractive or repulsive, and no excluded volume between the polymer segments. It is called the theta solvent because it happens at a critical temperature known as the theta temperature. In a poor solvent, polymer segments attract one another. A poor solvent can be converted to a theta solvent by adding certain solutes or by changing the temperature above or below the theta temperature (40).

Steric interactions played an important role to explain the interactions between polymer brushes on the bacterial surface and the AFM tip in many AFM studies (67, 91). For example, in one study the force images were taken between a bare silicon nitride tip and three different *Escherichia coli* K12 strains, each having a different length of LPS on their surface. The results showed that the force curves obtained on the top of the bacterial cell were identical for the three different strains indicating that there is a lack of steric contribution of LPS to the force curves (91). While in another study the short-range repulsive interactions between *E. coli* D21 bacteria and hydrophilic glass or hydrophobic N-octadecyltrichlorosilane (OTS)-treated glass substrates coated with the block copolymers, poly (ethylene glycol) (PEG)-lysine dendron or Pluronic F127 surfactant, showed that the polymer brushes appear not to only block the long-range attractive forces of interaction between bacteria and substrates but also to introduce repulsive steric effects (67).

The steric interactions between the AFM tip and cell surface polymers can be fitted by a model developed by Alexander (9) and de Gennes (20) for grafted or adsorbed polymers at relatively high surface coverage. The model describes the force per unit area between two parallel equal surfaces with adsorbed or grafted polymer using scaling analysis. The force per unit area expression is a function of the brush thickness, grafting density of the biopolymer, and the temperature.

$$f \approx k_B T \Gamma^{3/2} \left[\left(\frac{2L_0}{D} \right)^{9/4} - \left(\frac{D}{2L_\circ} \right)^{3/4} \right] \qquad (9)$$

Where;

f = Steric force per unit area between the two surfaces

k_B = Boltzmann constant

T = Absolute temperature (298°K)

Γ = Grafting density (m^{-2})

D = Distance between the two surfaces (nm)

L_0 = Polymer brush length (nm)

For $D/2L_0$ in the range 0.2 to 0.9 the above expression is roughly exponential and it was approximated by Israelachvili (40) to the following expression:

$$f \approx 100\, k_B T \Gamma^{3/2} e^{-\Pi D/L_0} \qquad (10)$$

When only one surface is covered with polymer, the term $D/2L_0$ in equation (9) will be replaced by D/L_0 to account for the reduced total layer thickness and in this case equation (10) for D/L_0 in the range 0.2 to 0.9 becomes:

$$f \approx 50 k_B T \Gamma^{3/2} e^{-2\Pi D/L_0} \qquad (11)$$

The Alexander-de Gennes equation was modified by Butt et al. (14) to describe the forces between the AFM-tip spherical surface and a flat surface.

1.5 van der Waals and Electrostatic Forces (The DLVO theory)

The DLVO theory of colloidal stability after Derjaguin, Landau, Verwey and Overbeek can be defined as the combined action of both van der Waals forces and the electrostatic forces to explain the total interaction that can occur between two surfaces or colloidal particles in a solution.

van der Waals forces, which are always present between any two interacting surfaces, are mainly attractive and are insensitive to variations in electrolyte concentration and pH. Electrostatic interactions, which are based on electric double layer interactions, are highly depending on the electrolyte concentration and surface charge density (40).

The DLVO theory has been typically used to describe microbial-surface interactions and often showed a qualitative agreement with bacterial-surface interactions (6). But in many cases the DLVO theory failed to predict the attachment of colloids to surfaces. For example, Elimelech and O'Melia found that the DLVO theory under low ionic strength conditions underpredicts the attachment of colloids to surfaces (23) and other researchers found that the DLVO theory was unable to predict the bacterial-surface interactions especially when microbial polymers play a significant role in the bacterial adhesion (7, 62, 75, 88). The failure in the DLVO theory can be due to the important role of the non-DLVO forces (40) as well as to some interactions which are not considered in

the van der Waals and the electrostatic forces under unfavorable deposition conditions (15, 23, 40). Possible explanations for the failure of the DLVO theory under unfavorable deposition conditions include; hydrodynamic interactions between the two surfaces, dynamic interactions between the double layers, distribution in the surface potential, occurring of reversible deposition instead of the irreversible one, and surface heterogeneity (15, 23). The non-DLVO forces can be monotonically attractive, monotonically repulsive, and they can be much stronger than the DLVO forces at small separations. These additional forces are steric interactions, specific ion effects, non-charge transfer Lewis acid base interactions, hydration forces, hydration pressure, born repulsion, polymer bridging, hydrogen bonding, and hydrophobic effects (6, 26, 37, 40, 68). To compensate for the inability of DLVO theory to explain the interactions between microbes and various surfaces, researchers applied a model which takes into account the sum of DLVO and short-range acid-base interactions (the extended-DLVO), and steric interactions to determine what types of forces influence the initial attachment of microbes to surfaces (6). This model could well-describe the interactions between lawns of *E. coli* D21f2 and mica, glass, teflon, or polystyrene surfaces (6, 62). However, the extended-DLVO model could not explain the interaction when the cell surface had a more complex structure because of the possible involvement of bridging effects and steric interactions caused by the LPS.

2 Materials & Methods

2.1 Microbial Growth

The experiments were performed on two strains of *Pseudomonas aeruginosa*. These two strains are; PAO1 a smooth strain of *Pseudomonas aeruginosa* and AK1401 which is a rough mutant of *Pseudomonas aeruginosa* PAO1. Original plates for both strains were provided by Professor Gerald Pier (Channing Laboratory, Department of Medicine, Brigham and Women's Hospital/ Harvard Medical School). Both strains were maintained at 4°C on Tryptic Soy Agar (TSA) (Sigma) plates. Each culture was replated every two weeks. The growth media used for both strains was Tryptic Soy Broth (TSB) (Sigma), prepared by dissolving 30g of TSB powder in 1 liter of ultrapure water (Milli-Q). The solution was sterilized by autoclaving at 121°C for 20 minutes before it was used. The two strains of *Pseudomonas aeruginosa* were grown in 5 ml TSB in 25 ml culture flasks (VWR). Cells were left overnight at 25°C on a radially oriented tube-spinner at 60 RPM. Cells were then transferred to 50 ml of the growth media (TSB) and grown in an orbital shaker bath at 37°C and 160 RPM until they reached an absorbance of 0.9 at 600 nm. Harvested cells were prepared for attachments on the clean glass slides or the Isophthalic Acid (IPA) gold slides for AFM experiments.

2.2 Cell Attachment

2.2.1 Glass Slide Cleaning

Glass slides (VWR) were cut into equal squares of 1" x 1" and rinsed with ultrapure water. They were sonicated in ultrasonic cleaner 2510 (Branson) for 30

minutes. Slides were washed in a 3:1 mixture of HCL and HNO_3 (Fisher) for 25 minutes, followed by elution. Slides were rinsed again in ultrapure water and washed with 4:1 mixture of H_2SO_4 and H_2O_2 (Fisher) for 25 minutes. Slides were rinsed again with ultrapure water and stored under fresh ultrapure water (31).

2.2.2 AK1401 Attachment to Clean Glass Slides

The clean glass slides were treated with 100 % ethanol (Fisher) for 5 minutes followed by 100 % methanol (Fisher) treatment for 5 minutes. Methanol was replaced with 10 ml of aminosilane solution. The aminosilane solution was prepared by adding 1 ml of 3-aminopropyl dimethoxysilane (Aldrich) to 9 ml of methanol. The slides were allowed to stay in the aminosilane solution for 15 minutes. The aminosilane solution was replaced with methanol. Then slides were rinsed with at least 50 ml of methanol followed by 25 ml ultrapure water. Finally, the slides were kept in methanol until the bacterial solution was ready to be poured on the slides (31).

18 ml of the AK1401 cell suspension was centrifuged at 1000 x g for 15 minutes. The supernatant was eluted and replaced with equivalent amount of ultrapure water. The resuspended cells were treated with 300 µL of 100 mM 1-Ethyl-3-(3-dimethylaminopropyl) carbodiimide.HCL (EDC) (Pierce), pH = 5.5, and left to equilibrate for 3 minutes. EDC solution was freshly prepared before each experiment by adding 0.192 g of EDC powder to 10 ml of ultrapure water. The resulting 100 mM solution was adjusted to pH = 5.5. The treatment with EDC was followed by addition of 300 µL of 40 mM N-Hydroxysulfosuccinimide (NHS) (Pierce), pH = 7.5. NHS solution was prepared by adding 0.0879 g of NHS powder to 10 ml of ultrapure water. The

resulting 40 mM solution was then adjusted to pH = 7.5. The bacterial solution with EDC/NHS was left to equilibrate for 10 minutes and then poured over the aminosilane treated glass slides. Samples were agitated for 10 hours on a shaker table, at 70 RPM, at room temperature, to allow the attachment process between the cells and the glass slides to take place.

Figure 1 shows the reaction that takes place upon the addition of both EDC and NHS to the bacterial cells.

2.2.3 PAO1 Attachment to IPA-Gold Slides

Isophthalic Acid (IPA) gold slides were kindly provided by Professor W.G. McMimpsey from Worcester Polytechnic Institute. The IPA-gold slide were treated with a mixture of 1 ml of 100 mM EDC solution, pH = 5.5 and 1 ml of 40 mM NHS solution pH = 7.5, slides were left to equilibrate for two hours at least.

12 ml of the PAO1 cells was centrifuged at 1000 x g for 15 minutes. The supernatant was eluted and replaced with equivalent amount of ultrapure water. The resusbended cells were poured over the EDC/NHS treated IPA-gold slides. The samples were agitated for 10 hours on a shaker table, at 90 RPM, at room temperature, to allow the attachment process between the cells and the IPA-gold slides to take place.

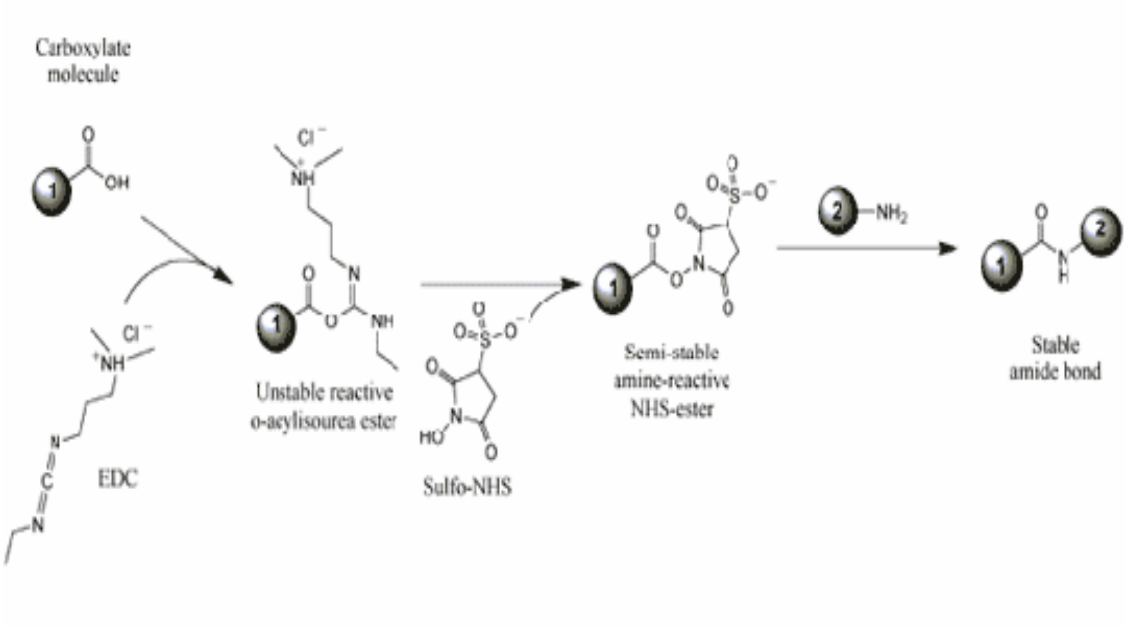

Figure 1. The reaction that takes place upon the attachment process of bacterial cells to glass slides. In this reaction the EDC reacts with a carboxyl group from molecule 1, forming an amine-reactive intermediate. This intermediate is unstable and short-lived in aqueous solution, and the addition of Sulfo-NHS stabilizes it by converting it to an amine-reactive Sulfo-NHS ester. The later reacts with an amine from molecule 2, yielding a conjugate of the two molecules joined by a stable amide bond (2).

2.3 Tip Modification

2.3.1 Cantilever Preparation

Silicon nitride cantilevers with silica sphere tips (1.0 μm) (Novascan) were cleaned immediately prior to each experiment by exposure to UV irradiation for 40 minutes. Each cantilever was then soaked in a 0.01 M NaOH solution (pH ~ 12) (Sigma) for 2-3 minutes and flushed with 5 ml of water.

2.3.2 Iron Oxide Coating

Iron oxide is a common constituent of natural waters colloids. Therefore, the oxide coated SiO_2 surface can be considered representative of the underlying mineral surface. The coating was performed by raising the pH of a 10^{-5} M $FeCl_3$ solution (Sigma) from 3.5 to 7.0 using small additions of NaOH solution over a period of 30 minutes. When the pH of the solution reached 7.0 the cantilever was soaked in the 10^{-5} M $FeCl_3$ solution for 15 hours to allow equilibration.

2.3.3 Adsorption of Poly (methacrylic) Acid (PMA) onto Fe_2O_3-Coated Silica Spheres

100 $mg \cdot L^{-1}$ of PMA solution (Polymer Source) was freshly prepared before each experiment. About 20 ml of the solution was added to the Fe_2O_3-coated cantilever in a small gel box. The cantilever was soaked in the solution for at least 16 hour to allow the

PMA to adsorb on and equilibrate with the iron oxide. After 16 hour the cantilever was allowed to dry and use in the AFM experiments.

2.3.4 Adsorption of Soil Humic Acid (SHA) onto Fe2O3-Coated Silica Spheres

100 $mg \cdot L^{-1}$ of SHA solution (International Humic Substances Society) was freshly prepared before each experiment. The solution was filtered using Acrodisc 25 mm syringe filter with 0.45 μm pore size (PALL Life Sciences). About 20 ml of the solution was added to the Fe_2O_3-coated cantilever in a small gel box. The cantilever was soaked in the solution for at least 16 hours to allow the NOM to adsorb on and equilibrate with the iron oxide. After 16 hours, the cantilever was allowed to dry and used in the AFM experiments.

2.3.5 Adsorption of Suwannee River Humic Acid (SRHA) onto Fe2O3-Coated Silica Spheres

100 $mg \cdot L^{-1}$ of SRHA solution (International Humic Substances Society) was freshly prepared before each experiment. The solution was filtered using Acrodisc 25 mm Syringe Filter with 0.45 μm pore size (PALL Life Sciences). About 20 ml of the solution was added to the Fe_2O_3-coated cantilever in a small gel box. The cantilever was soaked in the solution for at least 16 hours to allow the NOM to adsorb on and equilibrate with the iron oxide. After 16 hours, the cantilever was allowed to dry and used in the AFM experiments.

2.4 Optical Microscopy Experiments

2.4.1 Bacterial Imaging

The two strains of *Pseudomonas aeruginosa* were imaged using an optical microscope (Eclipse E400, Nikon) under FITC wavelengths (Objective Magnification = 100X). Bacterial cells which grown until they reached 0.9 absorbance were centrifuged at 1000 x g for 15 minutes. The supernatant was eluted and replaced with equivalent amount of ultrapure water. 2 ml of the resusbended cells were stained with 400 µl of 0.1 % acridine orange stain. After using the vortexer (Mini Vortexer) (Fisher Scientific) for 10 minutes the solution was poured onto a 0.2 µm filter (MF^{TM}-Membrane Filters) (Millipore). The solution was vacuum filtered (Welch Dry Vacuum Pump, Thomas Industries Inc.). Finally the filter was affixed to a clean glass slide and imaged using the optical microscope. Microscopy images were used to estimate the bacterial sizes. SigmaScan^{TM} version 5.0 was used to measure bacterial length. The average of 80 readings was calculated to determine the diameter of PAO1 bacteria and the average of 190 readings was calculated to determine the diameter of AK1401 bacteria.

2.4.2 Cell Counting

A Spermometer (Zander Spermometer™; Zander Medical Supplies) was used to obtain a calibration curve of number of bacterial cells per ml versus absorbance values in TSB for each strain of bacteria. The counting chamber dimensions are 1mm square with 0.01mm depth. The counting chamber is divided into ten strips vertical and ten strips horizontal, resulting in 100 squares of 0.1mm x 0.1mm each. Bacterial solution for this

experiment was prepared by growing the cells at 37°C until they reached the selected absorbance. Harvested cells were centrifuged at 1360 xg for 10 minutes then washed once in 0.1 M 2-[N-Morpholino]-ethanesulfonic acid (MES) buffer (Sigma). Bacterial solution was then sonicated for 5 minutes, this step was important to get individual cells of bacteria. Finally, around 200 μm from the bacterial solution was put into the chamber and imaged using an optical microscope under FITC wavelengths (Objective Magnification = 60X). For each absorbance 20 images were captured and the Adobe Photoshop Program 6.0 was used in counting the cells in each image.

2.4.3 Gram Staining

A 4-step staining test procedure was used to check whether the bacteria became contaminated and to verify that the bacteria are Gram-negative. Bacteria were applied to a clean glass slide in a manner yielded a thin, uniform smear. The smear was affixed to the slide using heat, by passing the slide through a low flame 2-3 times and leaving the slide to cool to room temperature before staining. Four materials were needed to carry out the test procedure. These materials are; Gram Crystal Violet, Gram Iodine or Stabilized Gram Iodine, Gram Decolorizer and Gram Safranin or Gram Basic Fuchsin. First the fixed smear was flooded with primary stain (Gram Crystal Violet) and stained for 1 minute. The primary stain was then removed by gentle washing with cold tap water. The slide was then flooded with mordant (Gram Iodine or Stabilized Gram Iodine) which retained on the slide for 1 minute. The mordant stain was then removed by gentle washing with cold tap water. Gram Decolorizer was then used to decolorize the slide until solvent running from the slide was colorless (30-60 seconds). The slide was gently

washed with cold tap water. The slide was then flooded with counterstain (either the Gram Safranin or Gram Basic Fuchsin) and stained for 30-60 seconds then the slide was gently washed with cold tap water. Finally, the slide was allowed to air dry and the smear was examined under an oil immersion lens using an optical microscope under FITC wavelengths (Objective Magnification = 100X).

2.5 Atomic Force Microscopy (AFM) Experiments

Experiments were carried out using a Dimension 3100 (AFM) with Nanoscope IIIa controller (Digital Instruments, Santa Barbara, CA).

2.5.1 Spring Constant Measurements

Spring constant measurements of silicon nitride cantilevers with 1 μm silica spheres (PT.GS.SN-type, Novascan Company) were carried out based on the work of Burnham et al. and Emerson and Camesano (13, 24).

2.5.2 Surface Morphology Experiments

Cell cultures were examined to establish cell morphology and interaction forces with the silicon tips. Glass slides, containing immobilized bacteria, were affixed to the AFM stage using a small piece of double-sided carbon tape. Images were captured for each cell found, and five force curves per each cell were recorded. All experiments were done under ultrapure water.

Three kinds of organic materials were used in the AFM experiments; poly (methylacrylic) acid (PMA) which is a simple polymer used to represent the NOM and

two complex natural organic materials; Soil Humic Acid (SHA) and Suwannee River Humic Acid (SRHA). A schematic of the PMA structure is shown in Figure 2.

The three types of NOM were examined using the AFM tapping mode in air with bare silicon probes, in order to understand the differences in their surface characteristics. In all cases, glass slide coated with the NOM, was affixed to the AFM stage and the bare silicon probe was allowed to scan different areas on the slide. AFM images of the three types of NOM were captured with 512 x 512 pixel resolutions.

2.5.3 Interactions Force Measurements

2.5.3.1 Probe Modification with Iron Oxide and NOM

Control experiments were done to study interaction forces between clean glass slides and modified silicon tips, with a manufacturer-reported spring constant of 0.12 N/m. Cleaned glass slides were placed on the AFM stage using a small piece of double-sided carbon tape. The unit was configured for tapping mode in liquid. Force curves were recorded with drive amplitude set to zero (approximating contact mode) for analysis. Experiments were done under 1mM NaCl solution (pH ~6.3) or water.

2.5.3.2 Adhesion Properties of Simple and Complex NOM

Control experiments to study the adhesion properties of simple NOM represented by PMA and complex NOM represented by SHA and SRHA were carried out using AFM tapping mode under ultrapure water. In each experiment the silicon probe was coated with one type of NOM, and the force interactions between the NOM-modified probe and clean glass slide were studied.

2.5.3.3 Interactions between Both Strains of *Pseudomonas aeruginosa* and NOM

Interaction forces between both strains and natural organic matter (NOM) coated silicon tips were examined. Glass slides, containing immobilized bacteria, were affixed to the AFM stage using a small piece of double-sided carbon tape and the NOM-coated tip was allowed to scan the bacterial surface. Images were captured for each cell found, and five force curves per each cell were recorded. All experiments were done under water.

The deflection voltage-separation distance curves obtained from the AFM were converted into force versus separation curves using the method of Ducker and Senden (22). In this method zero points of both cantilever deflection and scanner position were defined such as constant compliance region is aligned with the vertical axes and zero interaction regions at large distances is aligned with the horizontal axes. Deflection row data were converted to force data using Hooke's Law, which describes a linear relationship between force and deflection.

$$F = kx \qquad (11)$$

Where F is the interaction force

k the spring constant of the cantilever

and x is the deflection of the cantilever

Figure 3 shows a typical force curve of AFM tip interaction with polymer brush after determining both the point of zero distance and the range of zero force.

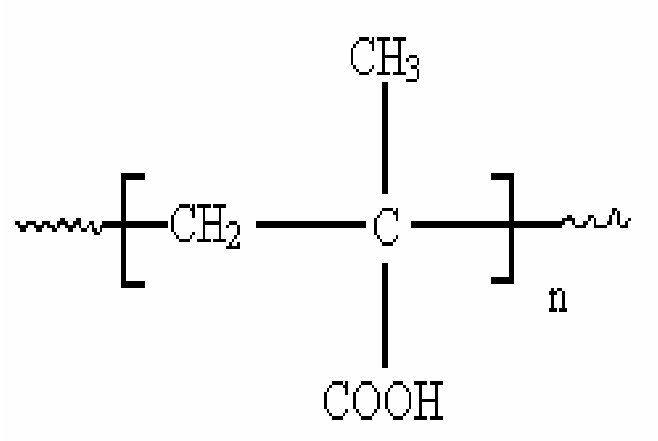

Figure 2. A schematic of the PMA structure showing the carboxylic group, which is the main functional group in humic substances.

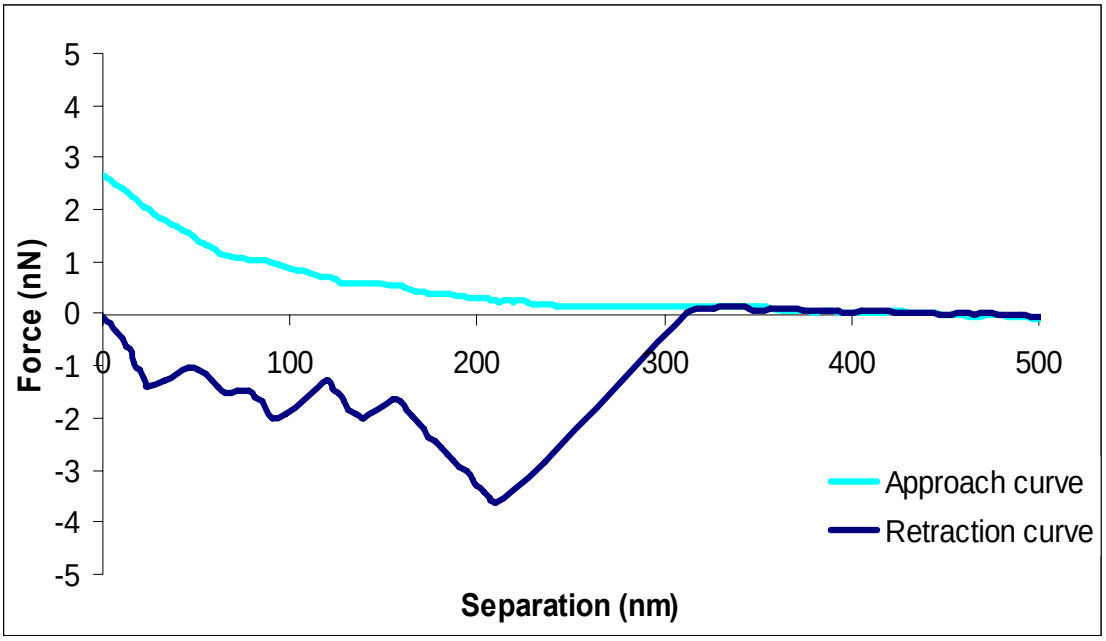

Figure 3. A schematic force curve showing both approach and retraction curves after zeroing.

3 Results

3.1 Microbial growth curve

Figure 4 shows typical growth curves for *Pseudomonas aeruginosa* PAO1 and AK1401. Both strains of *P. aeruginosa* were grown in TSB media at 37°C. Absorbance values were recorded with time. After examining the growth curves an absorbance value of 0.9 was selected as a reference point for all experiments, since it is in the early-mid exponential phase. The doubling time was calculated from the plot of the natural log of absorbance versus time and found to be around 60 minutes for both strains.

3.2 Optical Microscopy Results

3.2.1 Microscopy Images

Figure 5 shows an epifluorescent microscopy image of *Pseudomonas aeruginosa* PAO1 stained with 0.1% acridine orange under FITC wavelengths (Magnification = 100X).

Figure 6 shows an epifluorescent microscopy image of *Pseudomonas aeruginosa* AK1401 stained with 0.1% acridine orange under FITC wavelengths (Magnification = 100X). Microscopy images were used to estimate the size of both strains; for PAO1, the length of 80 bacteria was measured and the average value was 0.95 ± 0.192 μm while for AK1401, the length of 190 bacteria was measured and the average value was 1.12 ± 0.184 μm.

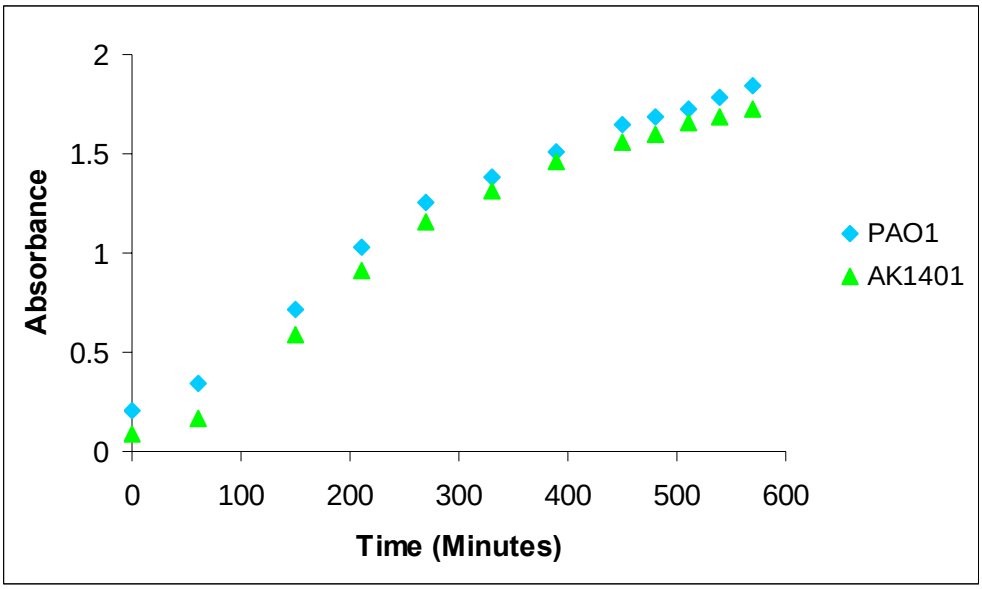

Figure 4. The growth curves of *Pseudomonas aeruginosa* strains, cells were grown in TSB media at 37°C and absorbance values were measured in TSB at 600 nm.

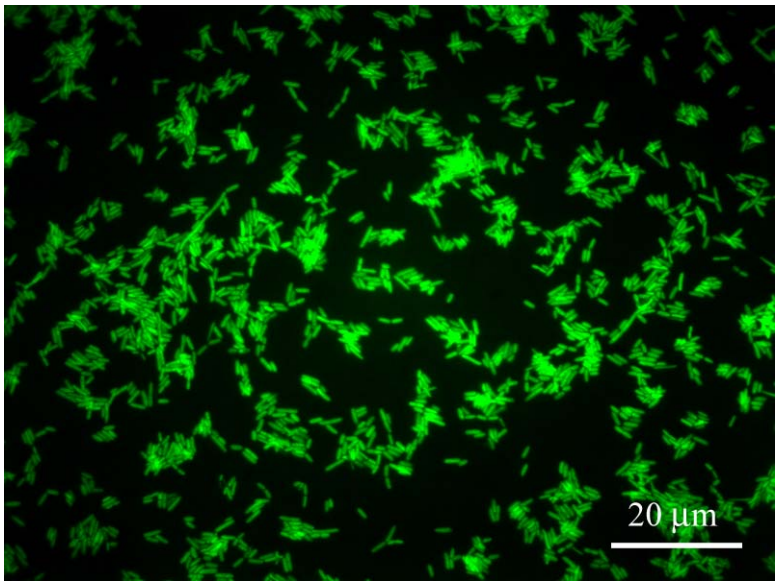

Figure 5. An epifluorescent microscopy image of *Pseudomonas aeruginosa* PAO1 under FITC wavelengths (Magnification = 100X).

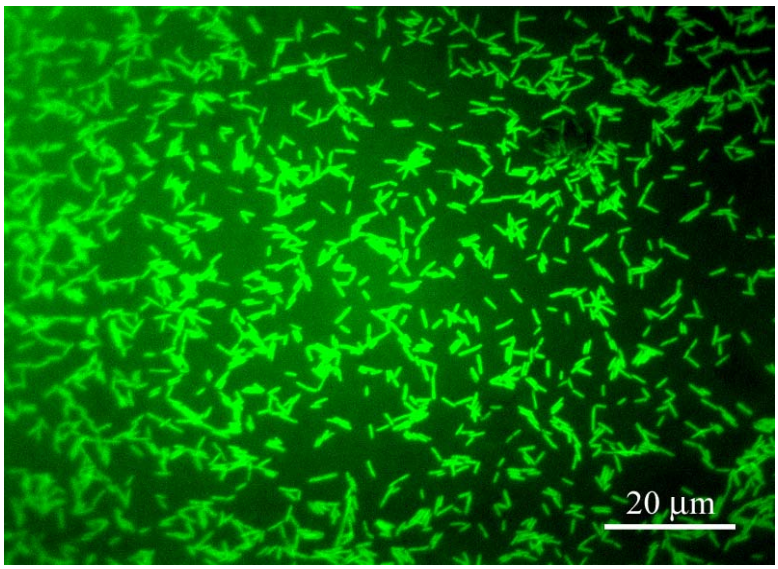

Figure 6. An epifluorescent microscopy image of *Pseudomonas aeruginosa* AK1401 under FITC wavelengths (Magnification = 100X).

3.2.2 Cell Counting

A counting chamber was used to find the number of bacterial cells per ml at different selected absorbance values for both strains of bacteria. Twenty images were captured at each absorbance and the Adobe Photoshop 6.0 program was used to count cells in each image. In order to have confidence in the values, at least 200 cells were counted at each absorbance value. The total number of counted cells was then divided by the number of squares used in counting them in order to find the number of cells per square. Finally, the number of cells per square was divided by the volume of one square to find the number of bacterial cells per ml. The data was used to calibrate the number of cells per ml at particular absorbance values in TSB media. Figure 7 shows a plot of the number of cells per ml for PAO1 strain versus absorbance values in TSB. The number of cells per ml at absorbance 0.9 was found to be 6.91×10^9 cells/ml.

Figure 8 shows a plot of number of cells per ml for AK1401 strain versus absorbance values in TSB. The number of cells per ml at absorbance 0.9 was found to be 8.34×10^9 cells/ml.

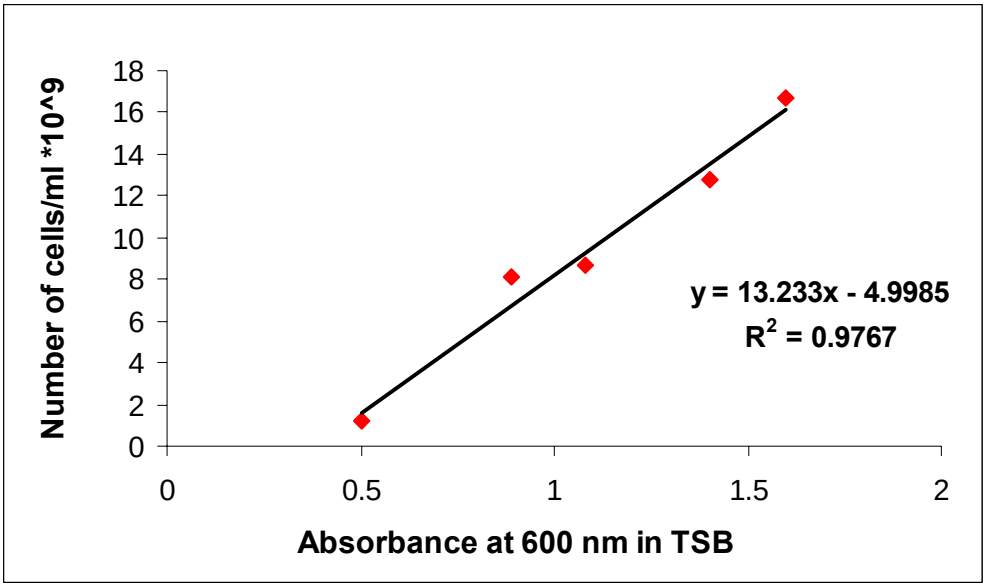

Figure 7. A calibration curve for *Pseudomonas aeruginosa* PAO1 showing the number of cells per ml versus absorbance values at 600 nm in TSB.

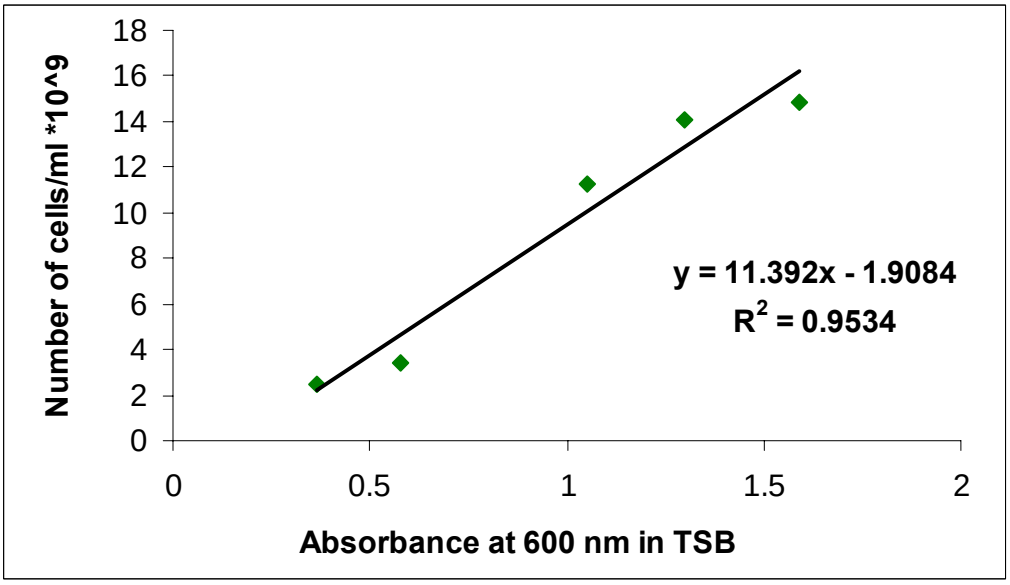

Figure 8. A calibration curve for *Pseudomonas aeruginosa* AK1401 showing the number of cells per ml versus absorbance values at 600 nm in TSB.

3.2.3 Gram Staining

A 4-step staining procedure was used to verify that bacteria were not contaminated and that they were Gram-negative. Slides were imaged using the optical microscope under FITC wavelengths (Magnification = 100X). Images for both strains were clear without any contamination and the color of the bacterial cells was red which confirms that the bacteria are Gram-negative. Figure 9 shows a microscopy image of *Pseudomonas aeruginosa* PAO1 Gram-stained under FITC wavelengths (Magnification = 100X).

Figure 10 shows a microscopy image of *Pseudomonas aeruginosa* AK1401 Gram-stained under FITC wavelengths (Magnification = 100X).

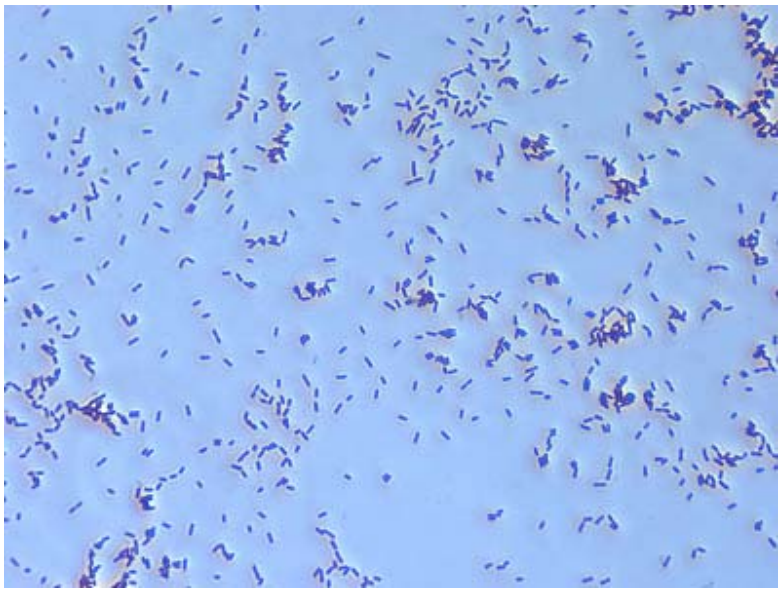

Figure 9. A microscopy image of *Pseudomonas aeruginosa* PAO1 Gram-stained under FITC wavelengths (Magnification = 100X).

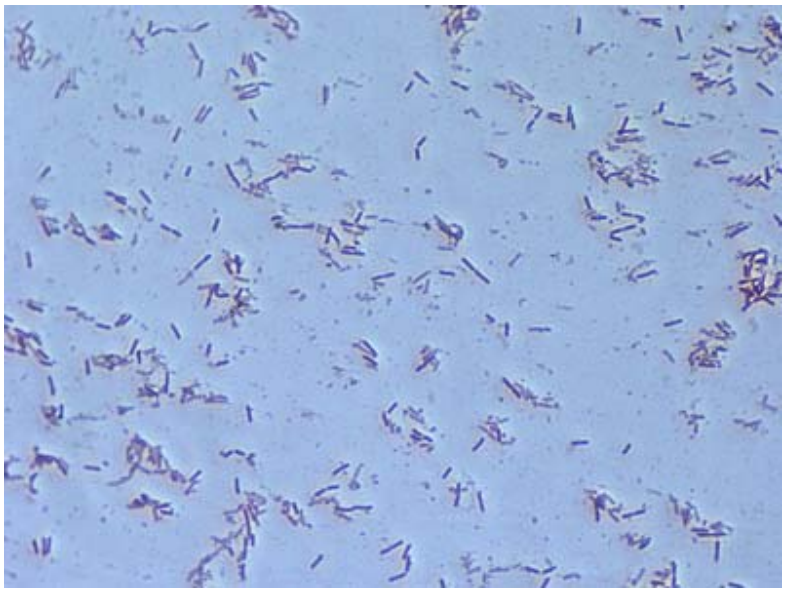

Figure 10. A microscopy image of *Pseudomonas aeruginosa* AK1401 Gram-stained under FITC wavelengths (Magnification = 100X).

3.3 Atomic Force Microscopy Results

3.3.1 Spring constant measurements

Spring constant measurements were carried out using four new silicon nitride cantilevers with 1 μm silica spheres attached. The manufacturer reported spring constant was 0.12 N/m.

Table 3 summarizes the average spring constant value of each experiment. The average spring constant for all measurements was 0.1175 ± 0.049 N/m, which was used in all AFM calculations.

3.3.2 Surface Morphology Results

Both strains of *P. aeruginosa* were imaged in water using tapping mode AFM with unmodified spherical silicon tips. A glass slide, containing immobilized bacteria, was affixed to the AFM stage and the unmodified silicon tip was allowed to scan different areas on the slide. Figure 11 and Figure 12 show AFM images of both strains of *Pseudomonas aeruginosa* captured under ultrapure water with 512 x 512 pixel resolution.

Three types of NOM (PMA, SRHA, and SHA) were imaged in air using tapping mode with bare silicon probes. In all cases, the glass slide coated with NOM was affixed to the AFM stage and the bare silicon probe was allowed to scan different areas on the slide. Figure 13, Figure 14, and Figure 15 show AFM images of the three types of NOM, respectively. The images were captured with 512 x 512 pixel resolution.

Table 3: Spring constant measurements of silicon nitride cantilevers with 1 µm silica spheres.

	Number of readings	Average Value of Spring Constant N/m	Standard Deviation Value
Cantilever # 1	5	0.19	0.021
Cantilever # 2	6	0.085	0.0094
Cantilever # 3	10	0.104	0.011
Cantilever # 4	9	0.091	0.006
Average value of all readings		0.1175	0.049

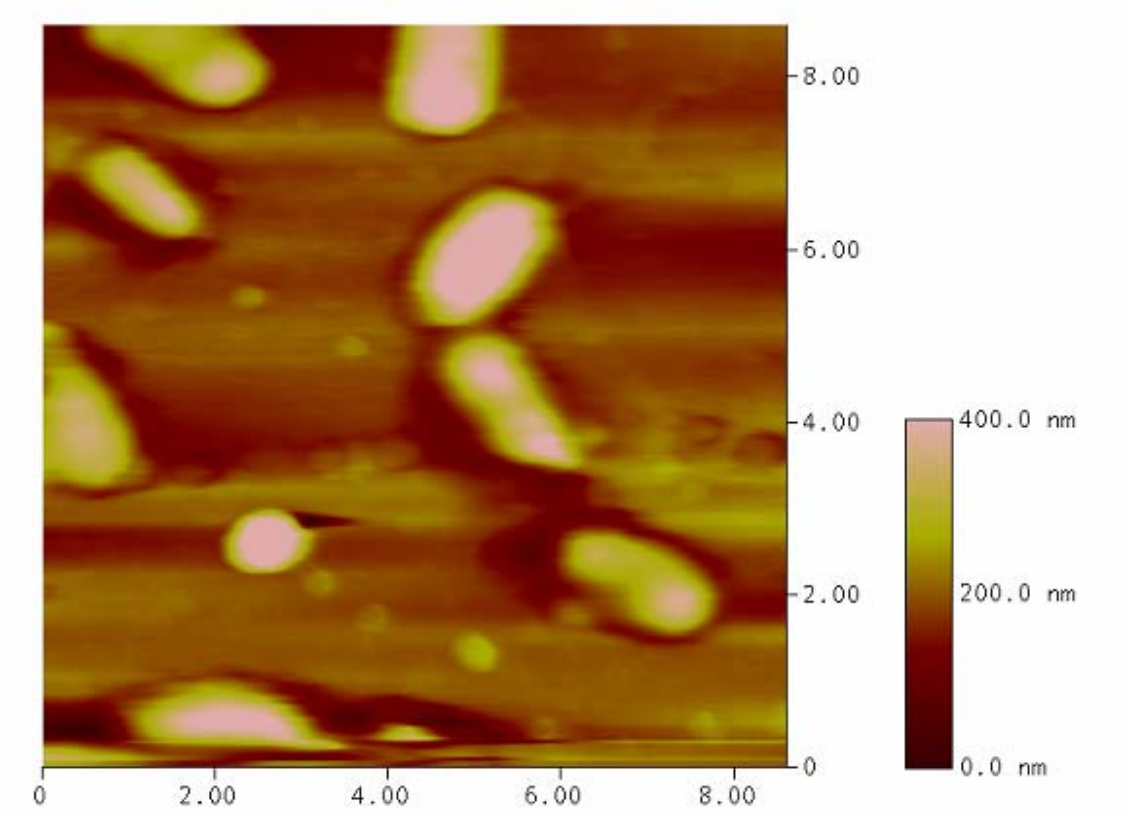

Figure 11. Tapping mode AFM image of *Pseudomonas aeruginosa* PAO1 under ultrapure water with 512 x 512 pixel resolution. x-y scale is in microns.

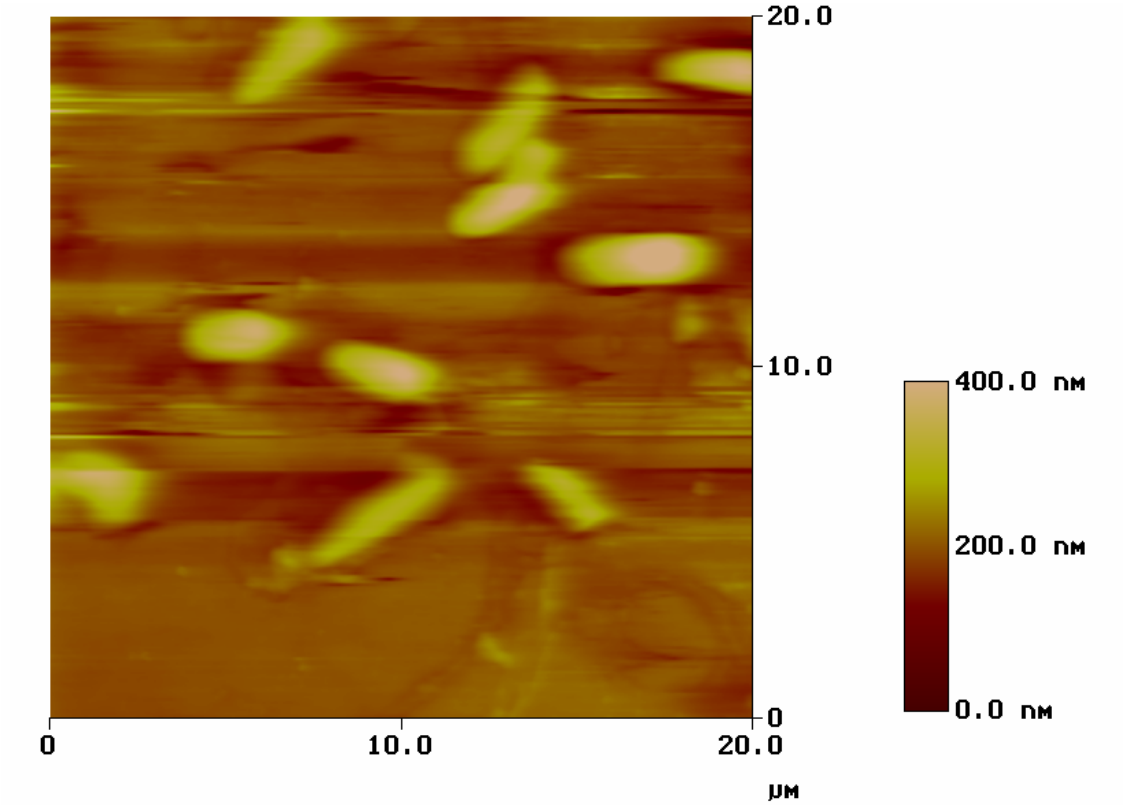

Figure 12. Tapping mode AFM image of *Pseudomonas aeruginosa* Ak1401 under ultrapure water with 512 x 512 pixel resolution. x-y scale is in microns.

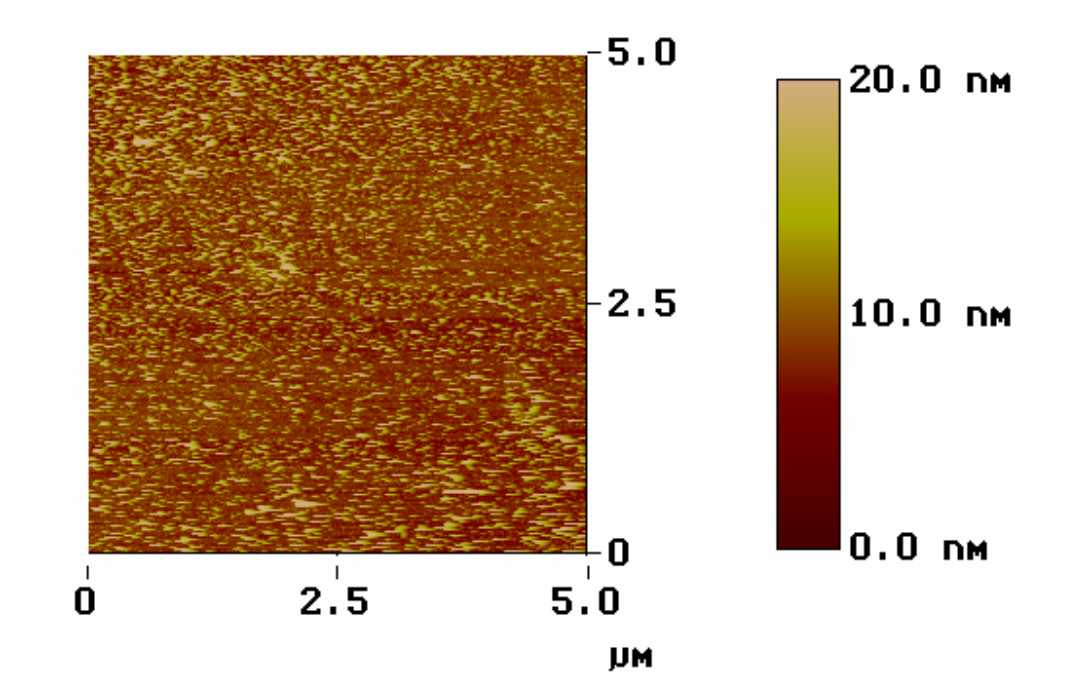

Figure 13. Tapping mode AFM image of PMA in air with 512 x 512 pixel resolution. x-y scale is in microns.

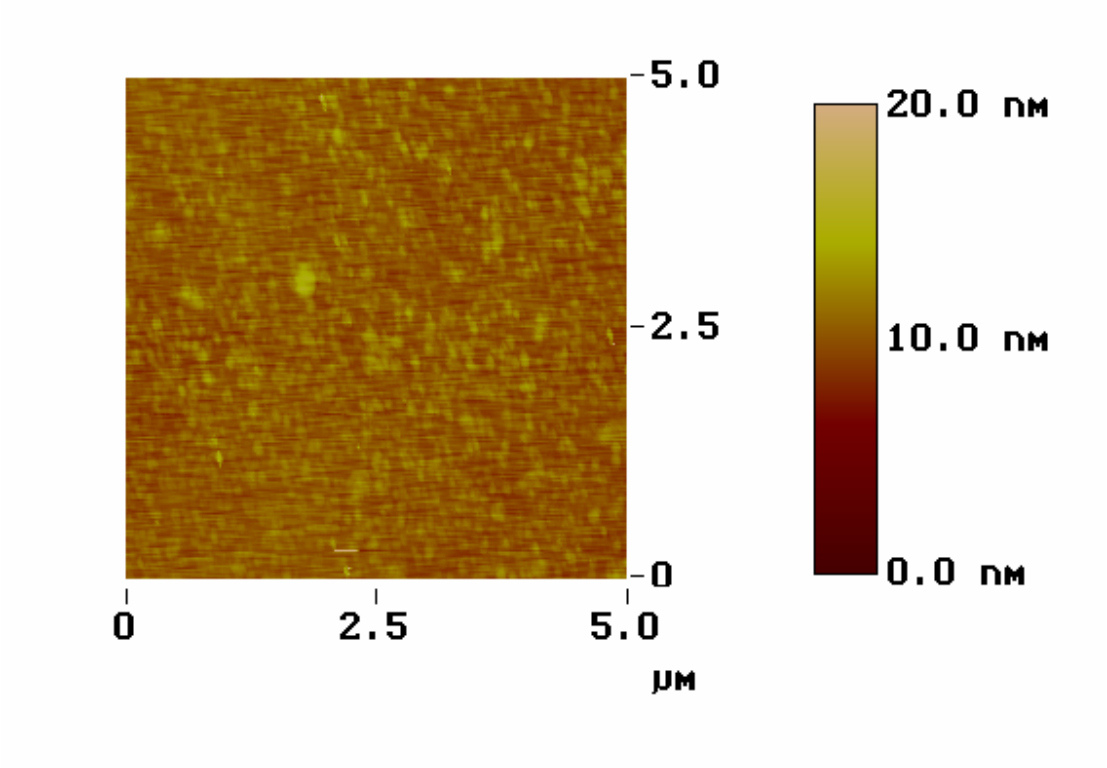

Figure 14. Tapping mode AFM image of SRHA in air with 512 x 512 pixel resolution. x-y scale is in microns.

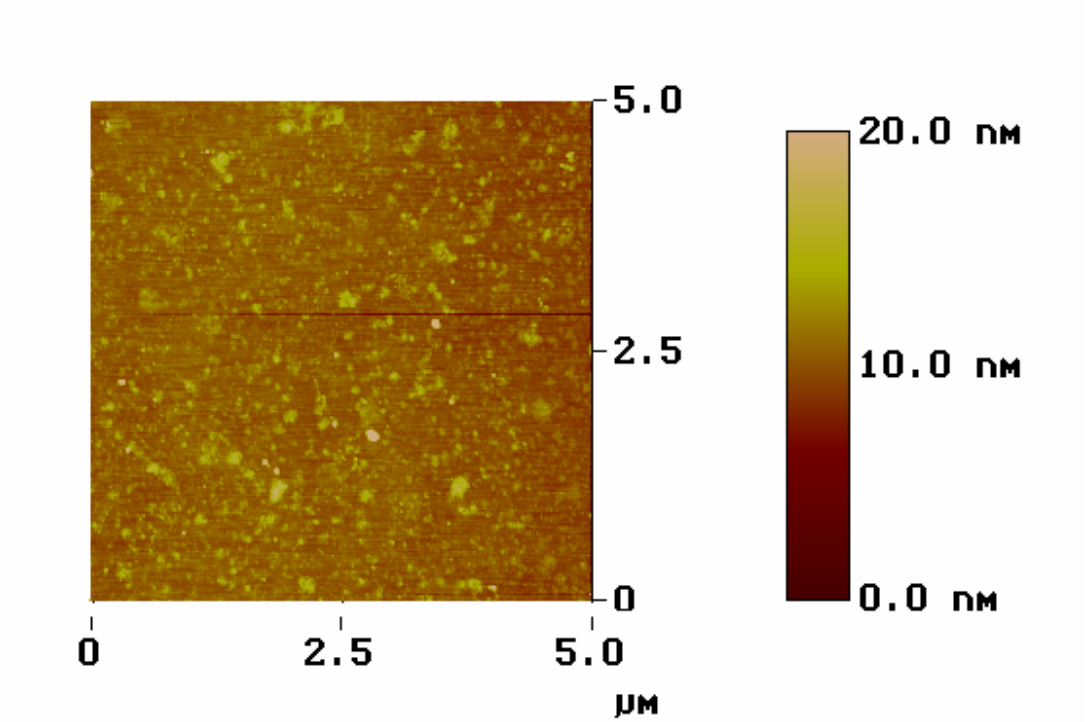

Figure 15. Tapping mode AFM image of SHA in air with 512 x 512 pixel resolution. x-y scale is in microns.

3.3.3 Interaction Force Measurements

3.3.3.1 Probe Modification with Iron Oxide and NOM

Control experiments to verify the successful modification of the silicon probes with iron oxide and natural organic matter were done in three parts using AFM tapping mode under 1 mM NaCl solution, pH = 6.3. In the first part, the interactions between a bare silicon probe and a clean glass slide were studied and the approach force-distance curves were analyzed using MATLAB 7.0.1 (1) . The approach curves of the force cycle illustrate the cantilevers interactions with the surface of the sample, from no interactions at large distances to maximum interaction at probe-surface contact. A positive value of the force indicates a repulsive interaction and a negative value of the force indicates an attractive interaction. Figure 16 shows the approach interaction curves between a bare silicon probe and clean glass slide. The interactions are purely repulsive; they start at 80 nm from the glass surface and reach a maximum repulsive force of 5.84 ± 0.18 nN at zero separation distance.

As the next step, the silicon probe was coated with a layer of iron oxide and the interactions between the iron oxide coated probe and clean glass slide were studied. Figure 17 shows the approach interaction curves of the iron oxide coated probe and clean glass slide. The interactions are purely repulsive; they start at 80 nm from the glass slide surface and reach a maximum repulsive force of 1.75 ± 0.05 nN at zero separation distance.

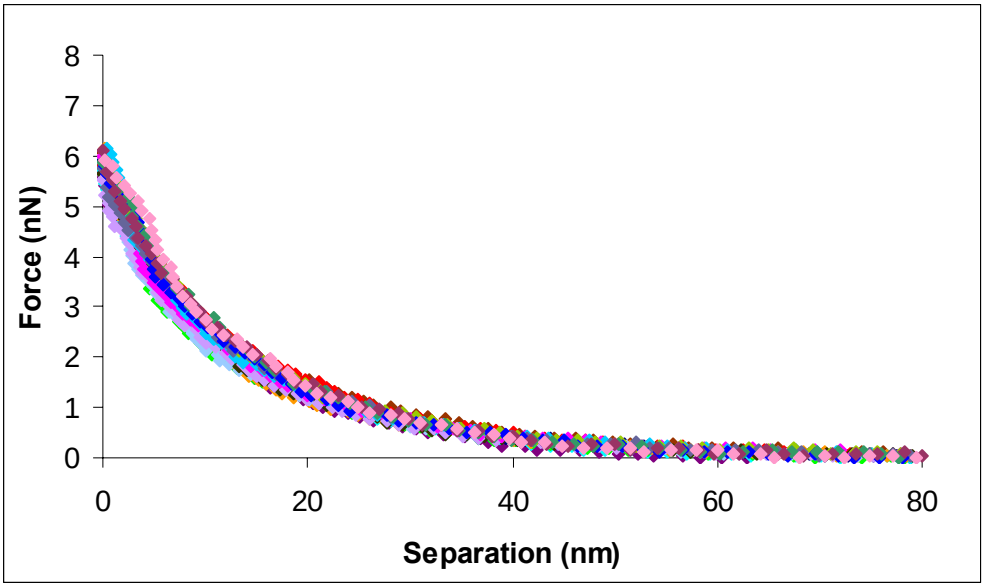

Figure 16. Approach curves for measurements between bare silicon probe and clean glass slide under 1mM NaCl solution, pH = 6.3. Each set of three curves was recorded from a single area of a cleaned glass slide, with five areas examined on each of three slides. The interactions begin at 80 nm and they reach a repulsive force of 5.84 ± 0.18 nN at zero separation distance.

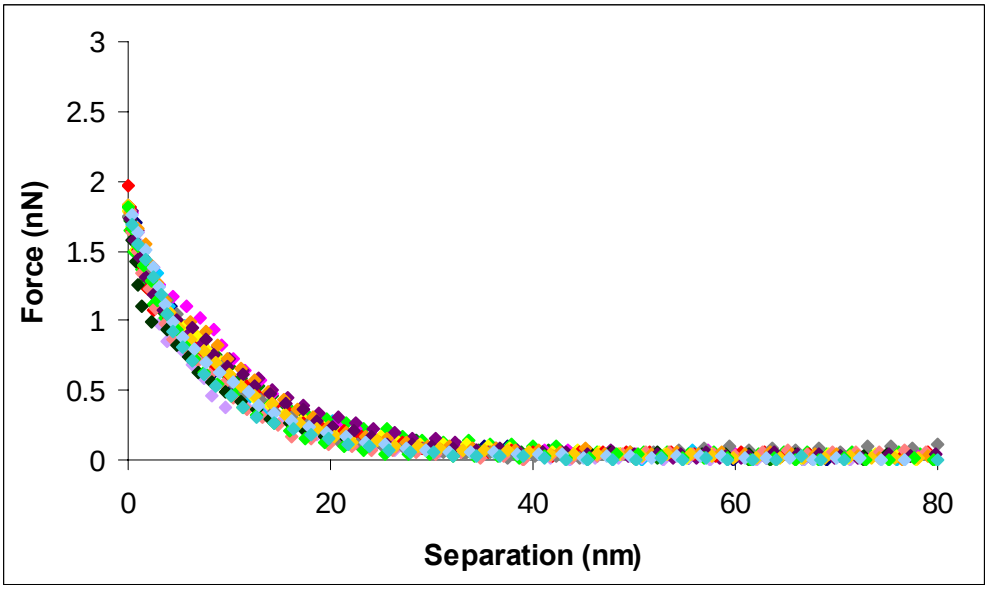

Figure 17. Approach interactions curves between iron oxide coated probe and clean glass slide under 1mM NaCl solution, pH = 6.3. Each set of three curves was recorded from a single area of a cleaned glass slide, with five areas examined on each of three slides. The interactions begin at 80 nm and they reach a repulsive force of 1.75 ± 0.05 nN at zero separation distance.

In the third step, the same probe which was previously modified with iron oxide was further modified with PMA. The interactions between the PMA-coated probe and clean glass slide were studied and the results of the approach curves of these interactions are shown in Figure 18. The interactions are purely repulsive; they start at 80 nm from the glass surface and reach a maximum repulsive force of 2.66 ± 0.20 nN at zero separation distance.

3.3.3.2 Adhesion Properties of Simple and Complex NOM

Control experiments to study the adhesion properties of simple NOM represented by PMA and complex NOM represented by SHA and SRHA were carried out using AFM tapping mode under ultrapure water. In each experiment the silicon probe was coated with one type of NOM, and the force interactions between the NOM-modified probe and the clean glass slide were studied. Retraction curves of the force cycle were analyzed and the resulting adhesion peaks were summed and plotted in histograms. The retraction curves of the force cycle represent the forces as the cantilever is being pulled away from the cell surface. The distance and force at which the pull-off event occurs are defined as the pull-off distance and the pull-off force. The pull-off distances and forces of the retraction peaks were collected and represented in histograms. The histograms are based on the normalized number of instances which occur in a certain force range and the normalized number of instances which occur in a certain distance range. For the three types of NOM the pull-off event took place at zero separation or at very short separation distances and so no pull-off distance histogram can be prepared. Figure 19 shows a

typical retraction curve of NOM-modified probe interacting with clean a glass slide. The histogram showing the results of the interactions between the three types of NOM and clean glass slide under ultrapure water is shown in Figure 20.

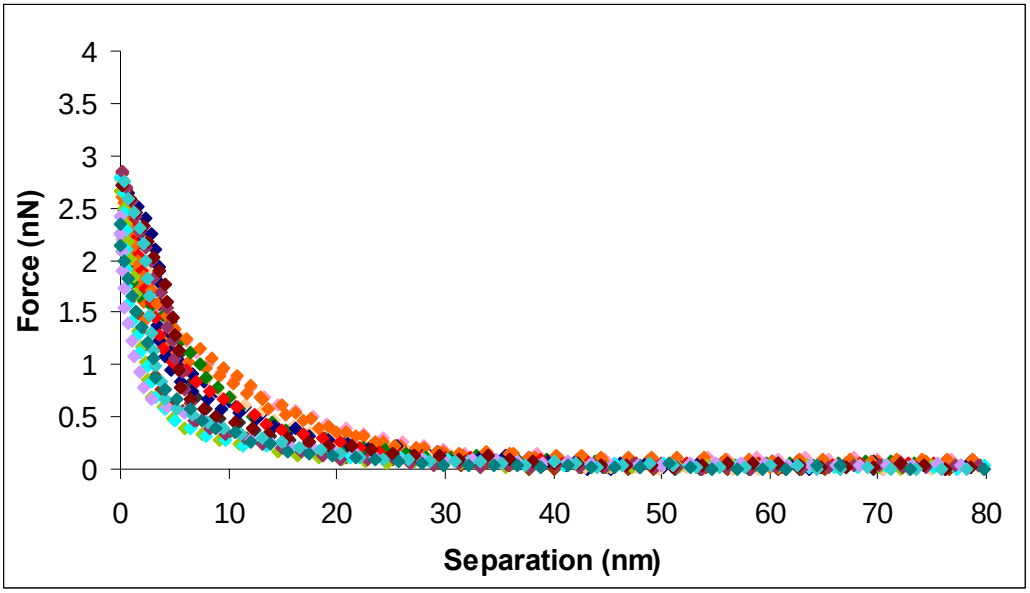

Figure 18. Approach curves showing interactions between PMA-coated probe and clean glass slide under 1mM NaCl solution, pH = 6.3. Each set of three curves was recorded from a single area of a cleaned glass slide, with five areas examined on each of three slides. The interactions begin at 80 nm and they reach a repulsive force of 2.66 ± 0.20 nN at zero separation distance.

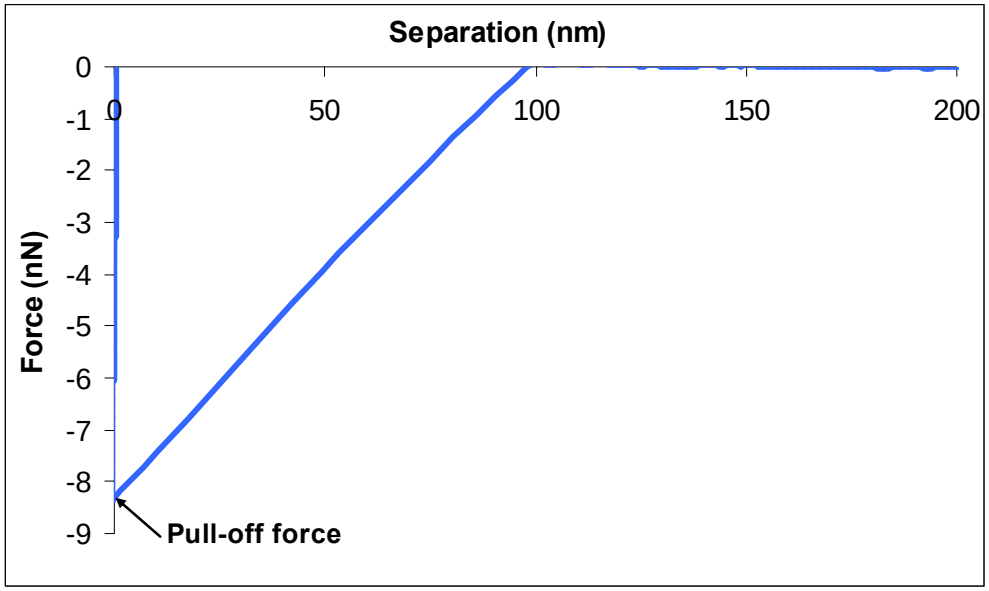

Figure 19. Typical retraction curve of SRHA-modified probe interacting with a clean glass slide under ultrapure water. In the curve there is only one peak which occurs at zero separation.

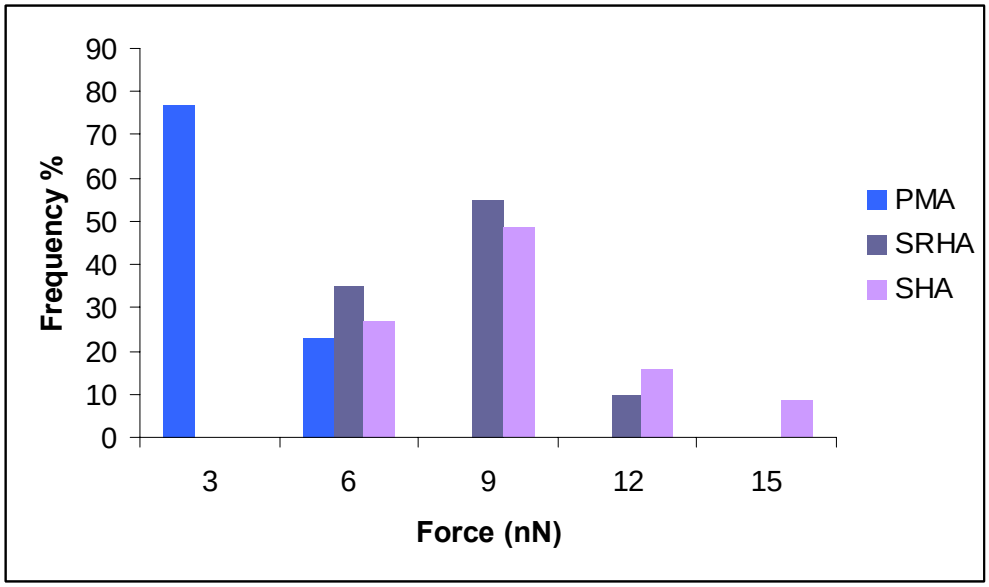

Figure 20. Normalized number of events occurring in a certain force range. The force ranges represent the ranges of adhesive pull-off forces exerted by three NOM-modified probes on clean glass slide surface. Each color in the graph refers to certain probe modification.

3.3.3.3 *Pseudomonas aeruginosa* PAO1

Measurements of the forces between *Pseudomonas aeruginosa* PAO1 and both unmodified and NOM-modified silicon probes were made in ultrapure water. Three types of natural organic compounds were used; PMA to represent a simple NOM with a known molecular weight and both SHA and SRHA to represent more complex NOM with unknown and distributed molecular weights. Fifty force curves on five individual cells of *Pseudomonas aeruginosa* PAO1 were captured in each experiment, analyzed using MATLAB® 7.0.1, and plotted using Microsoft Excel 2003.

3.3.3.3.1 Approach Curves

All the experiments with *Pseudomonas aeruginosa* PAO1 showed repulsive forces during the approach of the probe to the cell surface. Since force curves were captured at different ramp sizes, it was not possible to average them together. Instead, they were considered individually. However, it was possible to put individual force curves from five different cells on one graph showing the similarity among data sets. Figure 21 shows an example of the reproducibility of the approach curves for *Pseudomonas aeruginosa* PAO1 interacting with SHA-modified silicon probe under ultrapure water.

In order to compare the results of *Pseudomonas aeruginosa* PAO1 interacting with different modified probes, an average value of the force at zero distance and an average value of the decay distance at zero force were calculated from fifty individual force curves. A summary of the average decay length values and the average values of

the force at zero distance for all *Pseudomonas aeruginosa* PAO1 experiments is shown in Table 4.

3.3.3.3.2 Retraction Curves

During the pull-off process it is possible that some polymers from the bacterium attach to the probe through physical bonds, and their detachment from the probe eventually occurs as the tip is further retracted. Also, bacterial polymers can interact with the NOM molecules when modified tips were used. Each pull-off event will cause a single peak or multiple peaks in the retraction curve, depending on whether the studied surface has one polymer or multiple polymers, and on the number of contact points between the polymer and the probe. Figure 22 shows a representative retraction curve of *Pseudomonas aeruginosa* PAO1 interacting with the NOM-modified probe.

Figure 23 and Figure 24 show summaries of the distributions of force and distance, for *Pseudomonas aeruginosa* PAO1 interacting with different probes under ultrapure water.

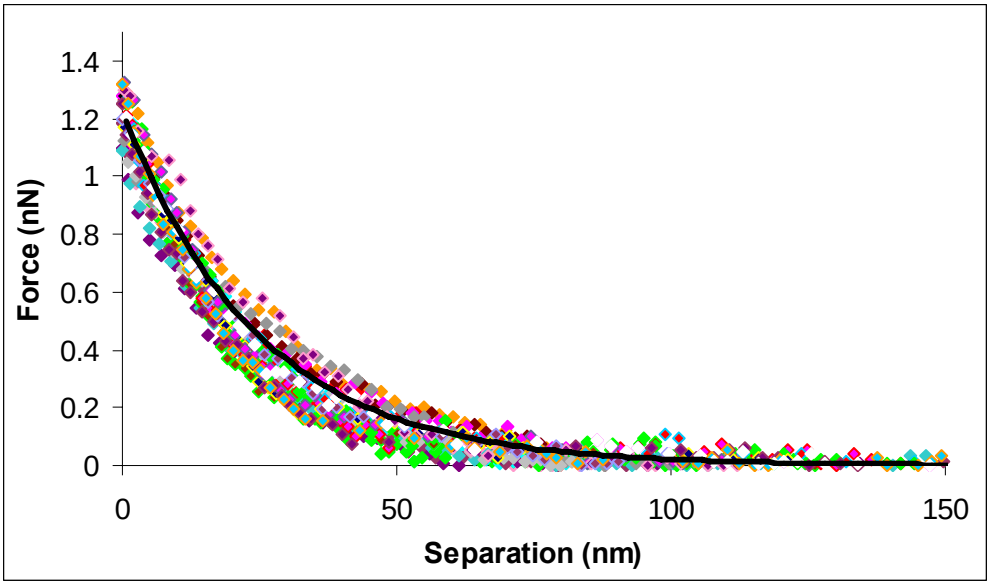

Figure 21. Representative example of 15 approach curves of *Pseudomonas aeruginosa* PAO1 interacting with SHA-modified probe under ultrapure water. The dotted curves represent the experimental data and the black solid line represents the average steric interactions fit. Five different bacterial cells were examined; with a set of three curves recorded from each individual bacterial cell. The interactions begin at 90 nm and they reach an approximate repulsive force of 1.2 nN at zero separation distance.

Table 4: A summary of decay length values and force at zero distance values for *Pseudomonas aeruginosa* PAO1 interacting with different modified probes under ultrapure water.

Probe Modification	Average Decay Length (nm) (n = 50)	Average Force at Zero Distance (nN) (n = 50)
Unmodified	286	2.27
PMA-modified	159	2.44
SRHA-modified	124	1.43
SHA-modified	84	1.21

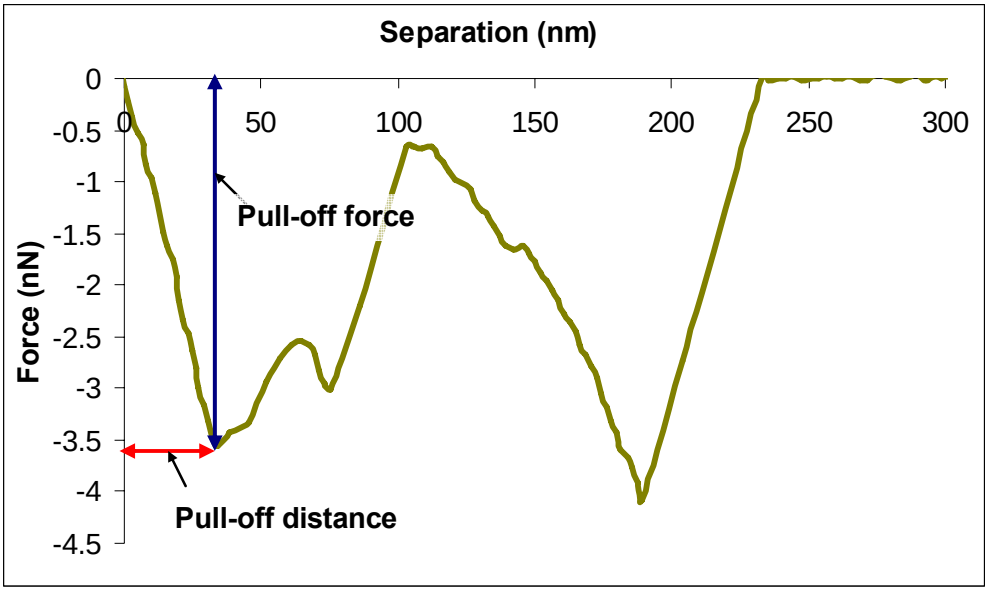

Figure 22. Typical retraction curve for interactions of *Pseudomonas aeruginosa* PAO1 with NOM-modified probe. The curve has multiple peaks, with the length of the blue line representing the magnitude of the first adhesive force, and the length of the red line representing the distance at which the first adhesive event occurs.

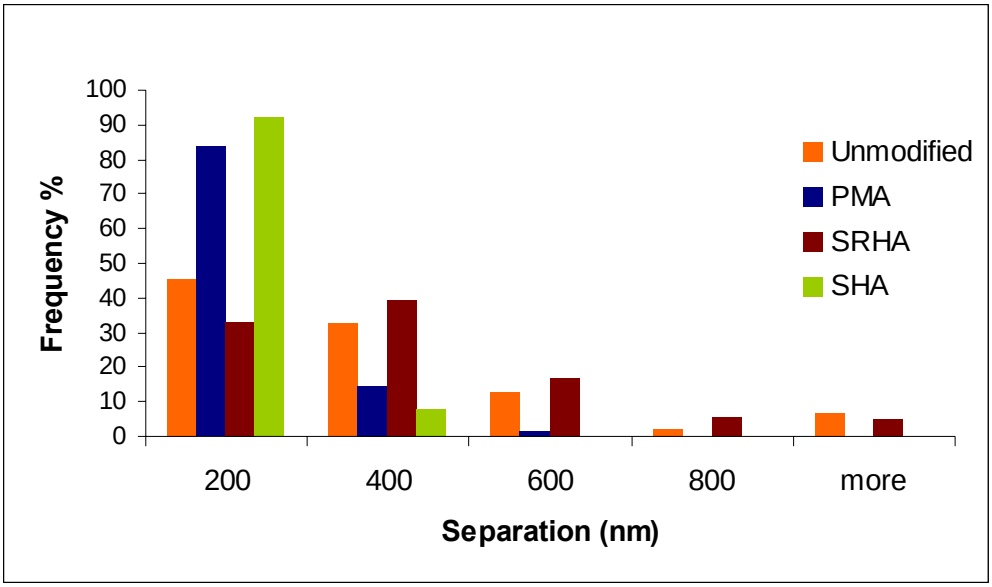

Figure 23. Normalized number of events occurring in a certain distance range. The distance ranges represent the ranges of break-off distances between *Pseudomonas aeruginosa* PAO1 and four different modified probes. Each color in the graph refers to certain probe modification.

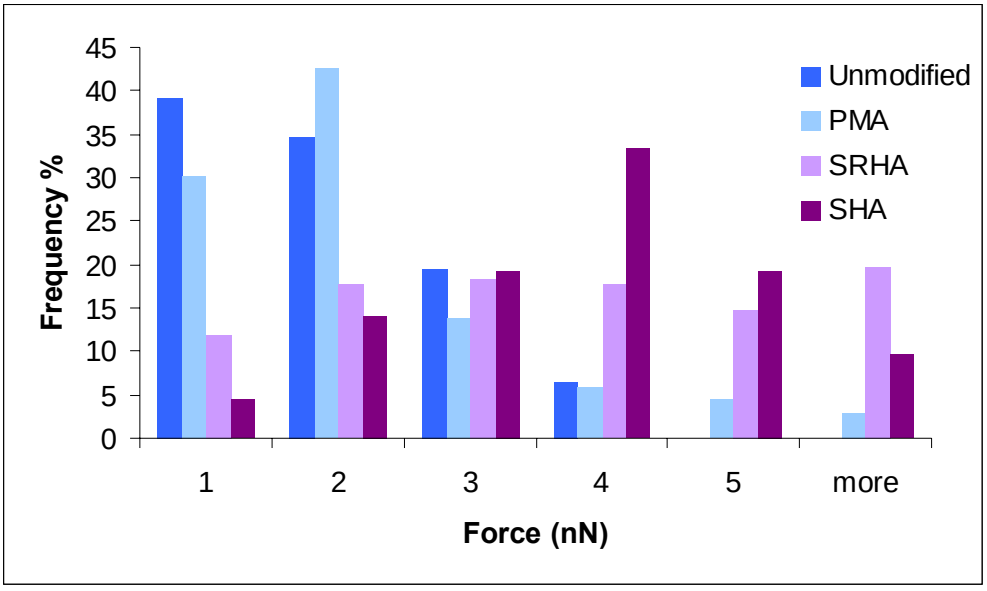

Figure 24. Normalized number of events occurring in a certain force range. The force ranges represent the ranges of adhesive pull-off forces exerted by four different modified probes on *Pseudomonas aeruginosa* PAO1 surface. Each color in the graph refers to certain probe modification.

3.3.3.3.3 Modeling of Steric Interactions

The model describing steric interactions was developed by Alexander (9) and de Gennes (20) for the interactions between two equal parallel surfaces with grafted or adsorbed polymers at relatively high surface coverage. The model was modified by Butt et al. (14) for the interactions between a spherical surface and a flat surface. We fit the experimental data for the approach of various probes to *Pseudomonas aeruginosa* PAO1 with the steric model. For the unmodified probe, we used the steric model corresponding to the case where only one surface is coated with a polymer brush.

An example of fitting the steric interaction model for a brush on one surface is shown with a typical approach curve of *Pseudomonas aeruginosa* PAO1. The polymer grafting density and equilibrium polymer length are the fitting parameters, as shown in Figure 25.

For the case of *P. aeruginosa* interacting with NOM-modified probes, we used a form of the steric model that was developed for two surfaces coated with (equal) polymer brushes. Figure 26 shows an example of this fitting for a typical approach curve of *Pseudomonas aeruginosa* PAO1, with the polymer grafting density and equilibrium polymer length as fitting parameters. The fitting parameters calculated from applying the steric model to the individual force curves in each experiment were averaged and used to generate the average theoretical steric interaction curve as shown in Figure 21. Thirty force curves captured on five different cells were used to calculate the fitting parameters in each experiment. Figure 27 shows four individual approach force-separation curves to represent *Pseudomonas aeruginosa* PAO1 interacting with different modified probes and

their theoretical steric interaction model fits. The fitted parameters values and the values of the force at zero separation are summarized in Table 5.

Figure 28 and Figure 29 show a comparison between the steric model parameters and the experimental values for *Pseudomonas aeruginosa* PAO1 interacting with different modified probes.

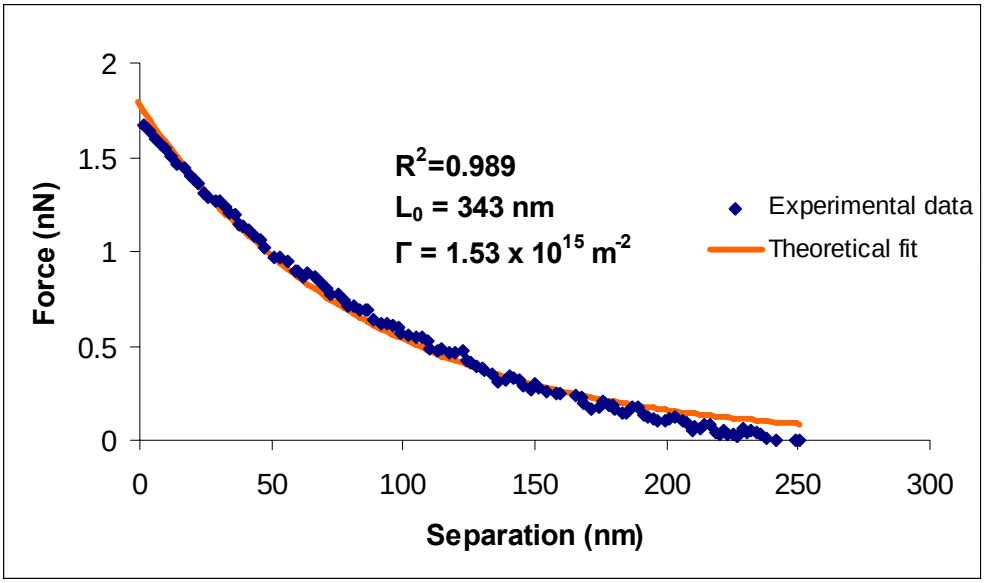

Figure 25. Using the steric interactions model for one surface bearing polymer brushes to fit one approach curve from the experimental data of *Pseudomonas aeruginosa* PAO1 interactions with unmodified probe under ultrapure water. The solid line represents the theoretical steric interactions fit and the dotted line represents the experimental curve.

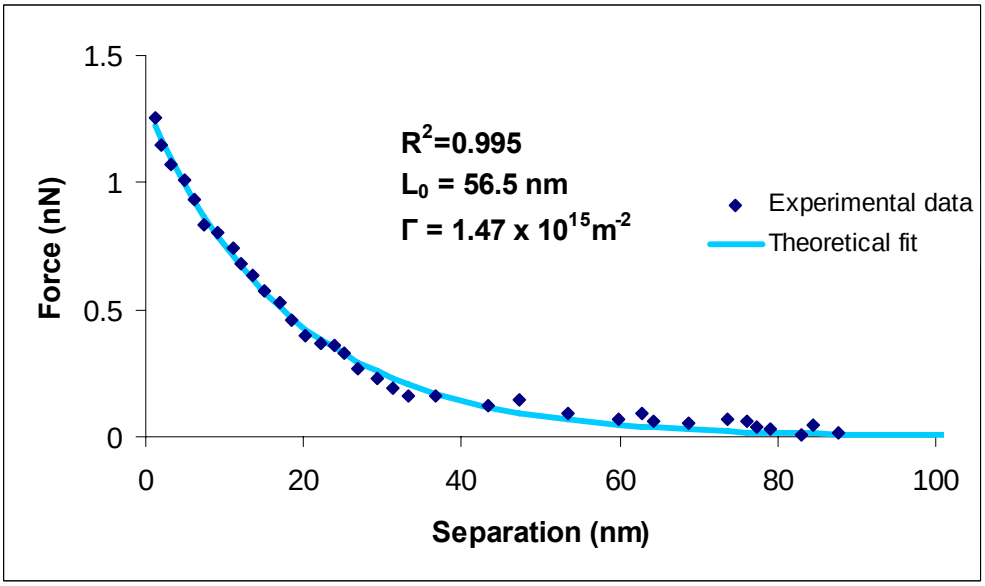

Figure 26. Using the steric interactions model for two surfaces bearing polymer brushes to fit one approach curve from the experimental data of *Pseudomonas aeruginosa* PAO1 interactions with NOM-modified probe under ultrapure water. The solid line represents the theoretical steric interactions fit and the dotted line represents the experimental curve.

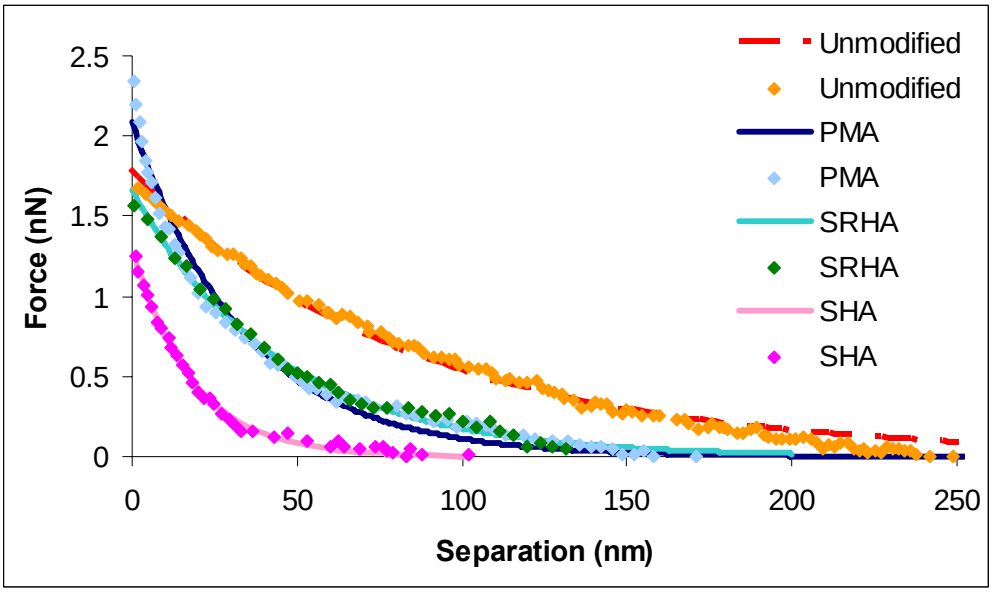

Figure 27. The theoretical steric interaction model fits and the experimental data of *Pseudomonas aeruginosa* PAO1 interacting with different modified probes. The dotted curves represent the experimental data. Each curve in the graph represents the fitting of one force curve captured on one *Pseudomonas aeruginosa* PAO1 cell. The dashed curve was generated using the steric interaction model for one surface coated with polymer brushes and the solid curves were generated using the steric interaction model for two surfaces coated with polymer brushes.

Table 5: A summary of equilibrium polymer length values, polymer grafted density values, and values of the force at zero separation from the theoretical steric interactions fits of *Pseudomonas aeruginosa* PAO1 interactions with different modified probes under ultrapure water.

Probe Modification	Average Equilibrium Polymer Length (L_0) (nm) (n = 30)	Average Polymer Grafting Density (γ) (m^{-2}) (n = 30)	Average Force at Zero Distance (nN) (n = 30)
Unmodified	358	1.61×10^{15}	2.38
PMA-modified	164	1.10×10^{15}	2.50
SRHA-modified	124	9.36×10^{14}	1.46
SHA-modified	88	1.10×10^{15}	1.32

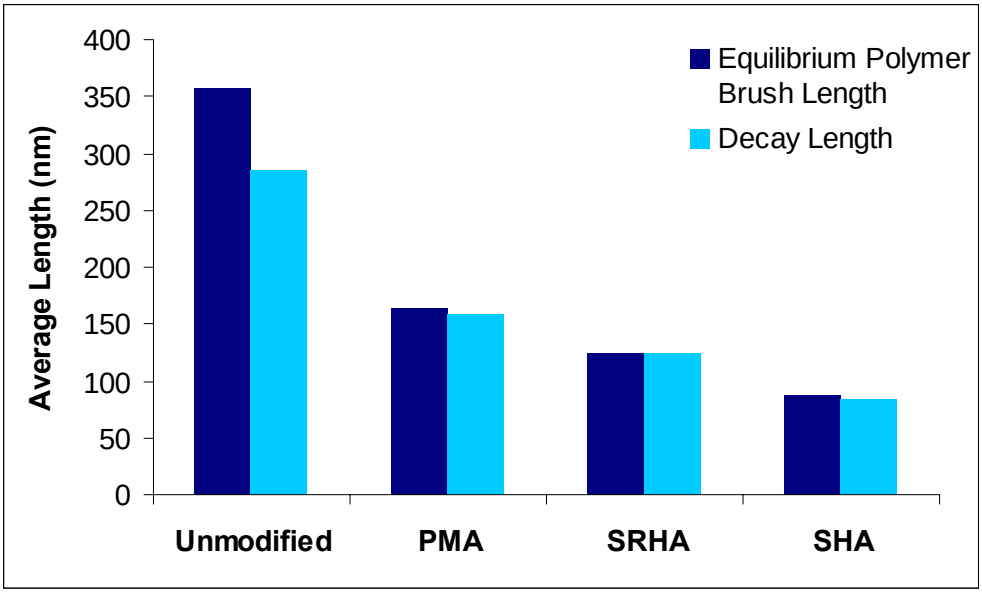

Figure 28. A comparison between average values of decay lengths and average values of equilibrium polymer brush lengths from all experiments of *Pseudomonas aeruginosa* PAO1 interacting with various probes.

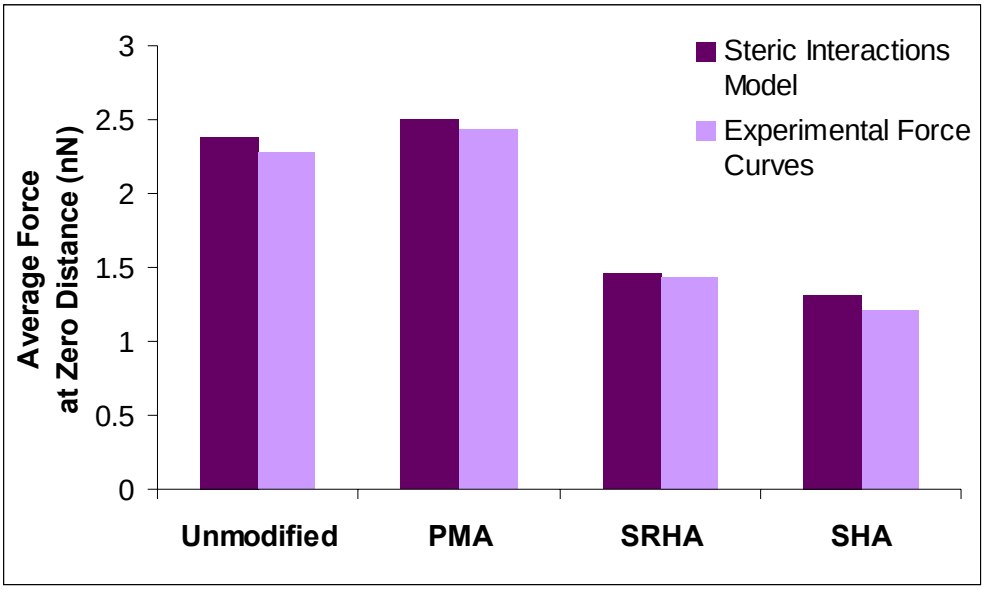

Figure 29. A comparison between average values of forces at zero distance from the experimental force curves and the steric interactions fits of *Pseudomonas aeruginosa* PAO1 interacting with various probes.

3.3.3.4 *Pseudomonas aeruginosa* AK1401

The adhesion interactions between *Pseudomonas aeruginosa* AK1401 and modified probes were studied with AFM under ultrapure water. Four experiments were done using *Pseudomonas aeruginosa* AK1401. In each experiment, fifty force curves were captured and analyzed, corresponding to five different cells of *Pseudomonas aeruginosa* AK1401.

3.3.3.4.1 Approach Curves

All the experiments done on *Pseudomonas aeruginosa* AK1401 showed repulsive forces during the approach of the probe to the cell surface. Force curves for each experiment were considered individually and in order to show their reproducibility they were put together on one plot. Figure 30 shows an example of the reproducibility of the approach curve for *Pseudomonas aeruginosa* AK1401 interacting with the SHA-modified silicon probe under ultrapure water. Averaging the individual force curves was not possible because they were captured at different ramp sizes. Instead an average value of the force at zero distance and an average value of the decay distance at zero force were each calculated from fifty individual force curves. Table 6 shows a summary of the average decay length values and the average values of the force at zero separation for all *Pseudomonas aeruginosa* AK1401 experiments with different modified probes.

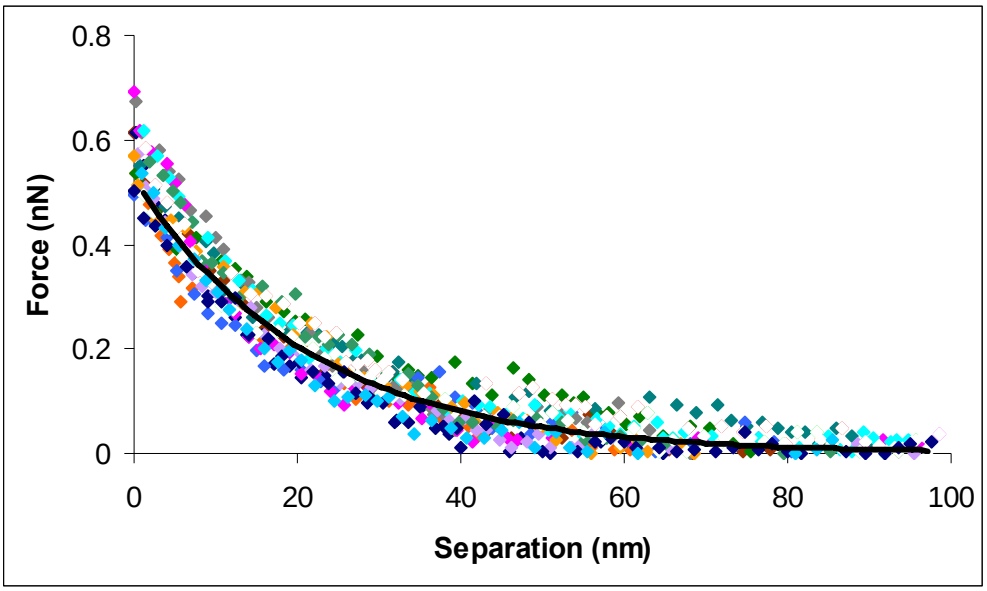

Figure 30. Representative example of 15 approach curves of *Pseudomonas aeruginosa* AK1401 interacting with SHA-modified probe under ultrapure water. The dotted curves represent the experimental data and the black solid line represents the average steric interactions fit. Five different bacterial cells were examined; with a set of three curves recorded from each individual bacterial cell. The interactions begin at 60 nm and they reach an approximate repulsive force of 0.6 nN at zero separation distance.

Table 6. A summary of decay length values and force at zero distance values from *Pseudomonas aeruginosa* AK1401 interacting with different modified probes under ultrapure water.

Probe Modification	Average Decay Length (nm) (n = 50)	Average Force at Zero Distance (nN) (n = 50)
Unmodified	156	0.89
PMA-modified	149	1.98
SRHA-modified	62	0.71
SHA-modified	56	0.57

3.3.3.4.2 Retraction Curves

The retraction curves of *Pseudomonas aeruginosa* AK1401 were analyzed using MATLAB 7.0.1, and presented in histograms based on the separation and force values of the retraction peaks. Figure 31 shows a typical retraction curve for *Pseudomonas aeruginosa* AK1401 interacting with NOM-modified probe. The results from the retraction curves for *Pseudomonas aeruginosa* AK1401 interacting with four different modified probes are summarized in Figure 32 and Figure 33.

3.3.3.4.3 Modeling of Steric Interactions

The modified steric interactions model for the interactions between a spherical surface and a flat surface with grafted or adsorbed polymers at relatively high surface coverage was used to fit the experimental approach curves of *Pseudomonas aeruginosa* AK1401interactions with different modified probes. The steric interactions equation with one surface only being coated with polymer brushes was used to fit the interactions between *Pseudomonas aeruginosa* AK1401 and unmodified probe. An example of fitting the steric interactions equation with one polymer surface to a single approach curve of *Pseudomonas aeruginosa* AK1401 with the polymer grafting density and equilibrium polymer length being the fitting parameters is shown in Figure 34. While the steric interactions equation for two equal polymer brushes coated-surfaces was used to fit *Pseudomonas aeruginosa* AK1401 interactions with NOM-modified probes. Figure 35 shows an example of fitting the steric interactions equation for two equal polymer brushes-coated surfaces to a single approach curve of *Pseudomonas aeruginosa* AK1401 with the polymer grafting density and equilibrium polymer length being the fitting

parameters. The fitting parameters values collected from fitting the steric interactions equation to the individual force curves in each experiment were averaged and used to generate an average theoretical steric interactions curve as shown in Figure 30. Fifty force curves captured on five different cells were analyzed in each experiment. Four approach force-separation curves of *Pseudomonas aeruginosa* AK1401 interacting with different modified probes and their theoretical steric interactions model fits are shown in Figure 36. The fitting parameters values with values of the force at zero separation from the theoretical fits of *Pseudomonas aeruginosa* AK1401 interacting with different modified probes are summarized in Table 7.

Figure 37 and Figure 38 show a comparison between the average values of the equilibrium polymer brush lengths and forces at zero distance calculated from the steric interactions fits and the average values of decay lengths and forces at zero distance from the experimental force curves of *Pseudomonas aeruginosa* AK1401 interacting with different modified probes.

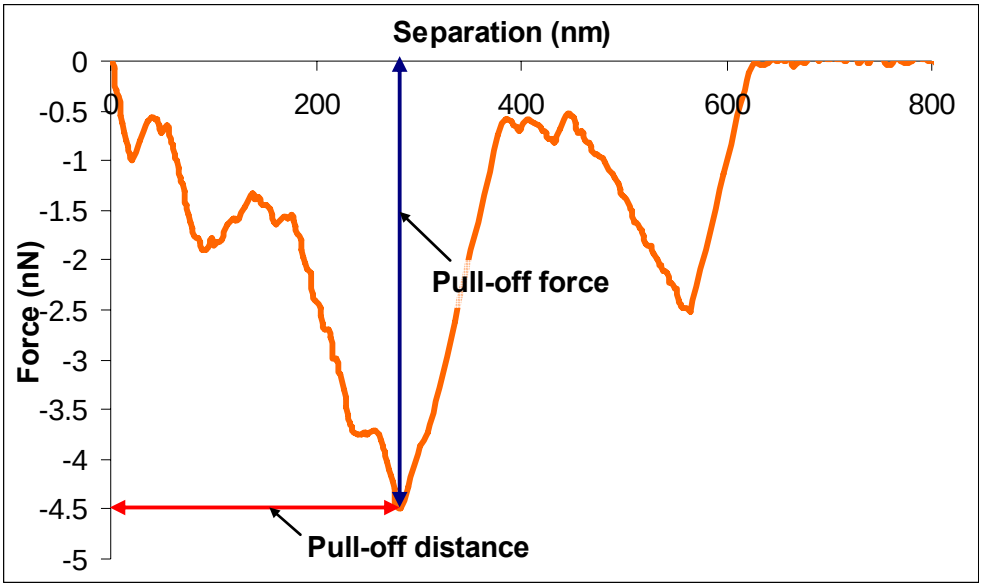

Figure 31. Typical retraction curve of *Pseudomonas aeruginosa* AK1401 interacting with an unmodified probe. The curve has multiple peaks, with the length of the blue line representing the magnitude of the third adhesive force, and the length of the red line representing the distance at which the third adhesive event occurs.

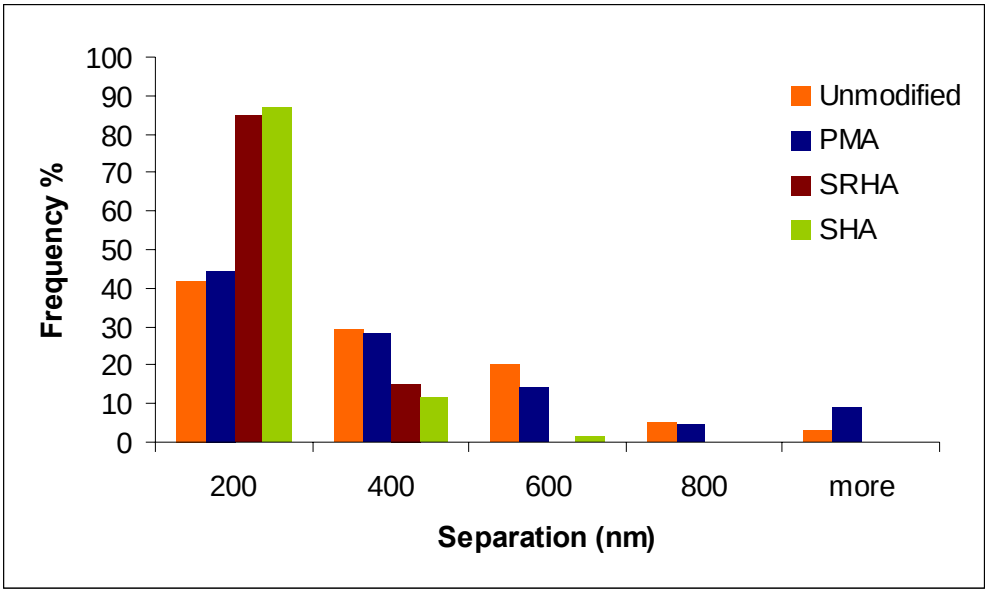

Figure 32. Normalized number of events occurring in a certain distance range. The distance ranges represent ranges of the pull-off distances between *Pseudomonas aeruginosa* AK1401 and four different modified probes.

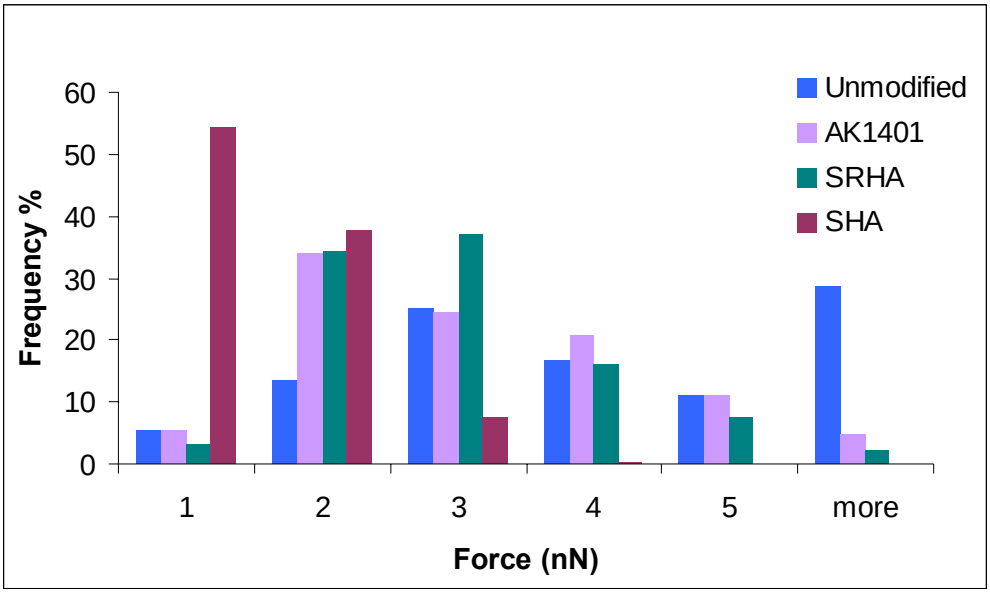

Figure 33. Normalized number of events occurring in a certain force range. The force ranges represent the ranges of adhesive pull-off forces exerted by four different modified probes on *Pseudomonas aeruginosa* AK1401 surface.

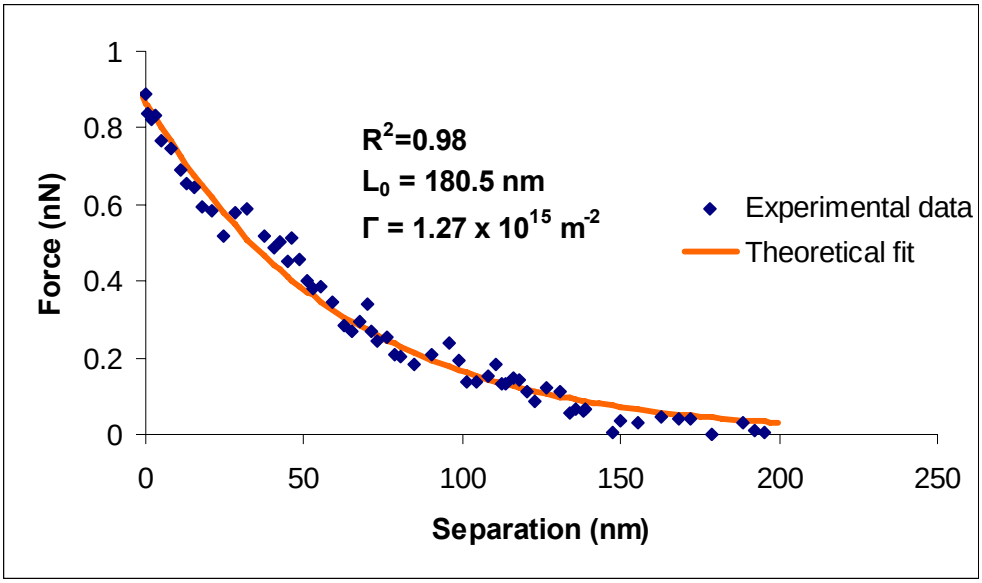

Figure 34. Using the steric interactions model for one surface bearing polymer brushes to fit one approach curve from the experimental data of *Pseudomonas aeruginosa* AK1401 interactions with unmodified probe under ultrapure water. The solid line represents the theoretical steric interactions fit and the dotted line represents the experimental curve.

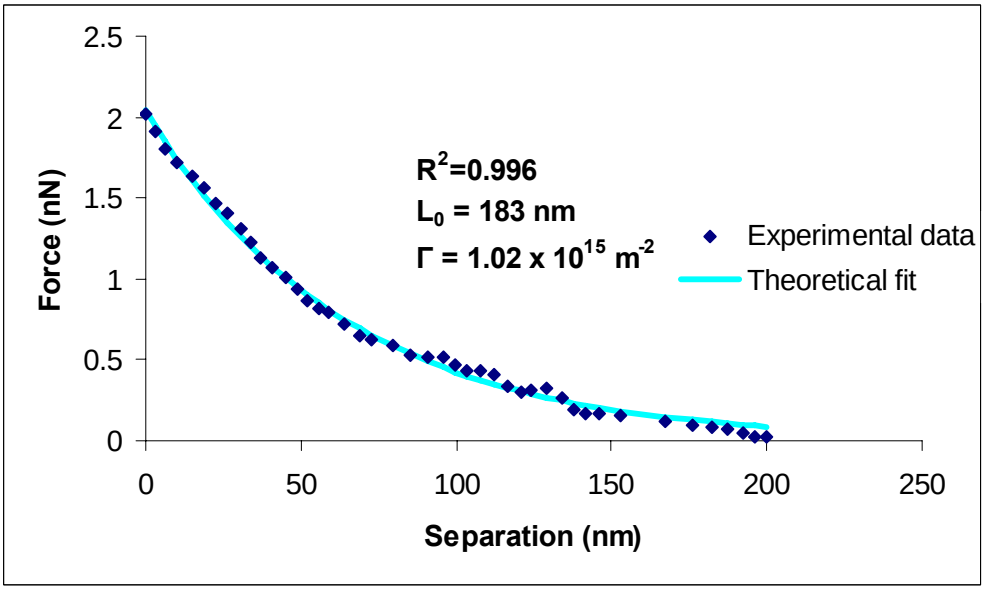

Figure 35. Using the steric interactions model for two surfaces bearing polymer brushes to fit one approach curve from the experimental data of *Pseudomonas aeruginosa* AK1401 interactions with PMA-modified probe under ultrapure water. The solid line represents the theoretical steric interactions fit and the dotted line represents the experimental curve.

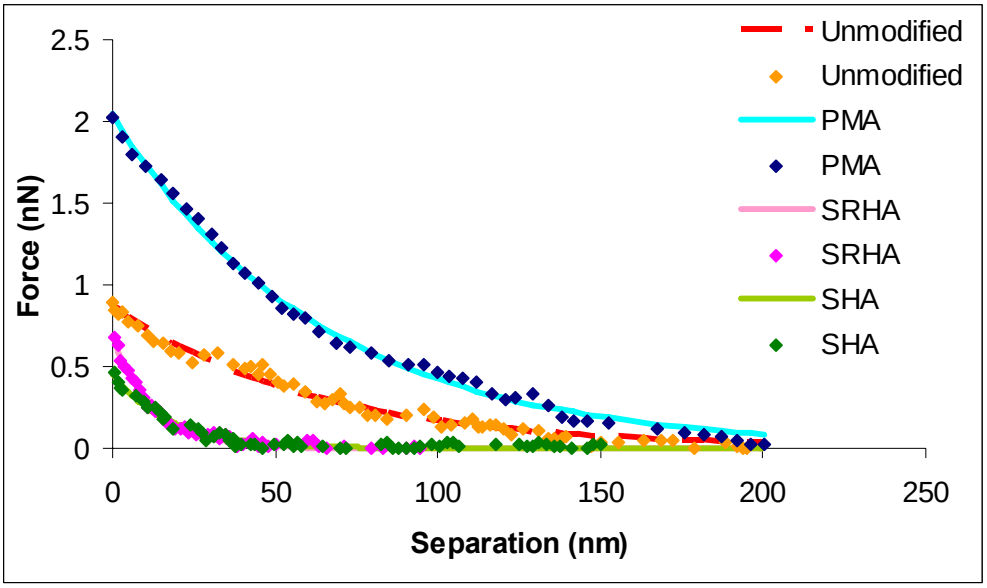

Figure 36. The theoretical steric interactions model fits and the experimental data of *Pseudomonas aeruginosa* AK1401 interacting with different modified probes. The dotted curves represent the experimental data. Each curve in the graph represents the fitting of one force curve captured on one *Pseudomonas aeruginosa* AK1401 cell by the steric interactions model. The dashed curve was generated using the steric interactions model for one surface coated with polymer brushes and the solid curves were generated using the steric interactions model for two surfaces coated with polymer brushes.

Table 7: A summary of equilibrium polymer length values, polymer grafted density values, and values of the force at zero separation from the theoretical steric interactions fits of *Pseudomonas aeruginosa* AK1401 interacting with different modified probes under ultrapure water.

Probe Modification	Average Equilibrium Polymer Length (L_0) (nm) (n = 30)	Average Polymer Grafting Density (γ) (m^{-2}) (n = 30)	Average Force at Zero Distance (nN) (n = 30)
Unmodified	168	1.38×10^{15}	0.90
PMA-modified	147	1.03×10^{15}	2.00
SRHA-modified	64	9.10×10^{14}	0.72
SHA-modified	52	9.30×10^{14}	0.61

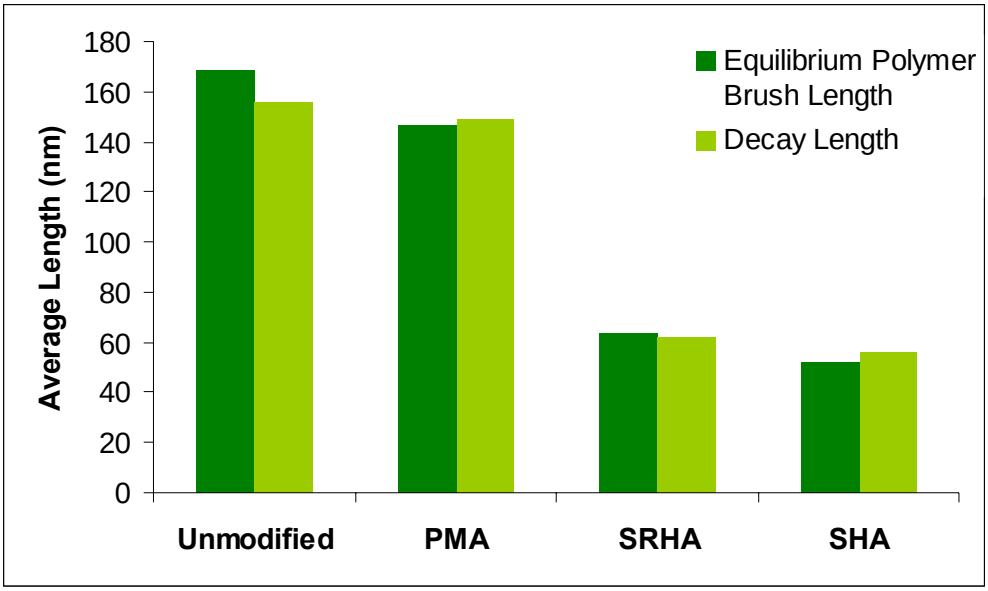

Figure 37. A comparison between average values of decay lengths and average values of equilibrium polymer brush lengths from all experiments of *Pseudomonas aeruginosa* AK1401 interacting with various probes.

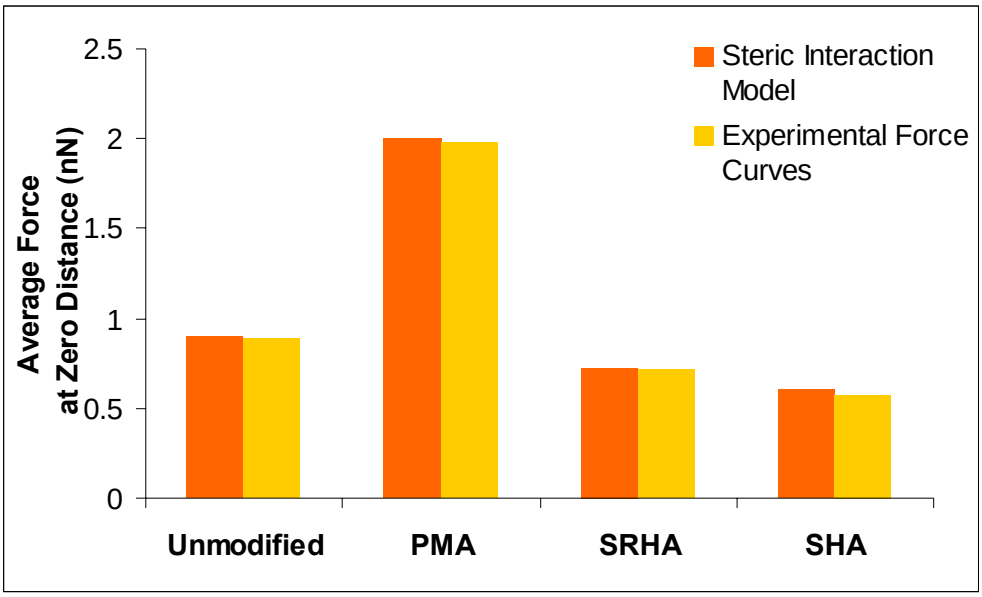

Figure 38. A comparison between average values of forces at zero distance from the experimental force curves and the steric interactions fits of *Pseudomonas aeruginosa* AK1401 interacting with various probes.

3.3.3.5 Comparison between Both *Pseudomonas aeruginosa* Strains

3.3.3.5.1 Approach Curves

In all experiments, both strains of *Pseudomonas aeruginosa* showed repulsive forces during the approach of the probe to the cell surface. However, in all cases *Pseudomonas aeruginosa* PAO1 has stronger repulsive forces and longer decaying distances than *Pseudomonas aeruginosa* AK1401 (Figure 39 and Figure 40).

3.3.3.5.2 Retraction Curves

Figure 41 show a comparison between the adhesive forces of both strains interacting with unmodified probes, simple NOM-modified probes, and complex NOM-modified probes. PAo1 has the lowest interactions with the unmodified probe among all interactions and the highest interactions with both the complex NOM. While AK1401 has the highest interactions with the unmodified probe among all interactions and the lowest interactions with both the complex NOM.

3.3.3.5.3 Modeling of Steric Interactions

The experimental data for the approach of various probes to both strains of *Pseudomonas aeruginosa* were fitted with the steric model. The fitting parameters values with values of the force at zero separation from the theoretical steric interactions fits of both *P. aeruginosa* strains interacting with different probes are summarized in Table 8.

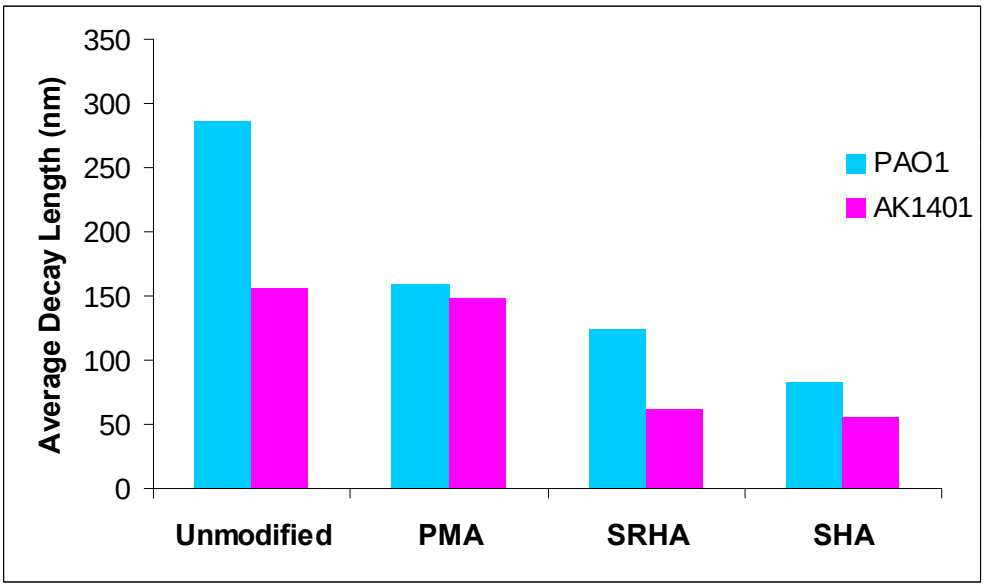

Figure 39. A comparison between average decay lengths values from both strains of *Pseudomonas aeruginosa* interacting with various probes. Each decay length value shown in the figure is the average of fifty decay length values from fifty approach curves captured on five different cells.

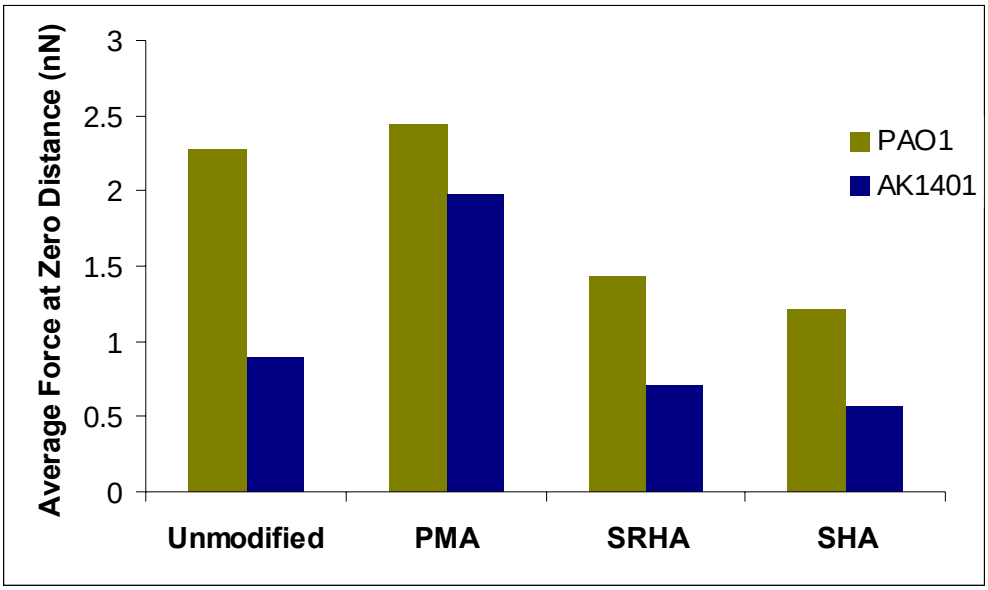

Figure 40. A comparison between average values of forces at zero distance from both strains of *Pseudomonas aeruginosa* interacting with various probes. Each value of force at zero distance shown in the figure is the average of fifty force values from fifty approach curves captured on five different cells.

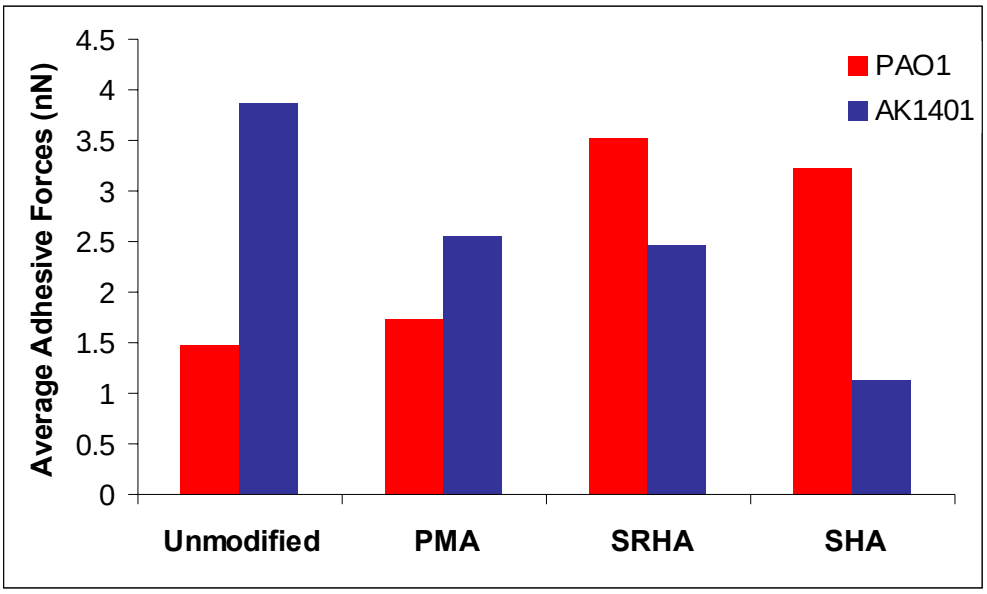

Figure 41. A comparison between average adhesive forces from both strains of *Pseudomonas aeruginosa* interacting with various probes. Each adhesive force shown in the figure is the average of all adhesive forces from fifty retraction curves captured on five different cells.

Table 8: A summary of equilibrium polymer length values, values of polymer grafted density, and values of the force at zero separation from the theoretical steric interactions fits of both *Pseudomonas aeruginosa* strains interacting with various probes under ultrapure water.

	Average Equilibrium Polymer Length (L_0) (nm) (n = 30)		Average Polymer Grafting Density (γ) (m^{-2}) (n = 30)		Average Force at Zero Distance (nN) (n = 30)	
	PAO1	AK1401	PAO1	AK1401	PAO1	AK1401
Unmodified	358	168	1.61×10^{15}	1.38×10^{15}	2.38	0.9
PMA-modified	164	147	1.10×10^{15}	1.03×10^{15}	2.5	2.00
SRHA-modified	124	64	9.36×10^{14}	9.1×10^{14}	1.46	0.72
SHA-modified	88	52	1.10×10^{15}	9.3×10^{14}	1.32	0.61

4 Discussion

4.1 Microbial Growth Curves

Harvesting the bacterial cells at a specific cell concentration is important for the valid comparison between different bacterial strains. An absorbance value of 0.9 at 600 nm was selected as a reference point in all experiments since it is in the early-mid exponential growth phase. As shown in Figure 4, the two strains of *Pseudomonas aeruginosa* have very similar growth behavior; both strains reach the selected absorbance value in about three and a half hours. This behavior is expected since the strains are genetically very similar.

4.2 Optical Microscopy Experiments

The optical microscope under FITC wavelengths was used to image both strains of *Pseudomonas aeruginosa*. The optical microscopy images are useful to estimate the size of each strain. The results of measuring the length of 80 bacteria for PAO1 and 190 bacteria for AK1401 showed that the sizes for both strains are within the typical size of bacteria (1-3 μm). For PAO1 strain the average length was 0.95 ± 0.192 μm while for AK1401 strain the average length was 1.12 ± 0.184 μm.

Optical microscopy also allowed us to confirm that the bacteria were Gram-negative and that the cultures were not contaminated.

In particular, optical microscopy was used to count the number of bacterial cells per ml and to calculate the cell number with the absorbance reading at 600 nm.

4.3 Atomic Force Microscopy (AFM)

4.3.1 Spring Constant Measurements

The calculation of precise and accurate value of the spring constant is of great importance, since the spring constant is the parameter which relates the cantilever deflection to the force of interaction.

There are different methods to calculate the cantilever spring constant. Some of these methods depend on the physical properties of the cantilever such as the geometry and density of the cantilever (17). Other methods depend on the thermal properties of the cantilever, and they require capturing the thermal distribution spectrum of the cantilever. Thermal techniques are in general more accurate than geometric techniques, since they are independent of the cantilever material or geometry, and they are based on standard physical theories (38).

In this work the method of Emerson and Camesano (24) was used for measuring and calculating the cantilever spring constant. This method is a thermal technique which only requires obtaining the thermal noise spectrum of the cantilever and its resonant frequency, and it was chosen because it is simple, accurate, and easy to apply.

Four new silicon nitride cantilevers with 1 μm silica spheres were used in measuring the cantilever spring constant. For each cantilever at least five readings were recorded and used in calculating an average value of the spring constant. The average value of the spring constant calculated from the four cantilevers was equal to 0.1175 N/m and it was applied in Hooke's Law in all the AFM experiments.

4.3.2 Surface Morphology Experiments

Capturing AFM images for both *Pseudomonas aeruginosa* strains in liquid was an important step in each experiment, since we had to ensure that the force curves were captured on the center of each bacterial cell. The clear AFM images of both bacterial strains in liquid shown in Figure 11 and Figure 12 are an indication of the strong attachment between the bacteria and the glass slide. The ellipsoidal shape and the dimensions of the bacteria verify that the bacterial surface was not affected or altered by the chemical binding materials which were used in immobilizing the bacteria. Specific chemical bonds were used in binding both strains to the glass slide. For PAO1, the IPA gold-coated glass slide interacted with the EDC\ NHS solution, and the EDC\ NHS molecules interacted with the amine groups on the bacterial surface, and the result of the reaction was forming a strong amide bond between the bacteria and the glass slide. While for AK1401, the aminosilane-coated glass slide interacted with the NHS\ EDC solution, and the NHS\ EDC molecules interacted with the carboxylic groups on the bacterial surface, and the result of the reaction was forming a stable amide bond between the bacteria and the glass slide.

The tapping mode AFM images for the three types of NOM in air showed that the adsorption of the NOM onto the glass slide was not in a monolayer. However, the PMA adsorption on the glass slide was more homogenous and more evenly distributed than the adsorption of both SRHA and SHA molecules. The uneven distribution of both SRHA and SHA molecules on the glass slide could be due to the fact that natural humic acids are mixtures of different substances with a wide molecular weight distribution (92).

The similarity between both natural humic acids AFM images is an indication of similar features and surface active groups comprising both materials.

4.3.3 Interaction Force Measurements

4.3.3.1 Probe Modification with Iron Oxide and NOM

The complete system of organo-mineral compounds was represented in this work by an adsorbed NOM into a surface film of iron oxide precipitated on spherical silica probes.

Silica spheres were chosen for the AFM experiments, because they are flat, easy to clean and mostly because they mimic the real soil colloidal particles (60). However, soil colloidal particles are not present alone in nature, or side by side with inorganic and organic particles, but often coated as organo-mineral compounds (92). Iron oxide was used in this work to model the mineral surface, since it is a common constituent of natural soil colloids (60). An iron oxide surface was generated by exposing the silica spheres to $FeCl_3$.

The results shown in Figure 16, Figure 17, and Figure 18 are approach force curves of interactions between different modified probes and clean glass slides under 1 mM NaCl solution, pH = 6.3. In each experiment, three clean glass slides were used, with five different areas examined on each of them. The reproducibility of the results it is a strong verification on the successful coating protocol followed in preparation of the iron oxide modified probes and the NOM-modified probes. Both the iron oxide coating and the adsorption of NOM into the iron oxide coated surface were done following the coating procedure of Mosley et al (60). For the NOM adsorption into iron oxide surface

they simply exposed the iron oxide colloidal particle to the natural or synthetic organic compounds. They showed that this technique was established in previous extensive work involved using the microelectrophoresis technique to examine the NOM-coated particles. The microelectrophoresis studies (53, 60) have established that after the simple exposure of iron oxide surfaces to NOM, such surfaces will be rapidly coated with strongly adhering NOM.

Vermohlen group (92) in their work of studying the influence of ionic strength, molar mass, and Ca^{2+} ions on the adsorption of polyelectrolytes onto different oxides, showed that the adsorption of polyelectrolytes onto aluminum oxide cannot only be described as a charge effect mechanism but that specific interactions must also be present.

The interactions between different modified probes and clean glass slides under 1 mM NaCl solution, pH = 6.3. are purely repulsive, with the highest repulsive forces measured for the bare silica probe-clean glass slide combination. This strong repulsion is presumably because both surfaces carry a large negative charge at pH values greater than ca. 4-5 (60), and these results are in agreement with previous research (60). The forces acting on the colloidal probes were lower after the formation of the iron oxide coating as shown in Figure 17. Under the same solution conditions, the smaller repulsive forces between the iron oxide-coated surface and clean glass slide compared to the forces between bare silica probe and clean glass slide could be due to the adsorption of positively charged Fe particles being electrostatically favorable (60). The measured repulsive forces in the presence of PMA are higher than the repulsive forces between the iron oxide-coated surface and clean glass slide, but still smaller than the repulsive forces

between bare silica probe and clean glass slide. This repulsive forces increase is due to the large negative charges carried on both the PMA surface and the glass slide surface, these results are in agreement with the work of Mosley et al (60).

4.3.3.2 Adhesion Properties of Simple and Complex NOM

The results of the retraction part of the force cycle were analyzed and represented in histograms in Figure 20. More than 75% of the adhesive forces of PMA are less than 3 nN. In contrast, the adhesive forces of both SRHA and SHA are distributed over a large force range with the majority of adhesion events between 6-9 nN. The large force distribution range for both the natural humic acids could be due to the polydispersity of their surfaces which are comprised of a mixture of different substances with wide molecular weight distributions (92). The Mann Whitney Rank Sum Test was used to see whether the adhesive forces for the three types of NOM are statistically different. The results showed that both SRHA and SHA are not significantly different with ($p = 0.684$), but both are significantly different from PMA ($p \leq 0.001$). These results suggest that the surface polymers of both natural humic acids are very similar and different from the surface polymers of PMA. The higher adhesive forces of SHA compared to SRHA could be a result of the higher maximum adsorption of SHA compared to SRHA because of it is higher molecular weight (44). Our results are in agreement with previous work of Johnson et al. on bacterial transport into porous media (44). They showed that SHA sorbed more strongly than SRHA to Fe-coated soil particles, and they explained that the stronger sorption of SHA relative to SRHA could be a result of the higher molecular weight of SHA.

4.3.3.3 *Pseudomonas aeruginosa* PAO1

4.3.3.3.1 Approach Curves

All the experiments with *Pseudomonas aeruginosa* PAO1 showed repulsive forces during the approach of the probe to the cell surface. In general, the repulsive forces are governed by the steric interactions experienced between the bacterial polymer brush and the silica probe or between two opposing polymer chains. In addition to the entropic and elastic interactions originated from the steric interactions, the surface polymer chains are influenced by the long-range electrostatic interactions. Our findings are in agreement with previous work of Abraham et al. (4) on interactions between strongly charged polyelectrolyte brushes. They suggested that the repulsive forces of higher magnitude are not of electrostatic nature but probably due to steric interactions or the physical contact of highly stretched polyelectrolyte brush surfaces. Also our results are in agreement with the work of Yamamoto et al. (97) on studying surface interaction forces between high density polymer brushes using the AFM. They observed repulsive forces at the brush surfaces, which originate from the steric interaction between the solvent-swollen PMMA brush and the probe sphere, and they suggested the strong dependency of the force curve on the graft density.

It can be noticed from Table 4 that PMA-modified probe has higher repulsive forces while interacting with PAO1 compared to both SRHA and SHA modified probes interacting with PAO1 which is expected, since the PMA surface has a higher charge density than both SRHA and SHA surfaces (92).

The Mann-Whitney Rank sum Test was used to check whether the repulsive forces at zero separation for both SRHA and SHA interacting with PAO1 are significantly different. The results of the test showed that there was a statistically significant difference between the values of repulsive forces at zero separation for both the SRHA-modified probe and the SHA-modified probe interacting with PAO1 strain with ($P \leq 0.001$), but it is still clear that the magnitudes of the forces at zero distance for both SRHA and SHA interacting with PAO1 are more alike than the forces at zero distance of PMA interacting with PAO1. This observation suggests that there are more common characteristics between the surfaces properties of both the natural humic acids if compared to the surface properties of PMA.

It can be noticed from the decay lengths values shown in Table 4 that the largest decay length is for the interactions between the unmodified probe and PAO1. Since the bacteria is interacting with polymer free surface there is a higher possibility for its surface polymer brushes to extend for a longer range of repulsion. While in the other cases the surface polymers of the bacteria are interacting with other polyelectrolytes. These polyelectrolytes with their own specific surface conformation may have more complicated interactions with the bacterial surface.

The results of using the Mann-Whitney Rank Sum Test for the decay length values of both SRHA and SHA interacting with PAO1 showed that, there was not a statistically significant difference between the decay lengths values for both the SRHA and the SHA modified probes interacting with PAO1 with ($P = 0.892$). This result supports the previous suggestion that both the natural humic acids might have similar surfaces.

4.3.3.3.2 Retraction Curves

The pull-off distances and the pull-off forces of the adhesion events were collected and presented respectively in Figure 23 and Figure 24. From the distance histograms for all experiments of PAO1 interacting with various probes it can be seen that the interactions between the unmodified probe and PAO1 persist to long distances up to a 1000 nm. While more than 80% of adhesion events of PMA-modified probe with PAO1 occur at distances shorter than 200 nm and more than 90% of adhesion events of SHA-modified probe with PAO1 are less than 200 nm. The long range of pull-off distances when the bacteria are interacting with a free polymer surface could be due to the flexibility of the polymer brushes to be stretched out further distances from the bacterial surface. While in the other cases, the probe also is covered with polymer brushes and the interactions between two polymer brushes are more complicated.

The first thing that can be noticed from the force histograms of various probes interacting with PAO1 is that adhesive forces between the unmodified probe and PAO1 are the least among all interactions with PAO1. The second thing that can be seen is that the adhesive forces between the NOM-modified probes and PAO1 increased with increasing the complexity of the NOM.

Our adhesive force results are in agreement with the work of Johnson et al. (45) on studying bacterial transport through porous media using column transport experiments. They showed that retention of Savannah River strain A1264 on iron oxide coated quartz pre-equilibrated with NOM was higher than it is retention on quartz porous media. That was true for both SRHA and SHA. The reason behind this behavior could be due to the surface charge heterogeneity resulting from the presence of iron oxide on the

quartz surface, and if the iron oxide surface is not fully covered with the NOM it would be expected that the bacterial deposition will increase relative to that on quartz alone.

Using the Mann-Whitney Rank Sum Test for the adhesive forces from all the experiments with PAO1 showed that there was not a statistically significant difference between the values of adhesive forces for both the PMA-modified probe and the unmodified probe interacting with PAO1 ($P = 0.371$). This finding supports our previous suggestion that PMA has similar behavior to the unmodified probe while interacting with PAO1 strain and that could be due to similar charge densities on both surfaces.

The Mann-Whitney Rank Sum Test was used also for both SRHA and SHA interacting with PAO1 and the results showed that there was not a significant difference between the adhesive forces of both SRHA and SHA interacting with PAO1 ($P = 0.651$). These results indicate that the surface polymers of both SRHA and SHA are very similar, which is in agreement with the repulsive forces of both SRHA and SHA from the approach force curves.

4.3.3.3.3 Modeling of Steric Interactions

The steric interaction model was used to fit the experimental data for the approach of various probes to *Pseudomonas aeruginosa* PAO1. For the unmodified probe, we used the steric model corresponding to the case where only one surface is coated with a polymer brush.

For the case of *P. aeruginosa* interacting with NOM-modified probes, we used a form of the steric model that was developed for two surfaces coated with (equal) polymer brushes. Although using this form of the steric model is not fully adequate since the

polymer brushes on both the bacterial surface and the NOM-coated surface are most likely unequal in length, the model fits showed excellent agreement with the experimental data as shown in Figure 26. This agreement suggests that when the surfaces of the opposed polymer layers approach each other, the steric repulsion becomes predominant.

Figure 28 and Figure 29 show another way to verify whether the steric model is a good fit for the experimental data. Figure 28 makes a comparison between the average decay length values from the experimental data and the average values of equilibrium polymer brush length from the interactions of the various probes with PAO1.

The results of using the Mann-Whitney Rank Sum Test showed that there was not a statistically significant difference between the average decay length values from the experimental data and the average values of equilibrium polymer brush length from all the different interactions with PAO1. These results strongly demonstrate that the steric model is a good fit for the experimental data.

Figure 29 makes a comparison between the average values of force at zero distance from the experimental data and the average values of force at zero distance calculated from the steric model fits of *Pseudomonas aeruginosa* PAO1 interacting with various probes. In all cases the similarity between the forces at zero distance from the experimental data and the steric model fits was so clear, with a slight increase in the reported values of the force at zero distance from the steric model fits. This overestimation is expected since the forces at zero distance of the theoretical fits are generated from average values of the steric model fitting parameters.

Table 5 summarizes the fitting parameters values from the theoretical fits of *Pseudomonas aeruginosa* PAO1 interacting with different modified probes. It can be noticed from the table that in most cases: the higher was the graft density the larger was the equilibrium polymer brush length.

Our results are highly supported by the work of Yamamoto et al. (97). They studied the effect of polymer grafting density on the interaction forces between Poly(methyl methacrylate) (PMMA) brushes and a silica particle attached to the end of a cantilever using the AFM. They found that the force curve is strongly dependant on the graft density, and the higher was the graft density, the larger was the separation where the interactions were observed. They concluded that as the graft density of the polymer increases the graft chains get more and more extended.

The highest graft density value and the largest equilibrium polymer brush length were associated with the interactions between the unmodified probe and *P.aeruginosa* PAO1. These characteristics of the interactions between the unmodified probe and *P.aeruginosa* PAO1; of high polymer density along with the strong resistance against compression are still not fully understood and difficult to explain and they could be related to the dynamic properties of the polymer brush.

4.3.3.4 *Pseudomonas aeruginosa* AK1401

4.3.3.4.1 Approach Curves

All the experiments with *Pseudomonas aeruginosa* AK1401 showed repulsive forces during the approach of the probe to the cell surface. In general, the repulsive forces are governed by the steric interactions experienced between the bacterial polymer brush

and the silica probe or between two opposing polymer chains. In addition to the entropic and elastic interactions originated from the steric interactions, the surface polymer chains are influenced by the long-range electrostatic interactions. Our findings are in agreement with previous work of Abraham et al. (4) on interactions between strongly charged polyelectrolyte brushes. They suggested that the repulsive forces of higher magnitude are not of electrostatic nature but probably due to steric interactions or the physical contact of highly stretched polyelectrolyte brush surfaces. Also our results are in agreement with the work of Yamamoto group (97) on studying surface interaction forces between high density polymer brushes using the AFM. They observed repulsive forces at the brush surfaces, which originate from the steric interaction between the solvent-swollen Poly(methyl methacrylate) (PMMA) brushs and the probe sphere, and they suggested the strong dependency of the force curve on the graft density.

It can be seen from Table 6 that AK1401 also has higher repulsive forces with PMA-modified probe than it does with both SRHA and SHA which is expected, since the PMA surface has a higher charge density than both SRHA and SHA surfaces (92).

The results of using the Mann-Whitney Rank sum Test for fifty values of repulsive forces at zero separation from all the experiments with AK1401 showed that, there was a statistically significant difference between the values of repulsive forces at zero separation from the three NOM-modified probes interacting with AK1401 with ($P \leq 0.001$) in all cases.

Although the results of using the Mann-Whitney Rank sum Test for fifty values of repulsive forces at zero separation from both experiments of SRHA and SHA interacting with AK1401 showed that, there was a statistically significant difference between the

values of repulsive forces at zero separation for both the SRHA-modified probe and the SHA-modified probe interacting with AK1401 strain with ($P \leq 0.001$), it is still obvious that the magnitudes of the forces at zero distance for both SRHA and SHA interacting with AK1401 are more alike than the force at zero distance of PMA interacting with AK1401. This observation suggests that there are more common characteristics between the surfaces properties of both the natural humic acids when compared to the surface properties of PMA.

It can be noticed from the decay lengths values shown in Table 6 that the largest decay length is for the interactions between the unmodified probe and AK1401. Since the bacteria is interacting with polymer free surface there is a larger possibility for it is surface polymer brushes to extend for a longer range of repulsion. While in the other cases the surface polymers of the bacteria are interacting with other polyelectrolytes. These polyelectrolytes with their own specific surface confirmation may have more complicated interactions with the bacterial surface.

The results of using the Mann-Whitney Rank Sum Test for fifty values of the decay lengths from the experiments of both SRHA and SHA interacting with AK1401 showed that there was a statistically significant difference between the decay lengths values for both the SRHA and the SHA modified probes interacting with AK1401 with ($P \leq 0.001$). However, it can be seen from Table 6 that the average values of decay lengths of both SRHA and SHA are very close and far from the average value of decay length of PMA. This result supports the previous suggestion that both the natural humic acids might have similar surfaces.

4.3.3.4.2 Retraction Curves

The pull-off distances and the pull-off forces of the adhesion events were collected and presented respectively in Figure 32 and Figure 33. From the distance histograms for all experiments of AK1401 interacting with various probes it can be seen that the interactions between AK1401and both the unmodified probe and PMA-modified probe persist to long distances up to a 1000 nm. While more than 80% of adhesion events of both SRHA-modified probe and SHA-modified probe interacting with AK1401 occur at distances shorter than 200 nm. The long range of pull-off distances for both the unmodified and PMA-modified probes interacting with AK1401 could be due to the flexibility of the polymer brushes to be stretched out further distances from the bacterial surface. While in the case of the natural humic acids, the probe is highly covered with polymer brushes which may complicate the interactions between the natural humic acids surfaces and the bacteria, besides that the probe now is considered soft material and not stiff enough to be able to stretch the bacterial surface polymers further distances. The similar pull-off distances distribution for both SRHA and SHA interacting with AK1401 suggests that both humic acids have similar polymer brushes covering their surfaces.

The first thing that can be noticed from the force histograms of various probes interacting with AK1401 is that adhesive forces between the unmodified probe and AK1401 are the highest among all interactions with AK1401. The second thing that can be seen is that the adhesive forces between the NOM-modified probes and AK1401 decreased with increasing the complexity of the NOM.

Our adhesive forces results for AK1401 are in agreement with the work of Johnson et al. (43) on facilitating transport of polycyclic aromatic hydrocarbons by NOM in aquifer sediments using column transport experiments. They showed that transport of hydrophobic contaminants in the presence of humic substances should be facilitated relative to transport of such contaminants alone. That was true for both SRHA and SHA.

Using the Mann-Whitney Rank Sum Test for the adhesive forces from all the experiments with Ak1401 showed that there was a statistically significant difference in the values of adhesive forces for all interactions between AK1401 and various probes with ($P \leq 0.001$).

4.3.3.4.3 Modeling of Steric Interactions

The steric interactions model was used to fit the experimental data for the approach of various probes to *Pseudomonas aeruginosa* AK1401. Figure 30 demonstrates that the steric model fit showed an excellent agreement with the experimental data. For the unmodified probe, we used the steric model corresponding to the case where only one surface is coated with a polymer brush.

For the case of *P. aeruginosa* interacting with NOM-modified probes, we used a form of the steric model that was developed for two surfaces coated with (equal) polymer brushes. The model showed excellent agreement with the experimental data as shown in Figure 35. This agreement suggests that when the two surfaces approach each other, the steric repulsion becomes predominant.

Figure 37 and Figure 38 show another way to verify whether the steric model is a good fit for the experimental data. Figure 37 makes a comparison between the average

decay length values from the experimental data and the average values of equilibrium polymer brush length from the interactions of the various probes with Ak1401. The results of using the Mann-Whitney Rank Sum Test showed that there was not a statistically significant difference between the average decay length values from the experimental data and the average values of equilibrium polymer brush length from all the different interactions with AK1401. These results strongly demonstrate that the steric model is a good fit for the experimental data.

Figure 38 makes a comparison between the average values of force at zero distance from the experimental data and the average values of force at zero distance calculated from the steric model fits of *Pseudomonas aeruginosa* AK1401 interacting with various probes. In all cases the similarity between the forces at zero distance from the experimental data and the steric model fits was so clear, with a slight increase in the reported values of the force at zero distance from the steric model fits. This overestimation is expected since the forces at zero distance of the theoretical fits are generated from average values of the steric model fitting parameters.

Table 7 summarizes the fitting parameters values from the theoretical fits of *Pseudomonas aeruginosa* AK1401 interacting with different modified probes. It can be noticed from the table that in most cases: the higher was the graft density the larger was the equilibrium polymer brush length.

Our results are highly supported by the work of Yamamoto et al. (97). They found that the force curve is strongly dependant on the graft density, and the higher was the graft density, the larger was the separation where the interactions were observed. They

concluded that as the graft density of the polymer increases the graft chains get more and more extended.

The highest graft density value and the largest equilibrium polymer brush length were associated with the interactions between the unmodified probe and *P.aeruginosa* AK1401. These characteristics of the interactions between the unmodified probe and *P.aeruginosa* AK1401; of high polymer density along with the strong resistance against compression are still not fully understood and difficult to explain and they could be related to the dynamic properties of the polymer brush.

4.3.3.5 Comparison between Both *Pseudomonas aeruginosa* Strains

4.3.3.5.1 Approach Curves

The repulsive forces of both strains interacting with different types of NOM have the same trend. Both strains had higher repulsive forces with PMA and less repulsive forces with both SRHA and SHA. However, in all cases *Pseudomonas aeruginosa* PAO1 has stronger repulsive forces and longer decaying distances than *Pseudomonas aeruginosa* AK1401 as shown in Figure 39 and Figure 40.

The difference in the repulsive forces and decaying distances between both strains interacting with various probes is due to differences in the polysaccharide component of the *Pseudomonas aeruginosa* lipopolysaccharide. The A-band polysaccharides of *Pseudomonas aeruginosa* AK1401 are composed of neutral D-rhamnose polysaccharides (36). The neutral polysaccharide component of the surface of *P. aeruginosa* AK1401 could be responsible for the less repulsive forces of AK1401 compared to PAO1.

Pseudomonas aeruginosa AK1401 does express the A-band polysaccharides only, while *Pseudomonas aeruginosa* PAO1 coexpress both the A-band and the B-band polysaccharides. The A-band and the B-band polysaccharides of *P. aeruginosa* PAO1 range up to 25 to 30 KDa in size, while the largest polymers of A-band polysaccharides *P.aeruginosa* AK1401 would be less than 6 KDa in size (36). Hence, it is reasonable that the polysaccharides of *P.aeruginosa* PAO1 would project out from the bacterial surface considerably further than the polysaccharides of *P.aeruginosa* AK1401.

Since the PMA surface has a higher charge density than both SRHA and SHA surfaces (92), it is expected that PMA-modified probe has higher repulsive forces while interacting with both strains if compared to both SRHA and SHA modified probes.

4.3.3.5.2 Retraction Curves

The two strains showed differences in their adhesive forces with the different NOM-coated probes as shown in Figure 41. Forexample, *P. aeruginosa* AK1401 has higher adhesive forces than *P. aeruginosa* PAO1 when interacting with the unmodified probe. While *P. aeruginosa* PAO1 has higher adhesive forces than *P. aeruginosa* AK1401 when interacting with both the SRHA and SHA-modified probes.

Using the Mann-Whitney Rank Sum Test for the adhesive forces from all the experiments of both strains interacting with various probes showed that there was a statistically significant difference between the values of adhesive forces for each single case from both strains ($P \leq 0.001$). The results of using the Mann Whitney Rank Sum Test along with our findings suggest that the two strains are very different while interacting with unmodified, simple NOM-modified, and complex NOM-modified probes. This difference is mainly due to differences in the LPS from both strains.

The results also showed inconsistency between the behavior of PMA and both SRHA and SHA while interacting with the two strains of *P.aeruginosa*. This finding suggests that the surface characteristics of the complex NOM are different from the surface characteristics of PMA and that could be due to many factors, one of them is the polydispersity of the natural humic acids (92).

4.3.3.5.3 Modeling of Steric Interactions

The steric interactions model was used to fit the experimental data for the approach of various probes to both strains of *Pseudomonas aeruginosa*. The steric model fit showed an excellent agreement with the experimental data. The fitting parameters of the steric model along with the values of the forces at zero distance from all the experiments with both *Pseudomonas aeruginosa* strains are summarized in Table 8.

It can be seen from Table 8 that for both strains the largest equilibrium polymer brush length was associated with the interactions between both strains and the unmodified probe, and that the equilibrium polymer brush length was decreasing with increasing the complexity of the NOM. Since both strains are interacting with polymer free surface when they are interacting with the unmodified probe, there is a larger possibility for the bacterial surface polymer brushes to extend for a longer range of repulsion. While in the other cases the surface polymers of the bacteria are interacting with other polyelectrolytes. These polyelectrolytes with their own specific surface confirmation they tend to have loops and tails in the adsorbed state (92), and hence they may have more complicated interactions with the bacterial surface. However, in all cases *Pseudomonas aeruginosa* PAO1 has longer equilibrium polymer brush length than *Pseudomonas aeruginosa* AK1401. This is expected since the A-band and B-band polysaccharides of *P. aeruginosa* PAO1 are much larger in the size (25-30 KDa) than the size of the A-band polysaccharides of *P. aeruginosa* AK1401 (< 6 KDa) (36).

It can also be noticed from the table that for both strains in most cases: the higher was the graft density the larger was the equilibrium polymer brush length, and in all cases PAO1 has higher graft density values than AK1401 which can be due to the big

difference between the size of polymer brushes covering the surface of PAO1 compared to the size of polymer brushes covering the surface of AK1401 (36, 78).

Our results are highly supported by the work of Yamamoto et al. (97). They found that the force curve strongly depends on the graft density, and the higher was the graft density, the larger was the separation where the interactions were observed. They concluded that as the graft density of the polymer increases the graft chains get more and more extended.

The highest graft density values were associated with the interactions between the unmodified probe and both *P. aeruginosa* strains. The characteristics of the interactions between the unmodified probe and *P. aeruginosa* are still not fully understood and difficult to explain and they could be related to the dynamic properties of the polymer brush.

The repulsive forces at zero distance calculated from the theoretical fits of both strains interacting with different types of NOM have the same trend. Both strains had higher repulsive forces at zero distance with PMA and less repulsive forces with both SRHA and SHA. However, in all cases *Pseudomonas aeruginosa* PAO1 has stronger repulsive forces at zero distance than *Pseudomonas aeruginosa* AK1401 as shown in Table 8.

The difference in the repulsive forces between both strains interacting with various probes is due to differences in the polysaccharide component of the *Pseudomonas aeruginosa* lipopolysaccharide. The A-band polysaccharides of *Pseudomonas aeruginosa* AK1401 are composed of neutral D-rhamnose polysaccharides (36). The neutral

polysaccharide component of the surface of *P.aeruginosa* AK1401 could be responsible of the less repulsive forces of AK1401 compared to PAO1.

Since the PMA surface has a higher charge density than both SRHA and SHA surfaces (92), it is expected that PMA-modified probe has higher repulsive forces while interacting with both strains if compared to both SRHA and SHA modified probes.

5 Conclusion

We studied the interactions between two well defined strains of *Pseudomonas aeruginosa* and three different NOM-coated surfaces. The two strains showed contrary adhesive interactions with the different NOM-coated surfaces. *P.aeruginosa* PAO1 had the highest adhesion with complex NOM while *P.aeruginosa* AK1401 had the lowest adhesion with the complex NOM. Since the LPS structure is the only difference between the two strains, it is supposed that the contrary adhesive interactions are due mainly to the effect of the LPS structure.

We demonstrated the effect of PMA as a simple model of the NOM, and both SRHA and SHA as two complex types of NOM on the adhesive properties of the two strains of *Pseudomonas aeruginosa*. The two natural humic acids were very similar in their interactions with each of the studied bacterial strains, and different from the behavior of PMA. The inconsistency between the effect of both the complex NOM and the effect of the simple NOM on both strains of *Pseudomonas aeruginosa* is an indication of different characteristics of the surface polymer brushes. Hence, PMA is not a good representation of the natural organic compounds.

Steric interactions are the dominant interactions that control the approach of the unmodified or the modified probes to the surface of both strains of *P.aeruginosa*. However, steric forces are not the only forces which are responsible for the repulsive forces in the approach curves; there are other forces such as the electrostatic forces which are present and play a role in explaining the repulsion in the force curves.

For both strains of *Pseudomonas aeruginosa*, the force curve strongly depends on the graft density: the higher was the graft density, the larger was the separation where the interactions are observed. This clearly shows that the polymer chains get more and more extended as the graft density is increased. Further studies on the properties of the polymer brushes are needed to explain the strong resistance of the high density polymer brushes against compression.

We were able to achieve a successful modification of the silicon probes with iron oxide and natural organic matter, in order to be used in examining the interactions between the NOM-coated surfaces and the two strains of *Pseudomonas aeruginosa*. AFM images of the NOM coated surfaces were obtained to verify the successful modification of the silicon probes with iron natural organic matter. Also reproducible force-distance curves of the interactions between the NOM coated surfaces and clean glass slide were obtained from three different experiments to verify the successful probe coating procedure.

6 References:

1. 2005. Personal communications with Ray Emerson.

2. 2002, posting date. Pierce Biotechnology, Inc. www.piercenet.com. [Online.]

3. **(SDWA). E. P. A. E. S. D. W. A.** 2005, posting date. National primary drinking water regulations: Groundwater rule. www.epa.gov/safewater. [Online.]

4. **Abraham, T., S. Giasson, J. F. Gohy, and R. Jerome.** 2000. Direct measurements of interactions between hydrophobically anchored strongly charged polyelectrolyte brushes. Langmuir **16:**4286-4292.

5. **Abu-Lail, N. I., and T. A. Camesano.** Atomic force microscopy and single-molecule force microscopy studies of biopolymers.

6. **Abu-Lail, N. I., and T. A. Camesano.** 2003. Polysaccharide properties probed with atomic force microscopy: A Review. Journal of Microscopy **212:**217-238.

7. **Abu-Lail, N. I., and T. A. Camesano.** 2003a. The role of lipopolysaccahrides in the adhesion, retention, and transport of E.coli JM109. Environmental Science & Technology **37:**2173-2183.

8. **Abu-Lail, N. I., and T. A. Camesano.** 2003. Role of lipopolysaccharides in the adhesion, retention, and transport of *Escherichia coli* JM109. Environmental Science & Technology **37:**2173-2183.

9. **Alexander, S.** 1977. Adsorption of chain molecules with a polar head a scaling description. Journal de Physique **38:**983-987.

10. **Arsenault, T. L., D. W. Hughes, D. B. MaClean, W. A. Szarek, A. M. B. kropinski, and J. S. Lam.** 1991. Structural studies on the polysaccharide portion of "A-band" lipopolysaccharide from a mutant (AK1401) of *Pseudomonas aeruginosa* strain PAO1. Canadian Journal of Chemistry **69:**1273-1280.

11. **Bales, R. C., S. R. Hinkle, T. W. Kroeger, K. Stocking, and C. P. Gerba.** 1991. Bacteriophage adsorption during transport through porous media:chemical perturbations and reversiblitiy. Environmental Science & Technology **25:**2088-2095.

12. **Bales, R. C., S. Li, K. M. Maguire, M. T. Yahya, C. P. Gerba, and R. W. Harvey.** 1995. Virus and bacteria transport in a sandy aquifer. Ground Water 33:653-661.

13. **Burnham, N. A., X. Chen, C. S. Hodges, G. A. Matei, E. J. Thoreson, C. J. Roberts, M. C. Davies, and S. J. B. Tendler.** 2003. Comparison of calibration methods for atomic-force microscopy cantilevers. Nanotechnology 14:1-6.

14. **Butt, H.-J., M. Kappl, H. Mueller, and R. Raiteri.** 1999. Steric forces measured with the atomic force microscope at various temperatures. Langmuir **15:**2559-2565.

15. **Camesano, T. A.** 1997. Enhancing bacterial transport in porous media by manipulation of flow velocity, cell concentration and solution ionic strength. University of Arizona. M. S. Thesis.

16. **Camesano, T. A., and B. E. Logan.** 1998. Influence of fluid velocity and cell concentration on the transport of motile and non-motile bacteria in porous media. Environmental Science & Technology **32:**1699-1708.

17. **Cleveland, J. P., S. Manne, D. Bocek, and P. K. Hansma.** 1993. A nondestructive method for determining the spring constant of cantilevers for scanning force microscopy. Review of Scientific Instruments **64:**403-405.

18. **Conboy, M. J., and M. J. Goss.** 2000. Natural protection of groundwater against bacteria of fecal origin. Journal of Contamination Hydrology **43:**1-24.

19. **Daniel, J. M., J. Harald, L. Tiina, K. Lars, and A. Kurt.** 2002. Observing structure, function and assembly of single proteins by AFM. Progress in Biophysics & Molecular Biology **79:**1-43.

20. **de Gennes, P. G.** 1987. Polymers at an interface: A simplified view. Advances in Colloid and Interface Science **27:**189-209.

21. **DeBorde, D. C., W. W. Woessner, Q. T. Kiley, and P. Ball.** 1999. Rapid transport of viruses in a floodplain aquifer. Water Research **33:**2229-2238.

22. **Ducker, W. A., and T. J. Senden.** 1992. Measurement of forces in liquids using a force microscope. Langmuir **8:**1831.

23. **Elimelech, M., and C. R. O'Melia.** 1990. Kinetics of deposition of colloidal particles in porous media. Environmental Science & Technology **24:**1528-1536.

24. **Emerson IV, R. J., and T. A. Camesano.** 2006. On the importance of precise calibration techniques for an atomic force microscope. Ultramicroscopy **106:**413-422.

25. **Fontes, D. E., A. L. Mills, G. M. Hornberger, and J. S. Herman.** 1991. Physical and chemical factors influencing transport of microorganisms through porous media. Applied and Environmental Microbiology **57:**2473-2481.

26. **Frank, B. P., and G. Belfort.** 1997. Intermolecular forces between extracellular polysaccharides measured with the atomic force microscope. Langmuir **13:**6234-6240.

27. **Frisbie, C. D., L. F. Rozsnyai, A. Noy, M. S. Wrighton, and C. M. Lieber.** 1994. Functional group imaging by chemical force microscopy. Science **265:**2071.

28. **Gannon, J. T., V. B. Manilal, and M. Alexander.** 1991. Relationship between cell surface properties and transport of bacteria through soil. Applied and Environmental Microbiology **57:**190-193.

29. **Gerba, C. P.** 1984. Applied and theoretical aspects of virus adsorption to surfaces. Advances in Applied Microbiology **30:**133-168.

30. **Gerba, C. P., C. Wallis, and J. L. Melnick.** 1975. Fate of wastewater bacteria and viruses in soil. Journal of Irrigation Drainage Division **101:**157-174.

31. **Grabar, K. C., R. G. Freeman, M. B. Hommer, and M. J. Natan.** 1995. Preparation and Characterization of Au Colloid Monolayers. Analytical Chemistry **67:**735-743.

32. **Grasso, D., B. F. Smets, K. A. Strevett, B. D. Machinist, C. J. Van Oss, R. F. Giese, and W. Wu.** 1996. Impact of physiological state on surface thermodynamics and adhesion of *Pseudomonas aeruginosa.* Environmental Science & Technology **30:**3604-3608.

33. **Gross, M. J., and B. E. Logan.** 1995. Influence of different chemical treatments on transport of Alcaligenes paradoxus in porous media. Applied and Environmental Microbiology **61:**1750-1756.

34. **Harvey, R. W., and S. P. Garabedian.** 1991. Use of Colloid Filtration Theory in Modeling Movement of Bacteria through a Contaminated Sandy Aquifer. Environmental Science & Technology **25:**178-185.

35. **Harvey, R. W., L. H. George, R. L. Smith, and R. D. LeBlanc.** 1989. Transport of microspheres and indigenous bacteria through a sandy aquifer: results of natural and forced gradient tracer experiments. Environmental Science & Technology **23:**51-56.

36. **Hatano, K., J. B. Goldberg, and G. B. Pier.** 1995. Biologic activities of antibodies to the natural-polysaccharide component of the *pseudomonas aeruginosa* lipopolysaccharide are blocked by O side chains and mucoid exopolysaccharide (Alginate). Infection and Immunity **63:**21-26.

37. **Heinz, W. F., and J. H. Hoh.** 1999. Spatially resolved force spectroscopy of biological surfaces using the AFM. Nanotechnology **17:**143-150.

38. **Hutter, J. L., and J. Bechhoefer.** 1993. Calibration of atomic-force microscope tips. Review of Scientific Instruments **64:**1868-1873.

39. **Huysman, F., and W. Verstraete.** 1993b. Water-facilitated transport of bacteria in unsaturated soil columns: influence of cell surface hydrophobicity and soil properties. Soil Biology and Biochemistry **25:**91-97.

40. **Israelachvili, J.** 1992. Intermolecular & Surface Forces, 2nd edition ed. Academic Press, London.

41. **Jin, Y., and M. Flury.** 2002. Fate and Transport of Viruses in Porous Media. Advances in Agronomy **77:**39-102.

42. **Jin, Y., M. V. Yates, S. Thompson, and W. A. Jury.** 1997. Sorption of viruses during flow through saturated sand columns. Environmental Science & Technology **31:**548-555.

43. **Johnson, W. P., and G. L. Amy.** 1995. Facilitated transport and enhanced desorption of polycyclic aromatic hydrocarbons by natural organic matter in aquifer sediments. Environmental Science & Technology **29:**807-817.

44. **Johnson, W. P., and B. E. Logan.** 1996. Enhanced transport in porous media by sediment-phase and aqueous-phase natural organic matter. Water Research **30:**923-931.

45. **Johnson, W. P., M. J. Martin, M. J. Gross, and B. E. Logan.** 1996. Facilitation of bacterial transport through porous media by changes in solution and surface properties. Colloids and Surfaces A: Physicochemical and Engineering Aspects **107:**263-271.

46. **Klaus, D. J.** 2001. Atomic force microscopy of biomaterials surfaces and interfaces. Surface Science **491:**303-332.

47. **Knapp, H. F., and A. Stemmer.** 1999. Preparation, comparison, and performance of hydrophobic AFM tips. Surface and Interface Analysis **27:**324-331.

48. **Korber, D. R., j. R. Lawrence, and D. E. Caldwell.** 1994. Effect of Motility on Surface Colonization and Reproductive Success of Pseudomonas fluorescens in Dual-Dilution Continuous Culture and Batch Culture Systems. Applied and Environmental Microbiology **60:**1421-1429.

49. **Kretzschmar, R., D. Hesterberg, and H. Sticher.** 1997. Effects of adsorbed humic acid on surface charge and flocculation of kaolinite. Soil Science Society of America Journal **61:**101-108.

50. **Leclerc, H., S. Edberg, V. Pierzo, and J. M. Delattre.** 1999. Bacteriophages as indicators of enteric viruses and public health risk in groundwaters. Journal of Applied Microbiology **88:**5-21.

51. **Leenheer, J. A., R. L. Malcolm, P. W. McKinley, and L. A. Eccles.** 1974. Occurrence of dissolved organic carbon in selected ground water samples in the United States. Journal of Research of the U.S. Geological Survey **2:**361-369.

52. **Litton, G. M., and T. M. Olson.** 1996. Particle size effects on colloid deposition kinetics: evidence of secondary minimum deposition. Colloids and Surfaces A: Physicochemical Engineering Aspects. **107:**273-283.

53. **Loeb, G. I., and R. A. Neihof.** 1975. Marine conditioning films. Advances in Chemistry **145:**319-335.

54. **Logan, B. E.** 1999. Environmental transport processes. John Wiley & Sons, Inc., New York.

55. **Logan, B. E., D. G. Jewett, R. G. Arnold, E. J. Bouwer, and C. R. O'Melia.** 1995. Clarification of clean-bed filtration models. Journal of Environmental Engineering **121:**869-873.

56. **MaClaine, J. W., and R. M. Ford.** 2002. Characterizing the adhesion of motile and nonmotile *Escherichia coli* to a glass surface using a parallel-plate flow chamber. Bioteechnology and Bioengineering **78:**179-189.

57. **Martin, Y., C. C. Williams, and H. K. Wickramasinghe.** 1987. Atomic force microscope-force mapping and profiling on a sub 100-.ANG. scale. Journal of Applied Physics **61:**4723-4729.

58. **McCarthy, J. F., and J. M. Zachara.** 1989. Subsurface transport of contaminants. Environmental Science & Technology **23:**496-504.

59. **McCaulou, D. R., R. C. Bales, and R. G. Arnold.** 1995. Effect of temperature-controlled motility on transport of bacteria and microspheres through saturated sediment. Water Resources Research **31:**271-280.

60. **Mosley, L. M., K. A. Hunter, and W. A. Ducker.** 2003. Forces between colloid particles in natural waters. Environmental Science & Technology **37:**3303-3308.

61. **Mueller, R. F., W. G. Characklis, W. L. Jones, and J. T. Sears.** 1992. Characterization of initial events in bacterial surface colonization by two *Pseudomonas* species using image analysis. Bioteechnology and Bioengineering **39:**1161-1170.

62. **Ong, Y. L., A. Razatos, G. Georgiou, and M. M. Sharma.** 1999. Adhesion forces between E. coli bacteria and biomaterial surfaces. Langmuir **15:**2719-2725.

63. **Pekdeger, A., and G. Matthess.** 1983. Factors of bacteria and virus transport in groundwater. Environmental Geology **5:**49-52.

64. **Pieper, A. P., J. N. Ryan, R. W. Harvey, G. L. Amy, T. H. Illangasekare, and D. W. Metge.** 1997. Transport and Recovery of Bacteriophage PRD1 in a Sand and Gravel Aquifer: Effect of Sewage-Derived Organic Matter. Environmental Science & Technology **31:**1163-1170.

65. **Pontius, F. W.** 1990. Water Quality and Treatment., Fourth ed. McGraw-Hill, New York.

66. **Rajagopalan, R., and C. Tien.** 1976. Trajectory analysis of deep bed filtration with the sphere-in-cell porous media model. AICHE Journal **3:**523-533.

67. **Razatos, A., Y.-L. Ong, F. Boulay, D. L. Elbert, J. A. Hubbell, M. M. Sharma, and G. Georgiou.** 2000. Force measurements between bacteria and poly(ethylene glycol)-coated surfaces. Langmuir **16:**9155-9158.

68. **Rijnaarts, H. H. M., W. Norde, J. Lyklema, and A. J. B. Zehnder.** 1995. The isoelectric point of bacteria as an indicator for the presence of cell surface polymers that inhibit adhesion. Colloids and Surfaces B: Biointerfaces **4:**191-197.

69. **Sadovskaya, I., J. Brisson, P. Thibault, J. C. Richards, J. S. Lam, and E. Altman.** 2000. Structural characterization of the outer core and the O-chain linkage region of lipopolysaccharide from *Pseudomonas aeruginosa* serotype O5. European Journal of Biochemistry **267:**1640-1650.

70. **Sadovskaya, I., J. R. Brisson, J. S. Lam, J. C. Richards, and E. Altman.** 1998. Structural elucidation of the lipopolysaccharide core regions of the wild-type strain PAO1 and O-chain-deficient mutant strains AK1401 and AK1012 from *Pseudomonas aeruginosa* serotype O5. European Journal of Biochemistry **255:**673-684.

71. **Scandura, J. E., and M. D. Sobsey.** 1997. Viral and bacterial contamination of groundwater from on-site sewage treatment systems. Water Science and Technology **35:**141-146.

72. **Schijven, J. F., W. Hoogenboezem, S. M. Hassanizadeh, and J. H. Peters.** 1999. Modeling removal of bacteriophages MS2 and PRD1 by dune recharge at Castricum, Netherlands. Water Resources Research **35:**1101-1111.

73. **Schwarzenbach, R. P., P. M. Gschwend, and D. M. Imboden.** 1992. Environmental Organic Chemistry. John Wiley & Sons, INC., New York.

74. **Shiming, L., C. Ji-Liang, H. Long-Sun, and L. Huan-We.** 2005. Measurements of the forces in protein interactions with atomic force microscopy. Current Proteomics **2:**55-81.

75. **Smets, B. F., D. Grasso, M. A. Engwall, and B. J. Machinist.** 1999. Surface physicochemical properties of *Pseudomonas fluorescens* and impact on adhesion and transport through porous media. Colloids and Surfaces B: Biointerfaces **14:**121-139.

76. **Smith, M. S., G. W. Thomas, R. E. White, and D. Ritonga.** 1985. Transport of *Escherichia coli* through intact and disturbed soil columns. Journal of Environmental Quality **14:**87-91.

77. **Stevens, S. M., S. Allen, M. C. Davies, C. J. Roberts, E. Schacht, S. J. B. Tendler, S. VanSteenkiste, and P. M. Williams.** 2002. The development, characterization, and demonstration of a versatile immobilization strategy for biomolecular force measurements. Langmuir **18:**6659-6665.

78. **Stoica, O., A. Tuanyok, X. Yao, M. H. Jericho, D. Pink, and T. J. Beveridge.** 2003. Elasticity of membrane vesicles isolated from *Pseudomonas aeruginosa*. Langmuir **19:**10916-10924.

79. **Stover, C. K., X. Q. Pham, A. L. Erwin, S. D. Mizoguchi, P. Warrener, M. J. Hickey, F. S. L. Brinkman, W. O. Hufnagle, D. J. Kowalik, M. Lagrou, R. L.**

Garber, L. Goltry, E. Tolentino, S. Westbrock-Wadman, Y. Yuan, L. L. Brody, S. N. Coulter, K. R. Folger, A. Kas, K. Larbig, R. Lim, K. Smith, D. Spencer, G. K.-S. Wong, Z. Wu, I. T. Paulsen, J. Reizer, M. H. Saier, R. E. W. Hancock, S. Lory, and M. V. Olson. 2000. Complete genome sequence of *Pseudomonas aeruginosa* PAO1, an opportunistic pathogen. Nature 406:959-964.

80. **Thurman, E. M.** 1985. Organic Geochemistry of Natural Waters. Martinus Nijhoff Publishers, The Hague, Netherland.

81. **Todar, K.** 2005 2002, posting date. Todar's online textbook of bacteriology. [Online.]

82. **Tufenkji, N., and M. Elimelech.** 2004. Correlation Equation for Predicting Single-Collector Efficiency in Physicochemical Filtration in Saturated Porous Media. Environmental Science & Technology **38:**529-536.

83. **Ubbink, J., and P. Scha¨r-Zammaretti.** 2005. Probing bacterial interactions: integrated approaches combining atomic force microscopy, electron microscopy and biophysical techniques. A review. Micron **36:**293-320.

84. **Vadillo-Rodriguez, V., H. J. Busscher, W. Norde, J. d. Vries, and H. C. van der Mei.** 2003. On relations between microscopic and macroscopic physicochemical properties of bacterial cell surfaces: an AFM study on Streptococcus mitis strains. Langmuir **19:**2372-2377.

85. **Van der Mei, H. C., and H. J. Busscher.** 2001. Electrophoretic mobility distributions of single-strain microbial populations. Applied and Environmental Microbiology **67:**491-494.

86. **Van Elsas, J. D., J. T. Trevors, and L. S. Van Overbeek.** 1991. Influence of soil properties on the vertical movement of genetically-marked *Pseudomonas fluorescens* through large soil microcosms. Biology And Fertility Of Soils **10:**249-255.

87. **Van Loosdrecht, M. C. M., J. Lyklema, W. Norde, G. Schraa, and A. J. B. Zehnder.** 1987. Electrophoretic mobility and hydrophobicity as a measure to predict the initial steps of bacterial adhesion. Applied and Environmental Microbiology **53:**1898-1901.

88. **Van Loosdrecht, M. C. M., J. Lyklema, W. Norde, G. Schraa, and A. J. B. Zehnder.** 1987. The role of bacterial cell wall hydrophobicity in adhesion. Applied and Environmental Microbiology **53:**1893-1897.

89. **Van Loosdrecht, M. C. M., W. Norde, J. Lyklema, and A. J. B. Zehnder.** 1990. Hydrophobic and electrostatic parameters in bacterial adhesion. Aquatic Sciences **52:**103-114.

90. **Vega, E., B. Lesikar, and S. D. Pillai.** 2003. Transport and survival of bacterial and viral tracers through submerged-flow constructed wetland and sand-filter system. Bioresource Technology **89:**49-56.

91. **Velegol, S. B., and B. E. Logan.** 2002. Contributions of bacterial surface polymers, electrostatics, and cell elasticity to the shape of AFM force curves. Langmuir **18:**5256-5262.

92. **Vermohlen, K., H. Lewandowski, H.-D. Narres, and M. J. Schwuger.** 2000. Adsorption of polyelectrolytes onto oxides-the influence of ionic strength, molar

mass, and Ca^{2+} ions. Colloids and Surfaces A: Physicochemical Engineering Aspects **163:**45-53.

93. **Wollum, A. G., II., and D. K. Cassel.** 1978. Transport of microorganisms in sand columns. Soil Science Society of America Journal **42:**72-76.

94. **Wozniak, D. J., T. J. O. Wyckoff, M. Starkey, R. Keyser, P. Azadi, G. A. O'Toole, and M. R. Parsek.** 2003. Alginate is not a significant component of the extracellular polysaccharide matrix of PA14 and PAO1 *Pseudomonas aeruginosa* biofilms. Proceedings of the National Academy of Sciences **100:**7907-7912.

95. **Xiaopeng, G., P. Jianhua, L. Ruixia, and T. Hongxiao.** 2004. Application of atomic force microscopy in the characterization of cell morphology of Bacillus cereus bacteria in the biosorption process of heavy metals. Huanjing Kexue Xuebao **24:**753-760.

96. **Xu, L., V. Vadillo-Rodriguez, and B. E. Logan.** 2005. Residence Time, Loading Force, pH, and Ionic Strength Affect Adhesion Forces between Colloids and Biopolymer-Coated Surfaces. Langmuir **21:** 7491-7500.

97. **Yamamoto, S., M. Ejaz, Y. Tsujii, and T. Fukuda.** 2000. Surface interaction forces of well-defined, high-density polymer brushes studied by atomic force microscopy. 2. effect of graft density. Macromolecules **33:**5608-5612.

98. **Yao, K., M. T. Habibian, and C. R. O'Melia.** 1971. Water and wastewater filtration:Concepts and applications. Environmental Science & Technology **5:**1105-1112.

99. **Yao, X., J. Walter, S. Burke, S. Stewart, M. H. Jericho, D. Pink, R. Hunter, and T. J. Beveridge.** 2002. Atomic force microscopy and theoretical

considerations of surface properties and turgor pressures of bacteria. Colloids and Surfaces, B: Biointerfaces **23:**213-230.

100. **Zhuang, J., and Y. Jin.** 2003. Virus retention and transport as influenced by different forms of soil organic matter. Journal of Environmental Quality **32:**816-823.

101. **Zhuang, J., and Y. Jin.** 2003. Virus retention and transport through Al-oxide coated sand columns: effects of ionic strength and composition. Journal of Contaminant Hydrology **60:**193-209.